UNIVERSITY OF NAPLES FEDERICO II

Department of Chemical, Materials and Industrial Production Engineering

Ph.D COURSE IN MATERIALS ENGINEERING AND STRUCTURES

XXV CYCLE

"Design of Bicomponent Electrospun Conduits for Peripheral Nerve Regeneration"

Tutors:

Dr. Vincenzo Guarino

Prof. Luigi Ambrosio

Candidate:

Valentina Cirillo

Coordinator:

Prof. Giuseppe Mensitieri

TABLE OF CONTENTS

AIM OF THIS RESEARCH

- To estimate the influence of solvent permittivity, polymer/solvent thermodynamic affinity and other technological parameters (i.e., concentration, flow rate) on the morphology and on the physical properties of poly(ε-caprolactone) (PCL) electrospun fibers in order to address cell response for nerve tissue engineering applications.
- To evaluate and define the effect of gelatin protein integration into PCL fibers on morphology and physico-chemical properties to identify the contribution of biochemical cues and scaffolds topography on cells (hMSC and PC-12) response.
- To design and produce electrospun conduits for *in vivo* implant in rat sciatic nerve model, in order to test them as artificial graft for peripheral nerve regeneration.

SUMMARY OF COVERED SUBJECTS

This thesis deals with the potential of the electrospinning process to create substrates composed of synthetic and natural polymers for use as alternative scaffolds for peripheral nerve regeneration.

Chapter 1 gives a brief overview on the history, on the theories about electrospinning process, on the effect of materials and process parameters, on different types of electrospinning equipments and on its several applications, mainly focusing on tissue engineering application.

Chapter 2 describes the preparation and characterization of electrospun poly(ε-caprolactone) (PCL) fibers changing solvent type and relates the differences in terms of morphology, crystallinity and cells response due to the employed polymer/solvent system.

Chapter 3 presents the design and the optimization of PCL/Gelatin fibers. By the investigation of membranes morphology, hydrophilicity, degradation rate and interaction with different cell lines, electrospun samples are proposed as scaffolds for peripheral nerve regeneration.

Chapter 4 concerns the design and optimization of electrospun conduits with a further assessment of their mechanical properties and interaction with primary cells.

Chapter 5 describes the *in vivo* implant of PCL and PCL/Gelatin electrospun conduits as graft for sciatic nerve in a rat model to repair a 5 mm gap after transection in a 18 weeks study. The estimation of occurred regeneration has been shown by electrophysiology and histological results.

Chapter 6 proposes the development of new electrospun devices with more complex characteristics, i.e. anisotropic or multilayer structures, to ensure the mechanical stability and to guide the regeneration process after peripheral nerve injury.

CHAPTER 1

The Electrospinning Technique

1.1 INTRODUCTION

Electrospinning is a versatile technique that allows the fabrication of continuous fibers with diameters ranging from micrometers down to a few nanometers. The method can be applied to synthetic and natural polymers as well as to metals and ceramics. By the implementation of specific electrospinning setups it is possible to produce fibers with complex architectures, such as core–shell or hollow fibers, with an ordered arrangements and 3-D structures, such as tubes [1].

Electrospinning, also known as electrostatic spinning, has its basis about 300 years ago. In 1745, Bose described aerosols generated by the application of high electric potentials to drops of fluids. In 1882, Lord Rayleigh investigated the question of how many charges needed to overcome the surface tension of a drop. Later, the first devices to spray liquids through the application of an electrical charge were patented by Cooley and Morton, in 1902 and 1903. In 1929, Hagiwaba et al. described the fabrication of artificial silk through the use of electrical charge. The crucial patent, in which the electrospinning of plastics was described for the first time, appeared in 1934 with Anton Formhals from Mainz as the author. Despite these early discoveries, the procedure was not utilized commercially. In the 1970s, Simm et al. patented the production of fibers with diameters of less than 1 mm. However, this work, which was followed by other patents, also remained unnoticed. Electrospun fibers were first commercialized for filter applications, as part of the nonwovens industry. Electrospinning gained substantial academic attention in the 1990s, which was partially initiated by the activities of the Reneker group. One reason for the fascination with the subject is the combination of both fundamental and application-oriented research from different science and engineering disciplines [1].

Since the invention of electrospinning in the early 20th century, there has been enormous activity in this area during the last two decades [2-5], with more than 1500 annual reports and 15,000 publications being written on the subject [6]. Electrospinning is not only used in university laboratories, but it is increasingly being applied in industry, too. The scope of applications, in fields

as diverse as filtration, catalysis, optoelectronics, sensor technology, tissue engineering scaffolds and medicine, is very broad [1, 7].

1.2 THEORETICAL BACKGROUND

Conventional production systems of large diameter fibers involve the drawing of molten polymer out through a die. The resultant stretched polymer melt dries to form individual strand of fiber. Similarly, electrospinning also involves the drawing of fluid, either in the form of molten polymer, polymer solution or different types of precursors, depending on the applications. However, unlike conventional drawing method, where there is an external mechanical force that pushes the melt through a die, electrospinning makes use of charges that are applied to the fluid to provide a stretching force [8].

The apparatus used for electrospinning consists of a high voltage power supply with positive or negative polarity, a syringe pump, in order to guarantee a constant flow of the fluid, a metal needle, and a conducting collector like an aluminium foil. The collector can be made of any shape according to the requirements, like a flat plate, a rotating drum, a disc, a cylinder (Figure 1.1).

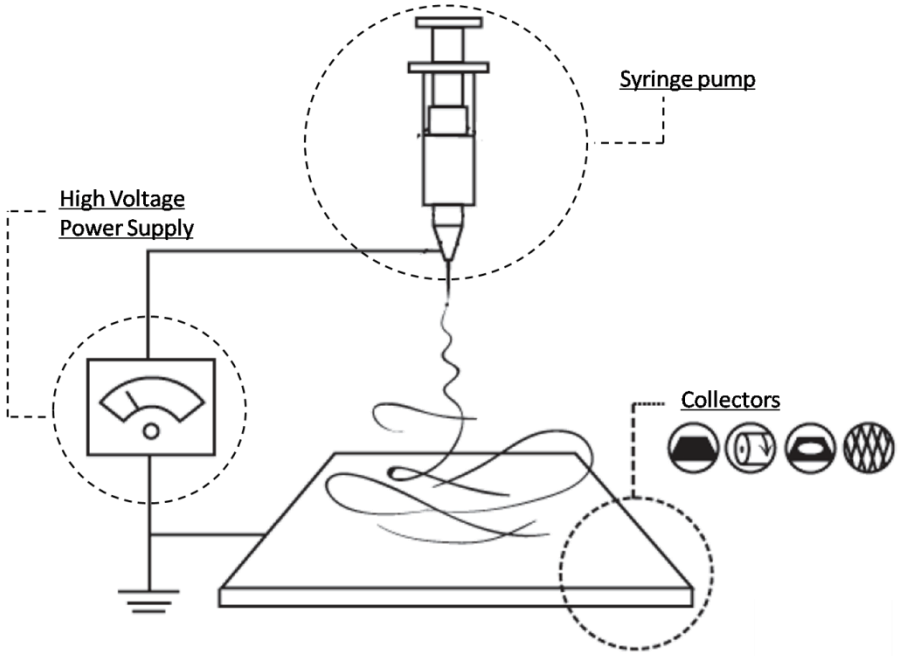

Figure 1.1: Electrospinning apparatus.

In this work electrospinning from polymer solution has been performed. The polymeric solution is forced through the syringe pump to form a pendant drop at the tip of the capillary. High voltage potential is applied to the polymer solution inside the syringe through an electrode connected via conductive clamps to the needle, thereby inducing free charges into the polymer solution. These

charged ions move in response to the applied electric field towards the electrode of opposite polarity or grounded, thereby transferring tensile forces to the polymer liquid [9]. Therefore at the tip of the capillary, indicated as base region, the pendant, hemispherical polymer drop takes a cone like projection, known as Taylor's cone (Figure 1.2).

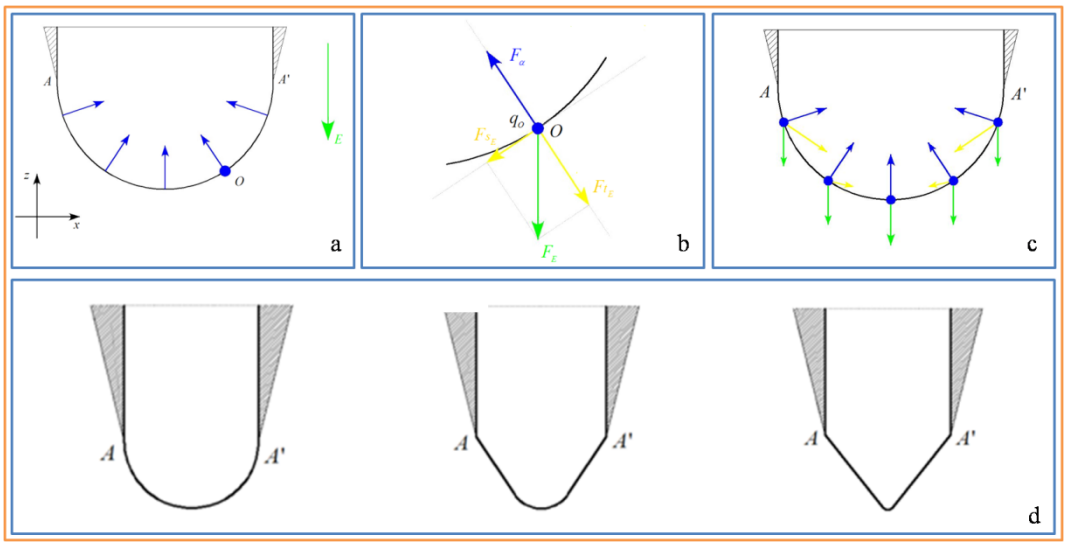

Figure 1.2: a) Surface tension effect on a polymer solution droplet, b) electric force acting on the droplet; c) balance between the electric field and the surface tension; d) Taylor's cone formation.

When the applied potential reaches a critical value required to overcome the surface tension of the liquid, a jet of liquid is ejected from the cone tip [10]. The shape of the base region depends upon the surface tension of the liquid and the force of the electric field; jets can be ejected from surfaces that are essentially flat if the electric field is strong enough [7], as represented in Figure 1.3.

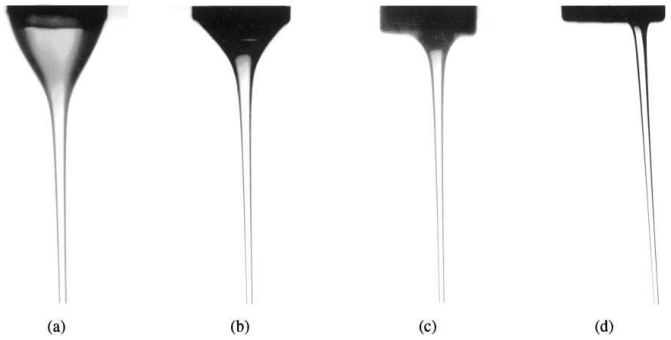

Figure 1.3: Stable jet profiles of PEO-water solution, a) E_∞= 0.47; b) E_∞= 0.53; c) E_∞= 0.6 ; d) E_∞= 1 kV cm^{-1} [11].

Electric forces then accelerate and stretch the polymer jet, causing the diameter to decrease as its length increases. After the initiation from the cone and a linear travel for a certain fraction of his path, the jet undergoes a chaotic motion or bending instability and as it goes through the atmosphere

towards the opposite charged collector (Figure 1.4), the solvent evaporates, leaving behind a dry fiber on the collecting device [12, 13]. The occurrence of bending instabilities is easily understood: even a simple linear arrangement of three equal charges elastically fixed along a chain becomes unstable towards lateral deflection, in this case a straight section of the jet turns sideways and forms loops in the horizontal plane. The loop diameters increase with time during the motion towards the counter electrode; thanks to these instabilities nanofibers can be produced [1].

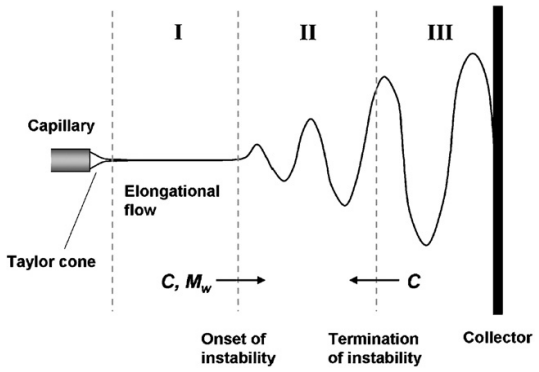

Figure 1.4: A scheme of evolving solution jet during electrospinning. The flight path is divided into three regions. When the parameters indicated (C: concentration, M_w: polymer molecular weight) are increased, regional borders may shift in the direction indicated by the arrows [14].

To the naked eye (and from the perspective of low-speed photography), this instability appears to be splaying, e.g., in the form of repeated bifurcations, of the initially single-jet stream (with each jet stream leading toward a single filament) into multiple jet streams (or subfilaments), giving the impression of a frayed rope, as seen in Figure 1.5, left. A reasonable explanation for the apparent splaying of the jet stream could be easily found in the increasing electrostatic repulsion of the different parts of the fiber surface [10]. However, subsequent experimental evidence gathered with highspeed cameras (Figure 1.5, right) and theoretical models suggested that the apparent splaying was an optical illusion in the form of a very fast whipping motion of the jet [15].

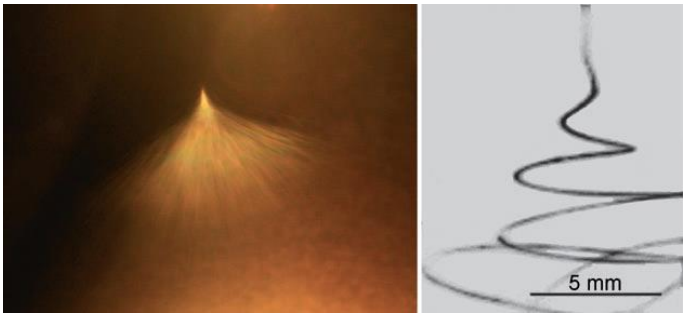

Figure 1.5: Left, photograph of a jet of PEO solution during electrospinning. Right, high-speed photograph of jet instabilities [1, 13].

Another instability is induced by the coupling of the liquid strand with the electric field during electrospinning. The so-called axisymmetrical instability provides a statistical variance of the jet radius that causes a modulation of the surface charge density (Figure 1.6). This modulation, in turn, generates tangential forces, which couples to the radius modulation and amplifies it. The end result is the formation of defects called beads, which are aligned along the fiber like pearls on a string [1].

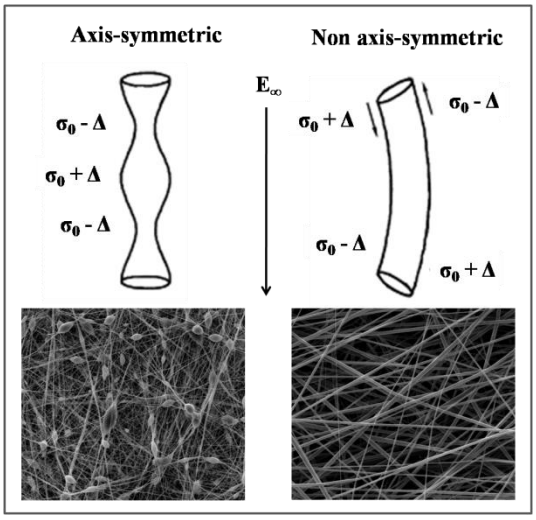

Figure 1.6: Representation of axis-symmetric and non axis-symmetric instabilities of electrospun jet.

Rutledge and co-workers examined the competition between these instabilities for various applied electric fields and the flow rate and determined the dominant mode. They constructed operating diagrams that outlined the conditions at which whipping could be expected; their predictions agreed well with experimental results [7, 16].

1.3 CONTROL OF THE ELECTROSPINNING VARIABLES

From the previous description of theory, it is clear that the electrospinning process can be controlled manipulating a number of variables which Doshi and Reneker classified in terms of materials properties, process and ambient parameters [7, 17].

The materials variables in solution electrospinning may be subdivided further in two groups. The first group is related to the nature of the components used, including chemical composition of the polymer and solvent, and for polymers, the corresponding molecular weight and molecular weight distribution. The second group mainly includes properties of solution, such as surface tension, concentration and viscosity, charge density, solution conductivity [15]. The applied voltage, the electrode separation distance and the flow rate are classified as process parameters, instead ambient variables include air composition and humidity [15].

1.3.1 Polymer Properties

Significant effects on morphology are primarily determined by the properties of the system used: changing the molecular weight of polymer, solvent type and solution concentration it is possible to pass from the creation of microspheres to fibers micro or nanosized, possibly characterized by a certain porosity and roughness, as summarized in Figure 1.7.

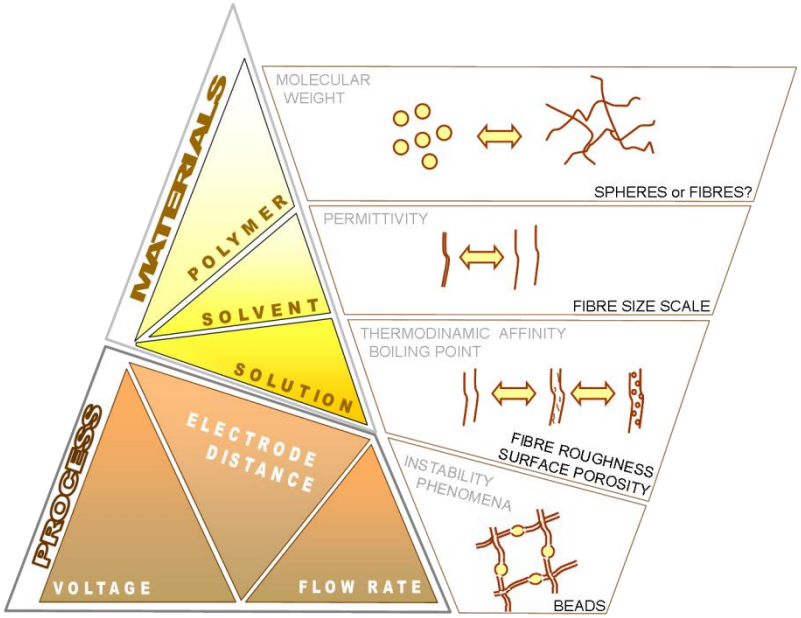

Figure 1.7: Dependence of morphology from materials and process parameters.

One of the conditions necessary for electrospinning to occur is that the solution must consists of polymer of sufficient **molecular weight** and the solution must be of sufficient viscosity. The molecular weight of the polymer represents the length of the polymer chain, it affects solution viscosity since the polymer length determines the amount of entanglement of the polymer chains in the solvent [8]. Generally, when a polymer of higher molecular weight is dissolved in a solvent, its viscosity is greater than solution of the same polymer but of a lower molecular weight.

During electrospinning as the jet travels from the needle tip towards the collection plate stretched by the electric field, it is the entanglement of the molecule chains that prevents the electrically driven jet from breaking up thus maintaining a continuous solution jet. As a result, monomeric polymer solution does not form fibers when electrospun [8, 18]. This means that there is a threshold in terms of molecular weight that allows the production of fibers instead of microspheres.

The polymer chain entanglements were found to have a significant impact on whether the electrospinning jet breaks up into small droplets or whether resultant electrospun fibers contain beads [19]. Although a minimum amount of polymer chain entanglements and viscosity are necessary for electrospinning, a viscosity that is too high makes it very difficult to pump the

solution through the syringe needle [20]. Moreover, when the viscosity is too high, the solution may dries at the tip of the needle before electrospinning can be initiated [21]. In fact, considering two different type of poly(ε-caprolactone) (PCL), one of low molecular weight (M_w 14 kDa) and another of high molecular weight (M_w 65 kDa), both dissolved in chloroform, fixing composition and process parameters, it is possible to switch from microspheres to fibers (Figures 1.8 A-B).

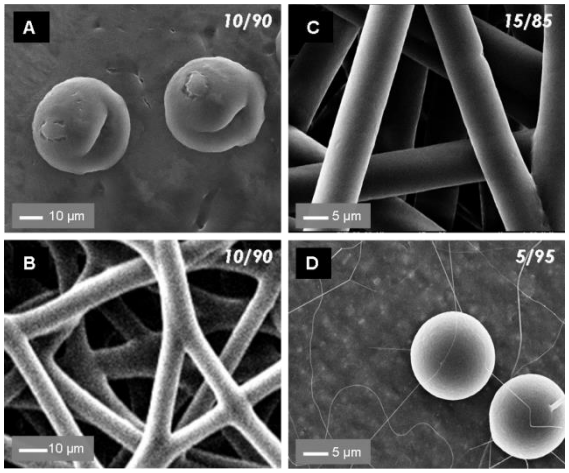

Figure 1.8: Comparison of polymer molecular weight and concentration effect on morphology of electrospun mats, fixing the remaining parameters: A) PCL M_w 14 kDa and 10% w/w, B) PCL M_w 65 kDa and 10% w/w, C) PCL M_w 65 kDa and 15% w/w, D) PCL M_w 65 kDa and 5% w/w.

1.3.2 Solvent Properties

Variation of solvent type greatly affects both the fiber spinnability and the final fiber morphology. The use of solvents with higher **dielectric constant**, which reflects the polarity of molecules, and higher dipole moment improves electrospinnability [22] and leads to the reduction of the resultant electrospun fiber diameter [23]. This is due to an increased bending instability of the electrospun jet, shown by a larger deposition area, and consequently to a longer jet path [8]. In fact it has been shown that the electric charges have a much greater effect to a polar solvent than to a non-polar solvent [23].

The greater bending instability and the reduction of fibers diameter due to higher polarity of solvents is evident comparing PCL membranes obtained from solutions in chloroform ($CHCl_3$), apolar, with low dielectric constant 4.8 [8] and in 2,2,2 trifluoroethanol (TFE) which is a fluorinated solvent showing a dielectric permittivity of 27.0 [8]. Scanning Electron Microscopy (SEM) images reported in Figure 1.9 demonstrate that changing solvent it is possible to control fiber size scale, reaching sub-micrometric dimensions.

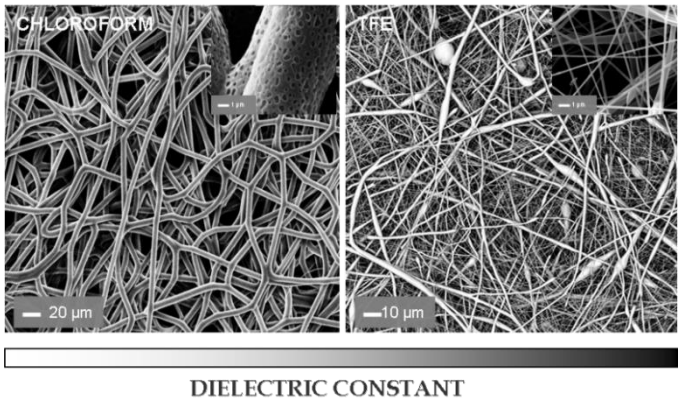

Figure 1.9: Influence of solvent dielectric permittivity and volatility on fibers size scale: A) PCL in $CHCl_3$; B) PCL in TFE.

In order to tune fiber size and improve electrospinnability, a solvent with higher dielectric constant can be added to the solution, since the dielectric constant of mixed solvents is the weighted average of the mixture components by assuming a simple additive function of solvents concentration. For example the dielectric properties of a PCL solution in chloroform (dielectric constant 4.8 [8]) can be increased with ethanol (EtOH) addition (dielectric constant 24.5 [8]) as co-solvent and lowering surface tension, the jet splays more easily, thereby reducing fibers diameter (Figure 1.10).

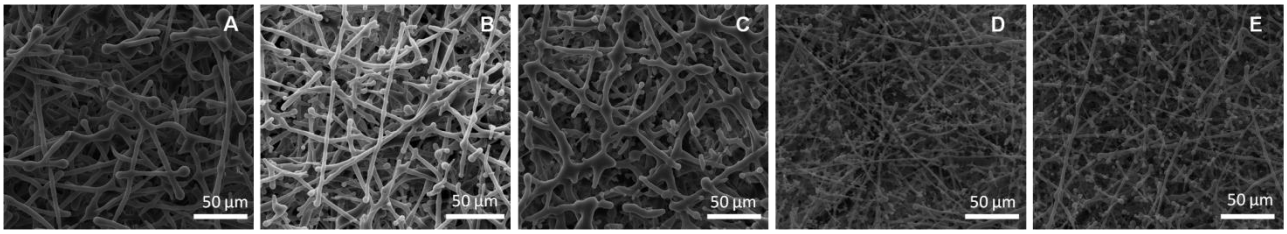

Figure 1.10: Influence of $CHCl_3$- EtOH ratio on fibers size scale: A) 100:0; B) 90:10; C) 80:20; D) 70:30, E) 60:40.

By assuming a linear relationship between pure solvents dielectric constant, the mixtures dielectric constants were estimated varying the ethanol amount (Figure 1.11 A).

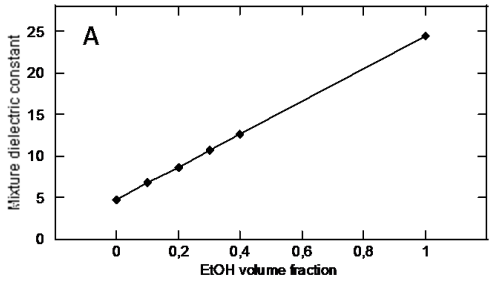

$CHCl_3$-EtOH ratio	Dielectric constant	Solubility parameter [$MPa^{1/2}$]
100:0	4,8 [8]	19,0 [24]
90:10	6,8	19,7
80:20	8,7	20,4
70:30	10,7	21,2
60:40	12,7	21,9
0:100	24,5 [8]	26,2 [24]

Figure 1.11: Influence of $CHCl_3$- EtOH ratio on mixture dielectric constant.

The limit to use co-solvents to improve solution relative permittivity is determined by the polymer/solvent thermodynamic affinity, expressed by the solubility parameter δ. It has been demonstrated that distributed defects along fibers occurred when there is a tendency towards the partial demixing of the solution due to sub-optimal thermodynamic coupling represented by a remarkable difference in terms of δ between the pure polymer and the pure solvents or mixture. In fact, for a 60:40 $CHCl_3$- EtOH ratio the permittivity increases but the solubility parameter of the mixture deviates from the PCL (20.2) (Figure 1.11 B).

Also solvents chemical structure influences system electrospinnability [25]: membranes obtained in the same conditions from PCL/chloroform solution, solvents with a linear chain, present less defects and more homogeneous diameters distribution than those produced from PCL/tetrahydrofuran (THF), which has symmetric cyclical chains, as shown in Figure 1.12. Linear solvent molecules easily tend to spread over the entangled polymer molecules thus reducing the tendency for the solvent molecules to come together under the influence of surface tension, leading to decrease beads formation.

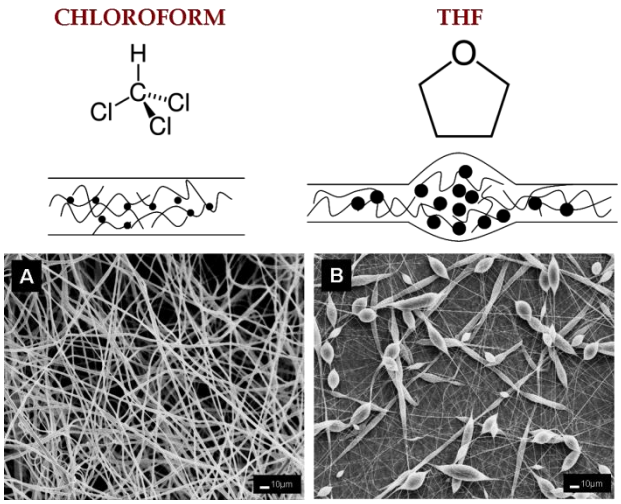

Figure 1.12: Effect of solvent properties on electrospinnability and defects formation: A) PCL in chloroform 20% w/w; B) PCL in THF 20% w/w.

In addition, solvent **density** can further affects the viscosity of solution, when this value is low, solvent molecules can congregate under the action of surface tension, determining the presence of defects, i.e. THF 0.87 g/cm^3 and $CHCl_3$ 1.47 g/cm^3 [25].

1.3.3 Solution Properties

The solution properties play a key role in the formation of electrospun fibers and defects. Similar to increasing the molecular weight, higher polymer **concentration** results in greater chain

entanglements within the solution which is necessary to maintain the continuity of the jet during electrospinning [8]. At low concentrations and so at low viscosities, surface tension is the dominant influence on fiber morphology and below a certain concentration drops form instead of fibers [26, 27]. Increasing concentration, there is a gradual change in the shape of the electrospun products, in fact drops are followed by fibers with beads from spherical to spindle-like until a smooth fiber is obtained [28].

These phenomena have been showed for a system composed of PCL in chloroform, at different composition (Figures 1.8 C-D) and it is compared with those due the increased polymer molecular weight. At high concentrations, processing is prohibited by an inability to control and maintain the flow of a polymer solution to the tip of the needle and by the cohesive nature of the high viscosity solutions [20, 21].

Once obtained defects-free fibers, a further increase in concentration causes a rise in fibers average diameter, probably due to the greater resistance of the solution to be stretched by the charges on the jet [29, 30]. In fact, if the concentration is high enough to guarantee a solution viscosity able to reduce bending instability, the deposition area is smaller and the jet path is reduced. In this way there is less stretching of the solution resulting in a larger fiber diameter [8, 28].

Although the range of concentrations that produce fibers obviously varies depending on the polymer/solvent system used and interactions between them, the forces of viscosity and surface tension determine the upper and lower boundaries of processing window, if all other variables are held constant [12].

In fact, the initiation of electrospinning requires the charged solution to overcome its **surface tension**. However, as the jet travels towards the collection plate, the surface tension may cause the formation of beads along the jet. Surface tension decreases the surface area per unit mass of a fluid. In this case, when there is a high concentration of free solvent molecules, there is a greater tendency for the solvent molecules to congregate and adopt a spherical shape due to surface tension. At higher viscosity the solvent interacts more with the polymer molecules thus, when the solution is stretched under the influence of the charges, the solvent molecules tend to spread over the entangled polymer molecules reducing the tendency for the solvent molecules to come together under the influence of surface tension [8].

Since electrospinning involves stretching of the solution caused by repulsion of the charges at its surface, if the **solution conductivity** is increased, more charges can be carried by the electrospinning jet influencing the stretching of the solution. As a result, smooth and finer fibers are formed [21] and the critical voltage for electrospinning to occur is also reduced [23]. Another effect

of the increased charges is that it results in a greater bending instability and so the deposition area of the fibers is increased [31].

Although organic solvents are known to be non-conductive, many of them do have a certain level of conductivity as mentioned previously otherwise the solution conductivity can be increased by the addition of ions. The size of the ions may have an influence in the fiber morphology. Electrospun fibers from a solution with dissolved NaCl was found to have the smallest diameter, while fibers from a solution with dissolved KH_2PO_4 had the largest diameter and fibers electrospun from solution with NaH_2PO_4 dissolved had intermediate diameter. As sodium and chloride ions have a smaller atomic radius than potassium and phosphate ions, they may have a greater mobility under an external electrostatic field. As a result, the greater elongational force on the electrospinning jet caused by the more mobile and smaller ions could yield fibers with smaller diameter [21].

1.3.4 Process Parameters

External factors such as the flow rate, voltage, type of collector, needle diameter and distance between the needle tip and collector have a certain influence on fibers morphology, though less significant than the solutions parameters.

The high **voltage** supplied induces the necessary charges on the solution and together with the external electric field, initiates the electrospinning process when the electrostatic force overcomes the surface tension of the solution [8].

The applied voltage affects the shape of the liquid surface from which the jet originates, this phenomenon reflects a change in the mass balance that occurs at the end of the capillary tip. In facts, the voltage can increase the spinning current, due to the charge transport during the flowing of polymer from the tip to the target, since ionic conduction in the polymer solution is usually assumed small enough to be negligible. Greater spinning current usually results in higher mass flow rate from the capillary tip to the grounded target when all other variables are held constant.

At low voltages, a droplet of solution remains suspended at the end of the syringe needle, and the fiber jet originates from a cone at the bottom of the droplet whose diameter is larger than the capillary. The nanofibers produced under these conditions have a cylindrical morphology with few bead defects present. As voltage is increased, the volume of the droplet decreases, the cone has receded and the jet originates from the liquid surface within the syringe tip. The electrospun fibers produced still have essentially a cylindrical morphology, but there is a distinct increase in number of bead defects present in the fiber mat. In fact, increasing the voltage causes the rate at which solution is removed from the capillary tip to exceed the rate of delivery of solution to the tip needed to maintain the conical shape of the surface. This shift in the mass balance results in a sustained but increasingly less stable jet, generating more defects [12].

When the voltage is increased, a stronger columbic repulsive force is present within the polymer jet causing greater stretching, a reduction of fiber diameter, a more pronounced whip-like motion of the ejected fiber due to bending instability [21, 32]. In addition, higher applied voltage increases the rate of solvent evaporation producing drier and a more distinguishable fibrous deposition as opposed to an interconnected mesh [33]. As with other electrospinning parameters, the voltage effects on fiber morphology are not standardized. It appears that the voltage effect on fiber diameter could be different, depending on the polarity of the solution and the electrical properties of the polymer [34]. This may also provide an explanation for the seemingly contradictory results reported by different electrospinning groups as some of the researchers found that the fiber diameter increased with voltage [30, 35-37] while others found that the fiber diameter decreased with increasing voltage [38-42], although the effect of voltage was not as strong as that of the polymer solution concentration as shown also in Figure 1.13 for PCL fibers.

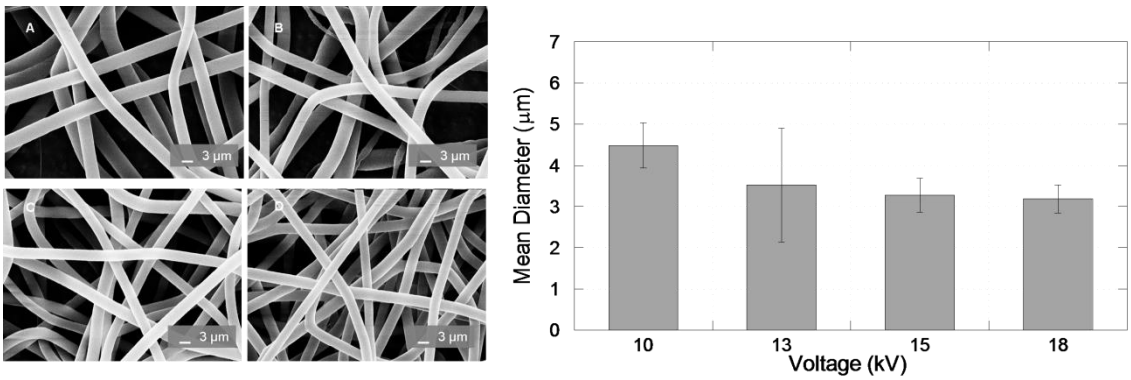

Figure 1.13: Evaluation of PCL fiber morphology changing the applied voltage: A) 10, B) 13, C) 15, D) 18 kV.

The struggle to maintain constant the Taylor cone requires frequent adjustments to the voltages strength in conjunction to monitoring other electrospinning parameters [43].

The solution **flow rate** is another process factor that has to be considered in order to obtain a stable Taylor's cone for given parameters and to influence electrospun fibers morphology. The feedrate determines the amount of solution available for electrospinning. When the feedrate is increased, there is a corresponding raise in the fiber diameter or beads size, simply because a greater volume of solution is drawn away from the spinneret [8, 21, 44, 45]. In Figure 1.14, SEM images and the relative image analysis showed an increase of fibers diameters ranging from 0.1 ml/h to 3 ml/h.

Due to the greater volume of solution drawn from the needle tip, the jet takes a longer time to dry. As a result, the solvents in the deposited fibers may not have enough time to evaporate given the same flight time. The residual solvents may cause the fibers to fuse together where they make contact forming web. A lower feed rate is more desirable as the solvent has more time for evaporation [46].

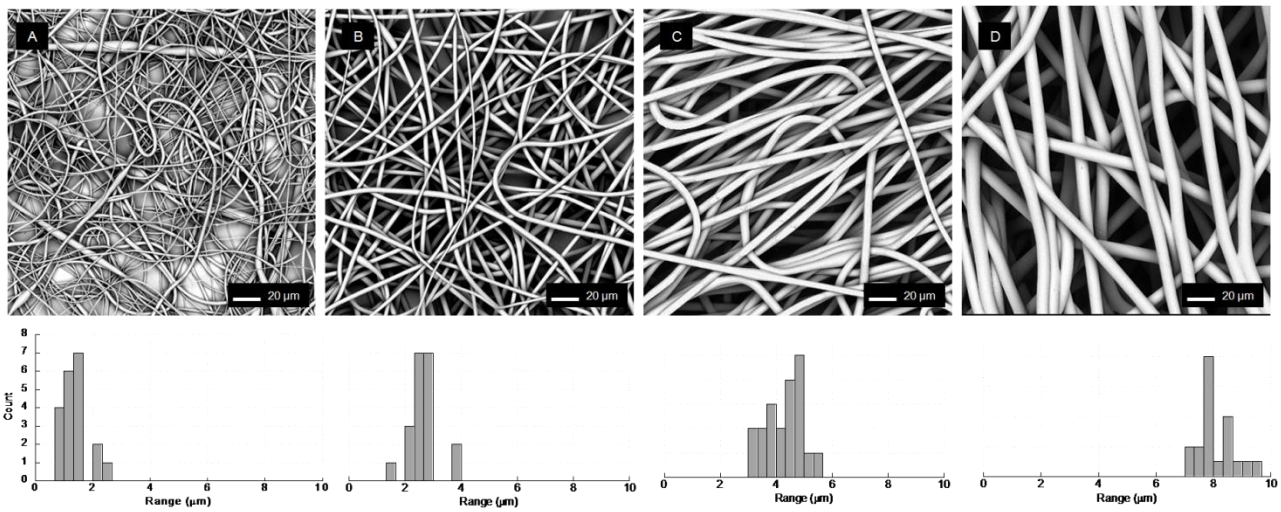

Figure 1.14: Evaluation of PCL fiber size from SEM images of membranes by using different flow rates: A) 0.1, B) 0.5, C) 1, D) 3 ml/h.

The **electrode separation distance** refers to measured distance between the dispensing needle and the grounded collecting plate. It contributes to the polymer fiber morphology by affecting flight time and electric field strength. As electrode separation distance increases and electric field strength decreases, the flight time of the ejected polymer jet increases which gives more time for solvent evaporation and the formation of independent fibers on a larger deposition area [8, 43]. Conversely, as electrode separation decreases, flight time shortens and the electric field strengthens allowing less time for solvents to evaporate. The resulting mat resembles a conglomeration of fibrous junctions instead of individual fibers on a narrower deposition area [43, 47].

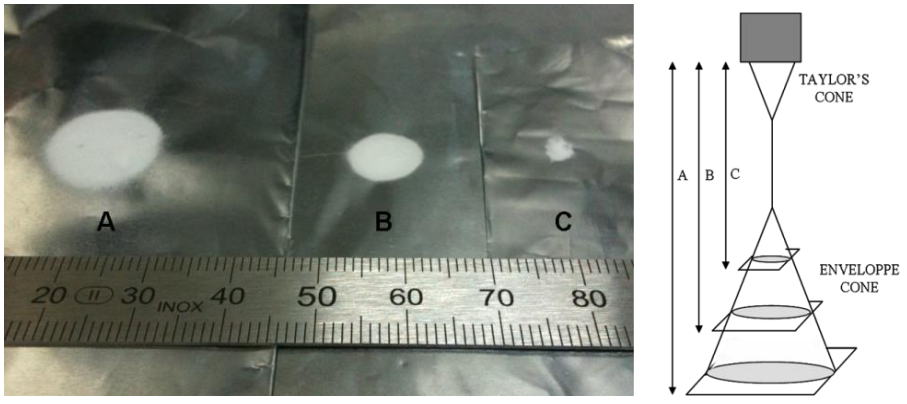

Figure 1.15: Deposition area reduction induced by decreasing electrodes distance during electrospinning of a PCL solution from 14 cm (A) to 10 cm (B) and 6 cm (C).

In Figure 1.15 it has been illustrated that deposition area effectively shrank decreasing electrodes distance from 14 cm to 6 cm during electrospinning of a PCL solution in chloroform, fixed

remaining parameters. Depending on the solution properties, the effect of varying the distance may or may not have a significant effect on the fiber morphology. In some cases, changing the distance has no significant effect on the fiber morphology.

1.3.5 Ambient Parameters

Any interaction between the surrounding and the polymer solution may have an effect on the electrospun fiber morphology.

High **humidity** for example was found to cause the formation of pores on the surface of the fibers: the surface of the jet cools and water from the air condenses on the surface of the fiber. As the fiber dries, the water droplets leave an imprint behind [48, 26]. On the contrary, experiments using Polysulfone (PS) dissolved in Tetrahydrofuran (THF) show that at humidity of less than 50%, the fiber surfaces are smooth. The humidity of the environment also determines the rate of evaporation of the solvent in the solution. At a very low humidity, a volatile solvent may dries very rapidly. The evaporation of the solvent may be faster than the removal of the solvent from the tip of the needle. As a result, the electrospinning process may only be carried out for a few minutes before the needle tip is clogged [8]. It has also been suggested that the high humidity can help the discharge of the electrospun fiber [49, 50]. However, more tests have to be carried out to determine the effect of humidity on the electrical discharge during electrospinning and the accumulation of residual charges on the collected fibers.

Under enclosed condition, it is possible to investigate the effect of **pressure** on the electrospinning jet. Generally, reduction in the pressure surrounding the electrospinning jet does not improve the electrospinning process. When the pressure is below atmospheric pressure, the polymer solution in the syringe has a greater tendency to flow out of the needle and there causes unstable jet initiation. As the pressure decreases, rapid bubbling of the solution occurs at the needle tip. At very low pressure, electrospinning is not possible due to direct discharge of the electrical charges.

Mit-Uppatham et al. spun polyamide-6 fibers at temperatures ranging from 25 to 60°C [28]. They found that increasing the **temperature** yielded fibers with a decreased fiber diameter, and they attributed this decline in diameter to the decrease in the viscosity of the polymer solutions at increased temperatures.

1.4 ELECTROSPINNING SETUPS

As well as fibers morphology can be adjusted to a certain extent by manipulating system and process parameters, also patterning and architecture of the final meshes can be tuned by using proper technological devices. Depending on the application, a number of collector configurations

can be used, including a stationary plate, a rotating mandrel, a cylinder. Typically the use of a stationary collector results in the formation of a randomly oriented fiber mat.

It is possible to control fibers deposition, inducing a preferential orientation in order to get aligned fibers rather than random meshes. The simplest form is through the use of a rotating mandrel at a very high speed, up to thousands of rpm (revolution per minute) so that the fibers can be taken up on its surface and wounded around it. This is a mechanical method of aligning the fibers along the circumference of the mandrel. If the rotation of the mandrel is slower than the alignment speed, the fibers deposited are randomly oriented [8].

An alternative method to align the electrospun fibers is based on the behavior of electrospinning jet in an electrostatic field: when two parallel conducting electrodes are placed below the needle with a gap between them as shown in Figure 1.16, the electric field lines in the vicinity of the parallel electrodes were split into two fractions pointing towards edges of the gap along the electrodes [51]. Since it is known that the electrospinning jet is influenced by the electrostatic field profile, the jet would stretch itself across the gap as the field lines are attracted towards the electrodes. This results in electrospun fibers aligning itself across the gap between the electrodes. Due to the presence of charges on the electrospun fibers, mutual repulsion between the deposited fibers enhances the parallel distribution of the fibers.

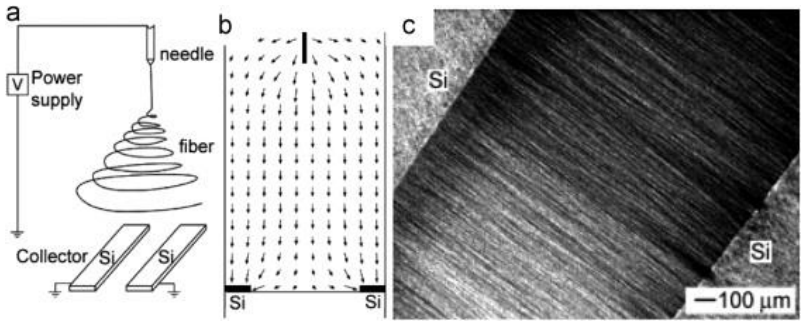

Figure 1.16: (a) Electrospinning with two parallel conducting collectors; (b) profile of the electric field; (c) electrospun fibers [52].

As shown in Figure 1.17 B, aligned fibers layers can be overlapped also changing the fibers orientation angle.

The potential application of electrospun fibers is greatly increased by the ability to obtain two-dimensional (2D) as well as three dimensional (3D) fiber architectures. Smaller diameter tube can be used as the rotating mandrel to form tubular structure made of electrospun fibers (Figure 1.17 C). Under normal electrospinning setup, only electrospun fibers of the same material are produced. However, to further improve on the versatility of electrospinning, some researchers have produced

fiber mesh composed of different types of polymer fibers. The fiber mesh may consist of layers formed by different types of polymer sequentially electrospun [39]. However, care must be taken to ensure that the second layer of fibers is deposited on top of the first fiber mesh. Accumulations of charges on the first layer of fiber mesh may discourage the subsequent layers of fibers from depositing directly on the previous layers. As consequence, the fiber mesh layers may not be of uniform thickness.

To obtain a fiber mesh with mixed polymer fibers, the simplest method is to use two different electrospinning source filled with the two different polymer solution and electrospun onto a moving collector [39, 53] as represented in Figure 1.17 D. This ease of use and adaptability is one of the main reasons for electrospinning's renewed popularity [3, 54].

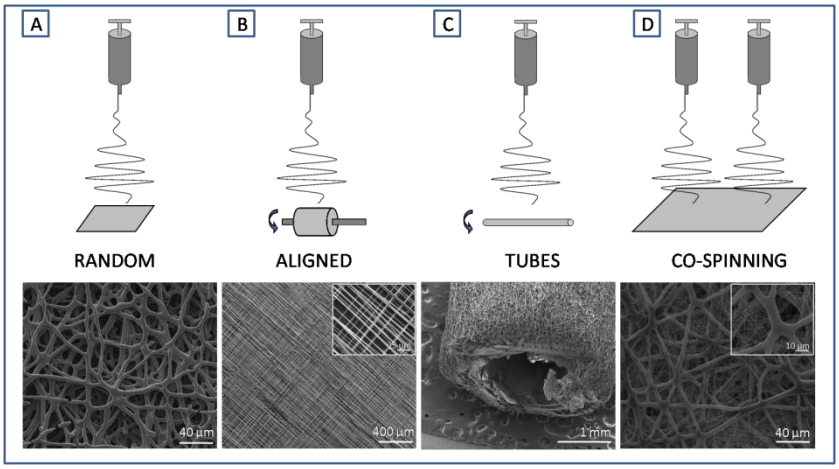

Figure 1.17: Electrospinning setups: A) random deposition; B) multilayer of fibers with a different angle of alignment; C) tubes; D) simultaneous electrospinning of different solutions.

1.5 APPLICATIONS

The possibility of large scale productions combined with the simplicity of the process makes this technique very attractive for many different applications [55]

Reviewing the number of patents, one can see that approximately two-thirds of all electrospinning applications are in the medical field. Of the remaining patents, one-half deals with filtration applications, and all other applications share the remaining half. The potential applications of electrospun fibers are shown schematically in Figure 1.18.

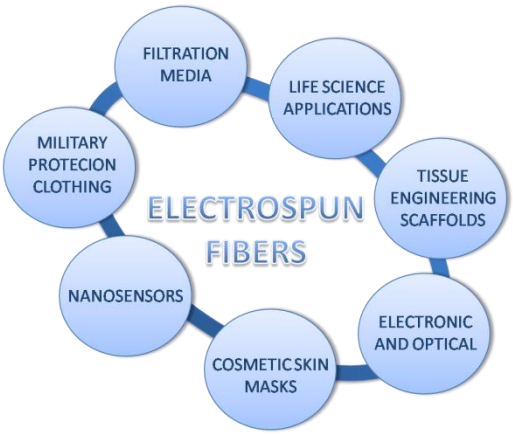

Figure 1.18: Electrospinning applications.

A very broad range of applications - including life sciences, medical, and filtration applications as well as sensors, protective clothing, and masks - is covered [15]. Here we would like to highlight the importance of electrospinning, in general, for biomedical applications like tissue engineering.

1.5.1 Tissue Engineering

As defined by Langer and Vacanti in 1993, tissue engineering is "an interdisciplinary field that applies the principles of engineering and life sciences toward the development of biological substitutes that restore, maintain, or improve tissue function" [7, 56].

For engineering living tissues, biodegradable scaffolds are generally considered as indispensable elements as these are used as temporary templates with specific mechanical and biological properties similar to native extracellular matrix (ECM) in order to modulate cell adhesion, invasion, proliferation, and differentiation prior to the regeneration of biologically functional tissue or natural ECM [7].

In vivo, ECM is composed of a network of nanometer-sized proteins and glycosaminoglycans [7]. The intricate complexities of this spatial and temporal environment dynamically influence phenotypic and other cellular behavior by providing indirect and direct informational signaling cues [7, 57].

Thus, the more closely the *in vivo* environment (i.e., chemical composition, morphology, surface functional groups) can be recreated, the more likely the success of the tissue engineering scaffold [58, 59].

Although the desired characteristics of a scaffold vary slightly with the tissue trying to be recreated, there are general properties that are desirable. First and foremost, the scaffold should be biocompatible, meaning that it integrates with the host tissue without eliciting a major immune response [60]. The scaffold should also be porous with a high surface-volume ratio to allow for cell attachment and in-growth, as well as exchange of nutrients during *in vitro* or *in vivo* culture [61].

Furthermore, the porous nature of the scaffold allows for angiogenesis upon implantation in a defect site (for vascularized tissues). Moreover, since the scaffold acts as a temporary support for the cells to adhere and proliferate, it should mimic native ECM both architecturally and functionally [62]. Finally, a tissue engineering scaffold should be biodegradable so that a second surgery is not required to remove the implant [62]. The rate of degradation should coincide or at least be controllable to mimic the rate of neo-tissue formation [7, 60].

Electrospinning generates connected porous mats with high porosity and high surface area which can mimic extra cellular matrix structure and therefore makes itself an excellent candidate for use in tissue engineering.

The diameter of electrospun fibers can be of similar magnitude as that of fibrils in ECM, mimicking the natural tissue environment [63]. Electrospinning has now become the most extensively used fabrication method for preparation of these nanofibrous scaffolds. When compared to other fiber forming processes such as self-assembly and phase separation techniques, electrospinning provides a simpler and more cost-effective means to produce fibrous scaffolds with an interconnected pore structure and fiber diameters in the sub-micron range [64].

Proper choice of biomaterials is required in terms of mechanical properties and degradation time which depends upon the type of scaffold required, type of the tissues to be regenerated and their regeneration time. This includes electrospinning of known and commercially available synthetic and natural biomaterials like polylactide (PLA), polycaprolactone (PCL), polyglycolic acid (PGA), and their copolymers etc. and especially synthesized novel biomaterials that are designed to direct the organization, growth, and differentiation of cells in the process of forming functional tissues [55].

Natural polymers are often used for preparing fibrous scaffolds because of their enhanced biocompatibility and bio-functional motifs such as collagen, alginate, silk protein, hyaluronic acid, fibrinogen, chitosan, starch and others and because their addition into synthetic polymers can improve the overall cytocompatibility of the scaffold [65-68]. A variety of polymeric fibers have been considered for use as scaffolds for engineering tissues such as cartilages [69, 70], dermal tissue engineering [71], bones [72, 73], arterial blood vessels [74-76], heart [77, 78], nerves [79,80].

REFERENCES

[1] Greiner A, Wendorff JH. Angew Chem. 2007; 46: 5670-5703.
[2] Huang ZM, Zhang YZ, Kotaki M, Ramakrishna S. Compos Sci Technol. 2003; 63: 2223-2253.
[3] Sill TJ, von Recum HA. Biomaterials. 2008; 29: 1989-2006.
[4] Jang JH, Castano O, Kim HW. Adv Drug Deliv Rev. 2009; 6: 1065-1083.
[5] Langer R, Tirrell DA. Nature. 2004; 428: 487-492.
[6] Shin SH, Purevdorj O, Castano O, Planell JA, Kim HW. J Tissue Eng. 2012; 3(1): 2041731412443530.
[7] Pham QP, Sharma U, Mikos AG. Tissue Eng. 2006; 12(5): 1197-1211.
[8] Ramakrishna S, Fujihara K, Teo WE, Lim WE, Ma Z. World Scientific Publishing Co Pte Ltd 2005.
[9] Reneker DH, Chun I. Nanotechnology. 1996; 7: 216-223.
[10] Deitzel JM, Beck Tan NC, Kleinmeyer J, Rehrmann J, Tevault D, Reneker D, Sendijarevic I, McHugh A. Army Research Laboratory. Aberdeen Proving Ground, MD 210055066
[11] Shin YM, Hohman MM, Brenner MP, Rutledge GC. Polymer. 2001; 42: 9955-9967.
[12] Deitzel JM, Kleinmeyer J, Harris D, Beck Tan NC. Polymer. 2001; 42: 261-272.
[13] Yarin AL, Koombhongse S, Reneker DH. J Appl Phys. 2001; 89 (5): 3018-3026.
[14] Eda G, Liu J, Shivkumar S. Mater Lett. 2007; 61: 1451-1455.
[15] Burger C, Hsiao BS, Chu B. Annu Rev Mater Res. 2006; 36: 333-368.
[16] Shin YM, Hohman MM, Brenner MP, Rutledge GC. Appl Phys Lett. 2001; 78: 1149-1151.
[17] Doshi J, Reneker DH. J Electrostat. 1995; 35: 151-160.
[18] Bucko CJ, Chen LC, Shen Y, Martin DC. Polymer. 1999; 40: 7397-7407.
[19] Shenoy SL, Bates WD, Frisch HL, Wnek GE. Polymer. 2005; 46: 3372-3384.
[20] Kameoka J, Orth R, Yang Y, Czaplewski D, Mathers R, Coates G, Craighead HG. Nanotechnology. 2003; 14: 1124-1129.
[21] Zong X, Kim K, Fang D, Ran S, Hsiao BS, Chu B. Polymer. 2002; 43: 4403-4412.
[22] Tungprapa S, Puangparn T, Weerasombut M, Jangchud I, Fakum P, Semongkhol S, Meechaisue C, Supaphol P. Cellulose. 2007; 14: 563-575.
[23] Son WK, Youk JH, Lee TS, Park WH. Polymer 2004; 45: 2959-2966.
[24] Barton AFM. Handbook of Solubility Parameters and Other Cohesion Parameters, 2nd edition. CRC Press 1991.
[25] Pattamaprom C, Hongrojjanawiwat W, Koombhongse P, Supaphol P, Jarusuwannapoo T, Rangkupan R. Macromol Mater Eng. 2006; 291: 840-847.
[26] Megelski S, Stephens JS, Chase DB, Rabolt JF. Macromolecules. 2002; 35: 8456-8466.
[27] Fong H, Chun I, Reneker DH. Polymer. 1999; 40: 4585-4592.
[28] Mit-uppatham C, Nithitanakul M, Supaphol P. Macromol Chem Physic. 2004; 205: 2327-2338.
[29] Jarusuwannapoom T, Hongrojjanawiwat W, Jitjaicham S, Wannatong L, Nithitanakul M, Pattamaprom C, Koombhongse P, Rangkupan R, Supaphol P. Euro Polym J. 2005; 41: 409-421.

[30] Demir MM, Yilgor I, Yilgor E, Erman B. Polymer. 2002; 43: 3303-3309.
[31] Choi JS, Lee SW, Jeong L, Bae SH, Min BC, Youk JH, Park WH. Int J Biol Macromol. 2004; 34(4): 249-256.
[32] Lee JS, Choi KH, Ghim HD, Kim SS, Chun DH, Kim HY, Lyoo WS. J Appl Polym Sci. 2004; 93: 1638-1646.
[33] Pawlowski KJ, Belvin HL, Raney DL, Su J, Harrison JS, Siochi EJ. Polymer. 2003; 44: 1309-1314.
[34] Tong HW, Wang M. Biomed Mater. 2010; 5: 1-15.
[35] Catalani LH, Collins G, Jaffe M. Macromolecules. 2007; 40: 1693-1697.
[36] Baker SC, Atkin N, Gunning PA, Granville N, Wilson K, Wilson D, Southgate J. Biomaterials. 2006; 27: 3136-3146.
[37] Fennessey SF, Farris RJ. Polymer. 2004; 45: 4217-4225.
[38] Katti DS, Robinson KW, Frank KK, Cato TL. J Biomed Mater Res B. 2004; 70B: 286-296.
[39] Kidoaki S, Kwon IK, Matsuda T. Biomaterials. 2005; 26: 37-46.
[40] Li Q, Yang Y, Jia Z, Guan Z. High Voltage Eng. 2007; 33: 186-189.
[41] Lyons J, Li C, Ko F. Polymer. 2004; 45: 7597-7603.
[42] Mo XM, Xu CY, Kotaki M, Ramakrishna S. Biomaterials. 2004; 25: 1883-1890.
[43] Vassalli JT. University of Missouri. 2008; 10-17
[44] Rutledge GC, Li Y, Fridrikh S, Warner SB, Kalayci VE, Patra P. National Textile Center, Annual Report (M98-D01). 2000; 1-10.
[45] Chen ZG, Wei B, Mo XM, Cui FZ. J Polym Sci Pol Phys. 2009; 47: 1949-1955.
[46] Yuan X, Zhang Y, Dong C, Sheng J. Polym Int. 2004; 53(11): 1704-1710.
[47] Sautter BP. University of Illinois at Chicago. 2005; 1-27.
[48] Casper CL, Stephens JS, Tassi NG, Chase DB, Rabolt JF. Macromolecules. 2004; 37: 573-578.
[49] Li D, Xia Y. Nano Lett. 2004; 4: 933-938.
[50] Li D, Ouyang G, McCann JT, Xia Y. Nano Lett. 2005; 5(5): 913-916.
[51] Li D, Wang Y, Xia Y. Nano Lett. 2003; 3(8): 1167-1171.
[52] Chang J, Dommer M, Chang C, Lin L. Nano Energy. 2012; 1(3): 356-371.
[53] Ding B, Kimura E, Sato T, Fujita S, Shiratori S. Polymer. 2004; 45: 1895-1902.
[54] Liu HQ, Hsieh YL. J Polym Sci Pol Phys. 2002; 40(18): 2119-2129.
[55] Agarwal S, Wendorff JH, Greiner A. Polymer. 2008; 49: 5603-5621.
[56] Langer R, Vacanti JP. Science. 1993; 260: 920-926.
[57] Behonick DJ, Werb Z. Mech Dev 2003; 120: 1327-1336.
[58] Li WJ, Laurencin CT, Caterson EJ, Tuan RS, Ko FK. J Biomed Mater Res. 2002; 60(4): 613-621.
[59] Smith LA, Ma PX. Colloid Surface B. 2004; 39: 125-131.
[60] Hutmacher DW. Biomaterials.2000; 21: 2529-2543.
[61] Sharma B, Elisseeff JH. Ann Biomed Eng; 2004; 32(1): 148-159.
[62] Rosso F, Marino G, Giordano A, Barbarisi M, Parmeggiani D, Barbarisi A. J Cell Physiol. 2005; 203(3): 465-470.
[63] Friess W. Eur J Pharm Biopharm. 1998; 45: 113-136.
[64] Bhardwaj N, Kundu SC. Biotechnol Adv. 2010; 28: 325-347.
[65] Pavlov MP, Mano JF, Neves NM, Reis RL. Macromol Biosci. 2004; 4: 776-784.

[66] Almany L, Seliktar D. Biomaterials. 2005; 26: 2467-2477.
[67] Wayne JS, Mcdowell CL, Shields KJ, Tuan RS. Tissue Eng. 2005; 11: 953-963.
[68] Yoo HS, Lee EA, Yoon JJ, Park TG. Biomaterials. 2005; 26: 1925-1933.
[69] Rho KS, Jeong L, Lee G, Seo BM, Park YJ, Hong SD, Roh S, Cho JJ, Park WH, Min BM. Biomaterials. 2006; 27: 1452-1461.
[70] Fertala A, Han WB, Ko FK. J Biomed Mater Res. 2001; 57: 48-58.
[71] Venugopal J, Ramakrishna S. Tissue Eng. 2005; 11: 847-854.
[72] Yoshimoto H, Shin YM, Terai H, Vacanti JP. Biomaterials. 2003; 24: 2077-2082.
[73] Chen JL, Chu B, Hsiao BS. J Biomed Mater Res. 2006; 79A: 307-317.
[74] Huang L, McMillan RA, Apkarian RP, Pourdeyhimi B, Conticello VP, Chaikof EL. Macromolecules. 2000; 33: 2989-2997.
[75] Nagapudi K, Brinkman WT, Leisen JE, Huang L, McMillan RA, Apkarian RP, Conticello VP, Chaikof EL. Macromolecules. 2002; 35: 1730-1737.
[76] Xu CY, Inai R, Kotaki M, Ramakrishna S. Biomaterials. 2004; 25: 877-886.
[77] Zong X, Ran S, Fang D, Hsiao BS, Chu B. Polymer. 2003; 44: 4959-4967.
[78] Zong XH, Bien H, Chung CY, Yin LH, Fang DF, Hsiao BS, Chu B, Entcheva E. Biomaterials. 2005; 26: 5330-5338.
[79] Yang F, Murugan R, Ramakrishna S, Wang X, Ma YX, Wang S. Biomaterials. 2004; 25: 1891-1900.
[80] Yang F, Xu CY, Kotaki M, Wang S, Ramakrishna S. J Biomat Sci-Polym E. 2004; 15: 1483-1497.

CHAPTER 2

Tuning Size Scale and Crystallinity of Poly(ε-Caprolactone) Electrospun Fibers via Solvent Permittivity

2.1 INTRODUCTION

In the previous chapter it has been reported as the scaling of fiber diameter to reach the desired morphology is dependent upon the synergistic effect of a large number of variables relating to polymer solution properties and process parameters, which ultimately control the final fiber characteristics. It has been demonstrated that fibers without beads may be electrospun by spinning within a certain concentration range in order to reduce surface tension [1], and that thinner fibers may be obtained from a polymer solution with a higher net charge density [2]. Several authors have recently noted that solution properties are the main factor which influences the transformation of the polymer solution into ultrafine fibers [3]. However, optimal materials and process parameters cannot be specified without a thorough knowledge of the chemical and physical properties of polymeric solutions, which influence the formation of the charged polymer jet during electrospinning. Some authors have recently discussed the influence of solvent features (e.g., volatility) on fiber surface morphology and fiber properties at the nanoscale [4]. Other studies have indicated the contribution of solvent boiling point in determining the final size of electrospun fibers [5] and co-solvent effects on the diameter and morphology of PVC fibers electrospun in tetrahydrofuran (THF)/dimethylformamide (DMF) mixtures. The effect of co-solvent has also been studied. A reduction in average fiber diameter was observed as the amount of DMF in a THF/DMF mixture increased, indicating the importance of solvent polarity in electrospinning [6]. All these studies show the real difficulty which exists in attempting to define a correlation between microscopic properties and macroscopic morphological features.

In this chapter, poly(ε-caprolactone) (PCL) electrospun membranes have been prepared using solvent systems of differing polarity. The objectives were to identify those solvent properties (e.g., permittivity, volatility and thermodynamic affinity with the polymer) which most affected fiber morphology and physical properties, as well as biological response of human Mesenchymal Stem Cells (hMSC)

2.2 EXPERIMENTAL SECTION

2.2.1 Materials

PCL pellets (M_w= 65 kDa) were purchased from Sigma-Aldrich (Italy). The solvents 1,1,1,3,3,3-hexafluoro-2-propanol (HFP), 2,2,2-trifluorethanol (TFE), (Fluka, Italy), chloroform ($CHCl_3$) and tetrahydrofuran (THF) (J.T. Baker, Italy) were used as received without further purification. PCL was dissolved separately in each solvent by magnetic stirring at 28°C overnight to attain a clear solution ready for electrospinning. Two different PCL/solvent ratios were used, namely lower (LC) and higher (HC), which were 10 and 20% w/v, respectively.

2.2.2 Electrospinning Setup

The electrospinning apparatus used in this work was comprised of three components: (i) a syringe pump system (Genie Plus k600, Kent Scientific), to control the mass flow of the solution as the process proceeded; (ii) two metal electrodes; (iii) a single-polarity high-voltage power supply (Gamma High Voltage Research, mod. ES30), capable of generating DC voltage in the range 0–30 kV, connected to (ii). The proposed apparatus was further enclosed in a Plexiglass box to insulate the system from external fields and to restrain sudden changes of environmental conditions during the electrospinning process. The solution was placed in a 5ml syringe (BD Plastipack, Italy), fixed on the pump system and joined to a stainless steel needle with an inner diameter of 18 Ga, connected to the positive pole. An earthed metallic plate covered by aluminium foil was used to collect fibers, with the distance between the tip of the needle and the collector set at 14 cm. The process was carried out in a vertical configuration, and a deposition time was adequate for the required thickness of the fibers to be deposited on the grid. The electrospun membranes investigated in this study were obtained by applying a high voltage of 13 kV at four different feed rates (i.e., 0.1, 0.5, 1 and 3ml/h).

2.2.3 Morphology and Image Analysis

A qualitative evaluation of the fiber morphology of the electrospun PCL membranes was performed using field-emission scanning electron microscopy (FESEM, QUANTA200, FEI, The Netherlands) after sputter-coating with gold-palladium. Samples were preliminarily kept under a fume hood in order to remove residual solvent traces, then directly located on metal stubs to preserve the fiber morphology. The accelerating voltage ranged between 5 and 20 kV. Moreover, on selected SEM images, the average diameter was determined by measuring ca. 30 representative fibers using freeware image analysis software (NIH Image J 1.37).

2.2.4 Thermodynamic Approach

To examine the ability of solvents to dissolve PCL, a procedure was adapted from earlier studies [7], based on estimating the χ parameter for different polymer/solvent pairings. The χ parameter shows the degree of solvent/polymer affinity; χ less than 0.5 indicates a favorable solvent interaction, whilst χ greater than 0.5 indicates that the solvent is unable to dissolve the polymer due to unfavorable polymer/solvent interactions. Assuming low polymer concentrations, χ may be expressed algebraically as

$$\chi = \frac{M_s}{RT\rho_s}(\delta_s - \delta_p)^2$$

where subscripts s and p denote solvent and polymer, respectively, M_S is the solvent molecular weight, R is the universal gas constant and δ is the solubility coefficient of the pure components. Some basic properties of the solvents (boiling point, density and solubility parameters) must be considered at room temperature, as summarized in Table 2.2 [7, 8]. χ values for each solvent were compared using that for PCL, reported elsewhere [9].

Table 2.1: Summary of solvent properties as a function of molecular polarity.

Solvent	**Chemical Formula**	**Polarity**	**Relative dielectric permittivity**
$CHCl_3$	$CHCl_3$	low	4.8 [10]
THF	C_4H_8O		7.5 [10]
HFP	$C_3H_2OF_6$	high	17.8 [11]
TFE	$C_2H_3OF_3$		27.0 [10]

Table 2.2: Solvent chemical parameters and thermodynamic affinity (χ parameter) of different PCL/solvents solutions.

Solvent	**Density ρ (g cm^{-3})**	**Boiling point T_b (°C)**	**δ (MPa$^{1/2}$)**	**χ**
$CHCl_3$	1.47	61.20	19.0 [7]	0.047
THF	0.87	66	19.1 [7]	0.038
HFP	1.60	59	20.0 [8]	0.002
TFE	1.38	73.6	22.5 [8]	0.155

2.2.5 Raman and IR Spectroscopy

Raman and IR spectroscopy were performed in collaboration with Dr. Paola Taddei from the Department of Biochemistry ‘‘G. Moruzzi’’, Alma Mater Studiorum, University of Bologna.

Raman spectra were recorded on a Bruker MultiRam FT-Raman spectrometer equipped with a cooled Ge-diode detector. The excitation source was a Nd^{3+}-YAG laser (1064 nm) in backscattering (180°) configuration. The focused laser beam diameter was about 100µm, the spectral resolution 4 cm^{-1}, and the laser power at the sample about 60 mW. At least three spectra were recorded on different points of each sample and averaged.

IR spectra were recorded on a Nicolet 5700 Fourier-transform infrared (FT-IR) spectrometer, equipped with a Smart Orbit diamond attenuated total reflectance (ATR) accessory and a deuterated triglycine sulfate (DGTS) detector. The spectral resolution was 4 cm^{-1} and the number of scans was 64 for each spectrum. The ATR area was 2 mm in diameter and the IR radiation penetration was about 2 µm. At least ten spectra were recorded at different points of each sample and averaged.

2.2.6 Differential Scanning Calorimetry (DSC)

DSC analysis was performed in collaboration with Dr. Paola Taddei from the Department of Biochemistry ‘‘G. Moruzzi’’, Alma Mater Studiorum, University of Bologna.

DSC measurements were made with a Mettler TA-STAR, DSC 821^e calorimeter from 25 to 120°C. The samples were heated at 2°C/min (1st run), then cooled at the same rate down to 25°C (2nd run) and finally reheated at 2°C/min (3rd run). For a crystalline polymer, the 1st run shows the melting peak of the polymer. From this, the crystallinity degree (*Xc %*) of the polymer was calculated according to:

$$X_c\ \% = 100(\Delta H_{m1}/\Delta H_m^\circ)$$

where ΔH_{m1} is the enthalpy of melting measured in the 1st run and ΔH°_m the enthalpy of melting of totally crystalline PCL (ΔH°_m = 139 J/g) [12]. The crystallization capability of the polymer (once melted in the 1st run) was evaluated as crystallizable fraction (*CF %*), calculated according to:

$$CF\ \% = 100(\Delta H_c/\Delta H_{m1})$$

where ΔH_c is the enthalpy of crystallization measured in the 2nd run.

2.2.7 Cell Culture

Biological assays were performed using a bone-marrow-derived human mesenchymal stem cell line (hMSC, PT-2501) obtained from Lonza. hMSC were cultured in a 75 cm^2 cell culture flask in Eagle’s alpha minimum essential medium (α-MEM) supplemented with 10% fetal bovine serum, antibiotic solution (streptomycin 100µg/ml and penicillin 100U/ml, Sigma Chem. Co.) and $2x10^{-3}$ M L-glutamin. The cells were incubated at 37°C in a humidified atmosphere with 5% CO_2 and 95% air. 4-6 passages of hMSC were used for all experimental procedures.

2.2.8 Cell Attachment

The cell adhesion of hMSC onto electrospun fiber mats of PCL scaffolds with both micro- and nanofibers was evaluated using the vibrant cell adhesion assay kit (MolecularProbes). hMSC, cultured in a 75 cm^2 cell culture flask, were washed with phosphate-buffered saline (PBS) and incubated with calcein AM stock solution to a final concentration of $5x10^{-6}$ M in serum-free medium for 30 min. After incubation, the cells were washed with PBS, trypsinized and the cell pellet was collected and diluted with culture medium to obtain the requisite cell concentration. hMSC were seeded onto electrospun fibers mats of PCL scaffolds and incubated for 4 h and 24 h. The fluorescence was quantified using a fluorescein filter set with a Wallac Victor3 1420 spectrophotometer (Perkin-Elmer, Boston, MA). The percentage cell adhesion was obtained by dividing the corrected (background subtracted) fluorescence of adherent cells by the total corrected fluorescence of control cells and multiplying by 100%. Conventional polystyrene 24 well culture plates were used as a control.

2.2.9 Cell Morphology

To observe cell morphology, hMSC were seeded onto electrospun fibers mats of PCL scaffolds at $1x10^4$ and grown for 24 h. At the end of the incubation time, non-attached cells were removed by rinsing three times with PBS. Cell fixation was carried out in 4% formaldehyde in 0.1 M phosphate buffer solution (pH = 7.3), washed with PBS and then dehydrated in graded series of ethanol (25–100%) and air dried. The samples without sputter-coating were examined by FESEM under low-vacuum conditions (SEM, Quanta- FEG 200, FEI, Netherlands).

2.2.10 Cell Viability

Cell viability of hMSC ($1x10^4$ cells) plated in triplicate onto electrospun fibers mats of PCL scaffolds was checked by the MTT assay for 2, 4 and 6 d of culture. This assay is based on the ability of mitochondrial dehydrogenases of living cells to oxidize a tetrazolium salt (3-4,5-dimethylthiazolyl-2-y-2,5-diphenyltetrazolium bromide) to an insoluble blue formazan product. The concentration of the blue formazan product is directly proportional to the number of metabolically active cells. The hMSCs seeded onto electrospun fiber mats of PCL scaffolds at the prescribed time were washed with PBS and incubated with fresh cultured medium containing 0.5mg/ml of MTT for 4 h at 37°C in the dark. The supernatant liquid was then removed and dimethylsulfoxide (DMSO) was added to each well. After 60 min of slow shaking, the absorbance was quantified by spectrophotometry at 570 nm with a plate reader. The culture medium was renewed every day.

2.2.11 Statistical Analysis

All numerical data are presented as mean ± standard deviation. All results were subjected to statistical evaluation using an unpaired Student's t-test to determine significant differences between groups. The significance level was set at $p<0.05$.

2.3 RESULTS

2.3.1. Morphology and Image Analysis

Different PCL fiber meshes from solutions with increasing solvent permittivity (i.e., $CHCl_3$<THF<HFP<TFE, (see Table 2.1) [10, 11], were investigated. Figure 2.1 shows the effect of the imposed flow rate (0.1-0.5-1-3ml/h) on the final diameter of the fibers. In the case of PCL/$CHCl_3$ solution, a fine weave of fibers was shown with an increasing fiber diameter as the flow rate increased (Figure 1A). A further increase in fiber diameter could also be detected as the polymer concentration switched from LC to HC configuration.

In the case of PCL/THF solution, a different morphology of fibers was shown to be attributable to reduced control of fiber formation during the electrospinning process. The higher permittivity of THF solvent determines a higher sensitivity of the polymer solution to the electric field, so amplifying the occurrence of jet instability phenomena. Consequently, fibers with several beads were obtained independently on the imposed flow rate condition. The use of higher concentrations (THF_{HC}) positively affected the cohesive forces among polymer chains, limiting the occurrence of instability phenomena, so that fine fibers meshes could be reached for higher values of flow rates. In the case of PCL/HFP and PCL/TFE solution, thinner fibers with an average fiber diameter on the nanometric scale were obtained. The higher permittivity values of HFP and TFE solution ensured stronger polar interactions among the polymer chains mediated by solvent molecules, but increased instability phenomena at lower flow rates, promoting the presence of several defects with uncontrolled morphology. Figures 2.1 B and C show a quantitative estimation of fiber size calculated by image analysis on selected SEM images. A marked increase in the fiber diameter was detected as the flow rate rose from 0.1 to 3ml/h. All trends in fiber size were substantially in agreement with SEM indications. A mean fiber diameter increasing from 1.32 ± 0.54 to 8.56 ± 0.73 μm was observed as the flow rate increased. Although the calculation of mean fiber diameter as a function of flow rate has been performed by neglecting the presence of beads along the fibers, such defects often affect the measurements.

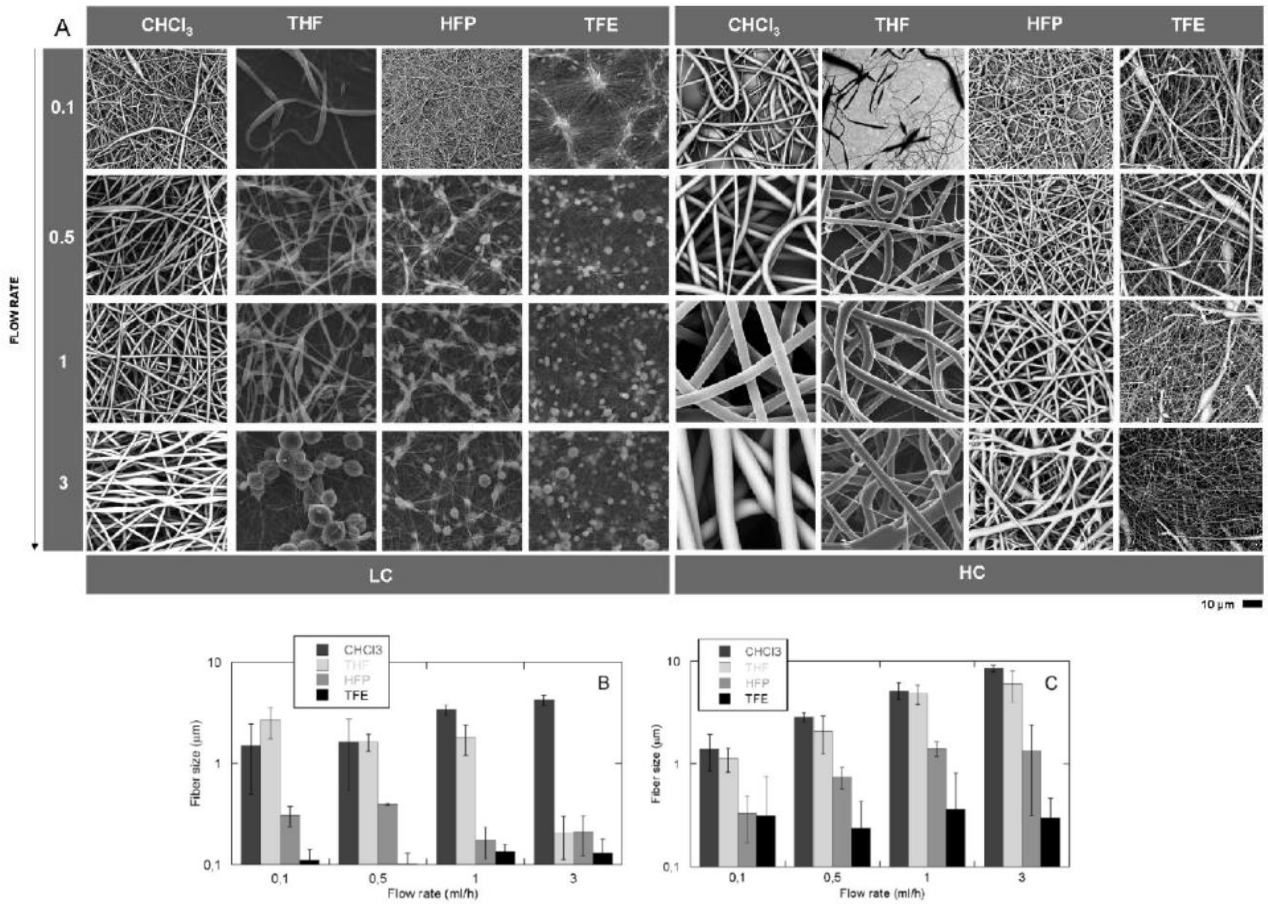

Figure 2.1: Evaluation of PCL fiber morphology from polymer solutions with different permittivity of solvent: A) SEM images of membranes using different polymer concentrations (i.e., LC, HC) and flow rates (i.e., 0.1, 0.5, 1, 3 ml/h); Estimation of fiber size as a function of flow rate via image of the scaffolds obtained from polymer solutions at low (B) and high (C) concentrations.

The presence of beads appeared more evident in the case of polymer solutions with lower densities, ρ (e.g., THF) and higher χ (e.g., TFE) (Table 2.2) where efficient interactions among polymer chains mediated by solvents molecules are more limited.

In response to this, a more accurate investigation (Figure 2.2) was focused on the comparison of samples at the same flow rate value, i.e., 0.5 ml/h, which was evaluated as optimal to minimize fiber defects. In Figure 2.2 B, a comparative analysis of PCL fiber morphology as a function of the solvent permittivity is reported for LC and HC samples, respectively. SEM images supported by image analysis showed that the mean fiber diameter decreased from 1.63 ± 1.09 to 0.10 ± 0.03 µm as the dielectric permittivity increased. A concurrent increase in fiber size from 0.24 ± 0.19 to 2.86 ± 0.31 µm was seen moving from lower (LC) to higher (HC) polymer concentration systems. The effect of solvent permittivity on fiber size was still compromised by the presence of fiber defects, which preferentially occurred in the case of LC solutions, due to the tendency of beads to form bridges between adjacent thin fibers.

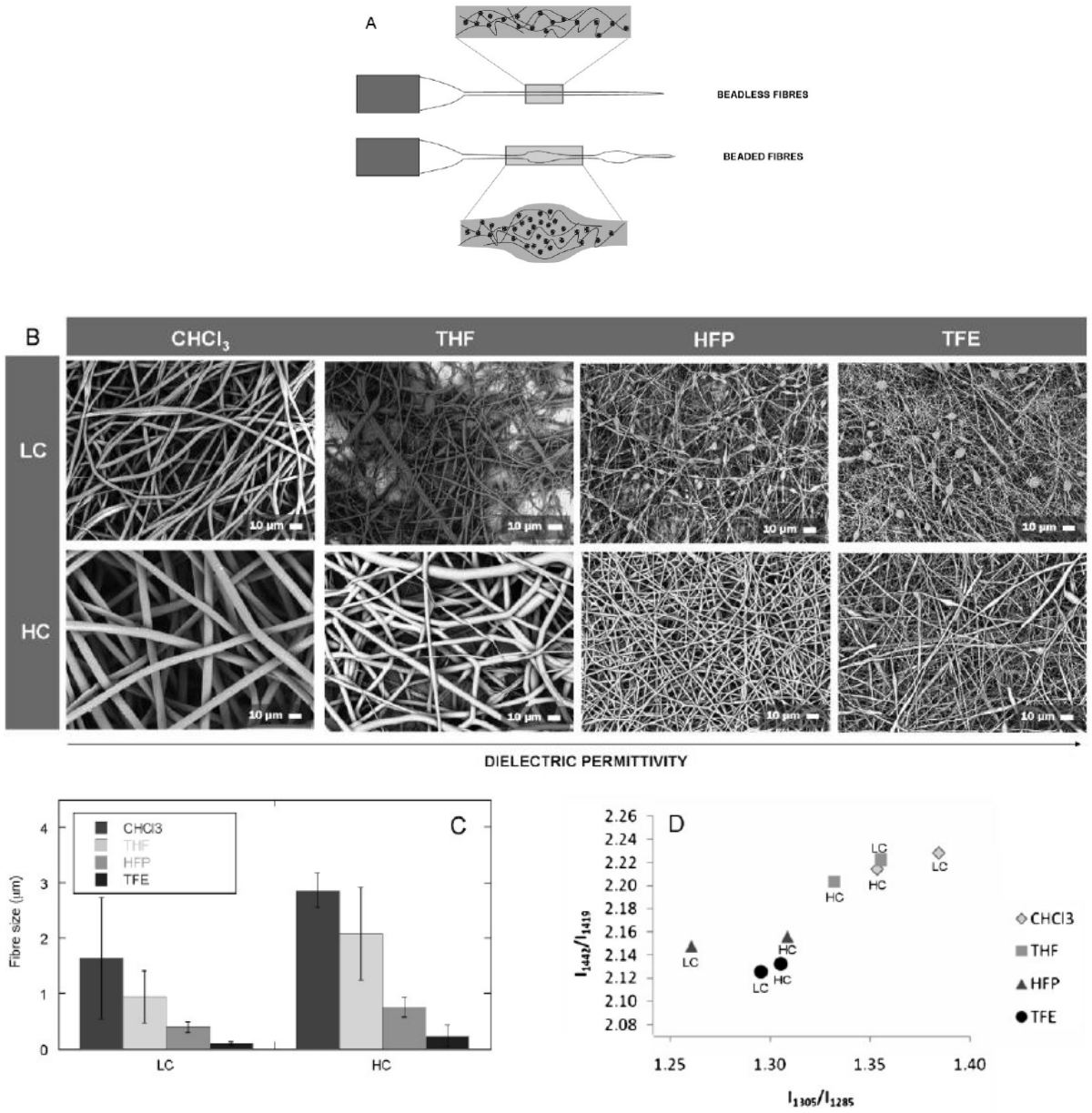

Figure 2.2: Beaded vs. beadless PCL fibers: A) Scheme of microscopic polymer and solvent combination; B) Effect of solution permittivity and polymer concentration on the average fiber diameter of PCL electrospun membranes from SEM images; C) Quantitative estimation of fiber diameters by image analysis; D) Fiber crystallinity map from the evaluation of the I_{1442}/I_{1419} vs. I_{1305}/I_{1285} Raman intensity ratios.

This effect is also apparent in the fiber size distribution of PCL fibers in Figures 2.3 (A–D), which show a comparison of selected samples (one for each solvent) with optimal fiber morphology. A wider distribution of fiber sizes was detected in THF and TFE solutions, i.e., in the solvents with the lowest density and highest χ values, respectively. There is also a clear reduction in mean fiber size in membranes spun from highly polar solvents (HFP, TFE), which were in the micrometer range, compared to those spun from solvents of low polarity ($CHCl_3$, THF), where fiber sizes were of the order of a few hundred nanometers.

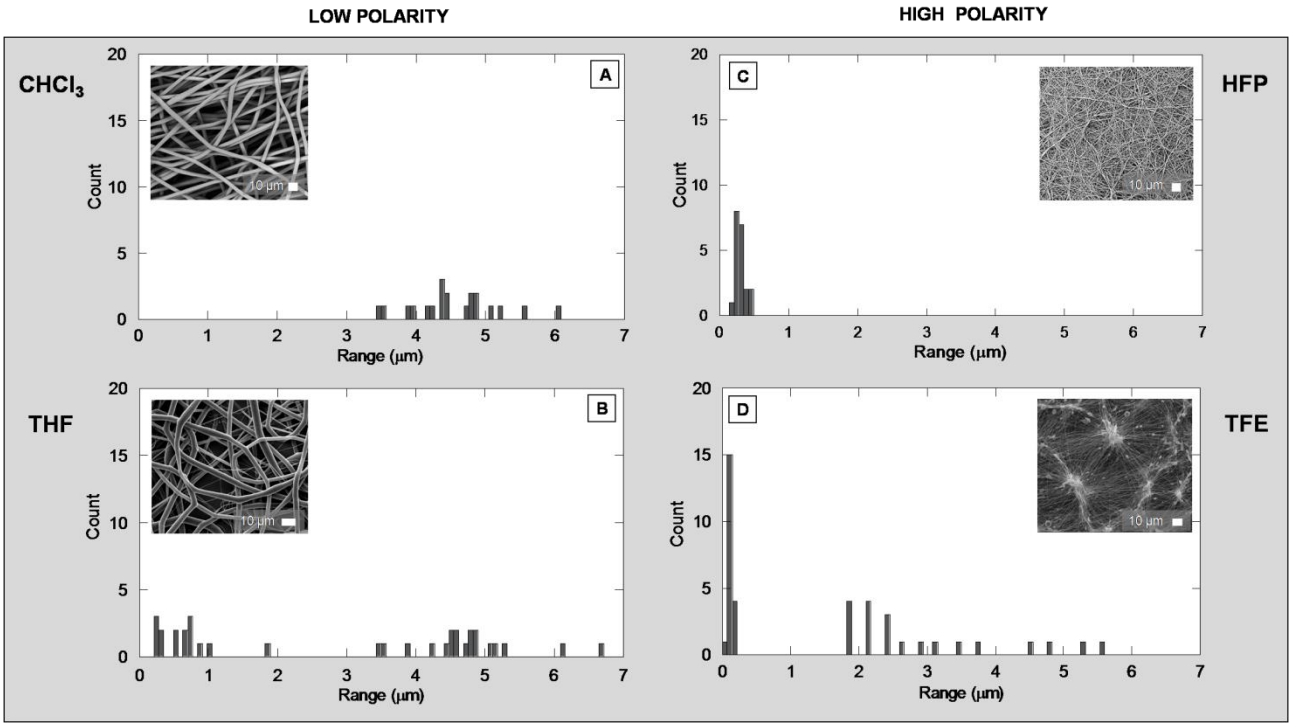

Figure 2.3: Fiber diameter distribution via image analysis of PCL membranes from low polarity, A) chloroform and B) THF, and highly polar solvents, C) HFP and D) TFE.

2.3.2 Vibrational and Thermal Analyses

The vibrational spectra of PCL have been widely investigated and various authors have tried to identify marker bands of PCL morphology and correlate their intensity with the crystallinity of the polymer. In Figure 2.2 D, the I_{1442}/I_{1419} vs. I_{1305}/I_{1285} Raman intensity ratio was reported to indicate the crystallinity of PCL fibers obtained from different polymer solutions. The samples from fluorinated solvents (TFE, HFP) showed the lowest I_{1305}/I_{1285} and I_{1442}/I_{1419} values, indicating the highest crystallinity. Samples from low polarity solvents ($CHCl_3$, THF) had the highest I_{1305}/I_{1285} and I_{1442}/I_{1419} values and were the least crystalline. These data also suggest an influence of polymer concentration on the fiber crystallinity as a function of the solvent polarity. An increase in crystallinity at increasing PCL concentration was detected for samples obtained from non-fluorinated samples, whereas an opposite effect was generally recognized for the samples obtained from fluorinated solvents. A more detailed investigation of fiber crystallinity was performed through the comparison of PCL vibrational spectra related to fibers with different fiber size scales of micrometric and nanometric size, respectively. Figures 2.4 and 2.5 show the most significant Raman and IR spectra of the samples analyzed. The trend of the Raman spectra clearly indicated that the fibers obtained from fluorinated HFP and TFE solvents were more crystalline than those obtained from the other solvents. For the former samples, the bands assignable to crystalline PCL were observable with higher intensities than those of the latter. In the spectra of the fibers obtained

from HFP and TFE, the component at 1285 cm^{-1} appeared increased in intensity with respect to the 1305 cm^{-1} band. Since the component at lower wavenumber is attributable to the CH_2 wagging mode of crystalline PCL [13] while the other is due to the same mode in both amorphous and crystalline PCL [13], this spectral trend indicates a higher crystalline content in the polymer fibers obtained from fluorinated solvents. The same behavior was observed for the component at 1419cm^{-1} (CH_2 bending of crystalline PCL) [13], which resulted in increasing the intensity with respect to the 1442 cm^{-1} band (CH_2 bending of crystalline and amorphous PCL) [13]. The I_{1305}/I_{1285} intensity ratio, which had already proved a valid marker of PCL crystallinity, was calculated [14, 15]. In the skeletal stretching region, the band attributable to crystalline PCL at 1110 cm^{-1} appeared intensified with respect to the component at 1095 cm^{-1} due to amorphous PCL [13] and more defined components at 1043 and 1035 cm^{-1} were observable. The 915 cm^{-1} band ($\nu_{C\text{-}COO}$ mode in crystalline PCL) [13] was also stronger.

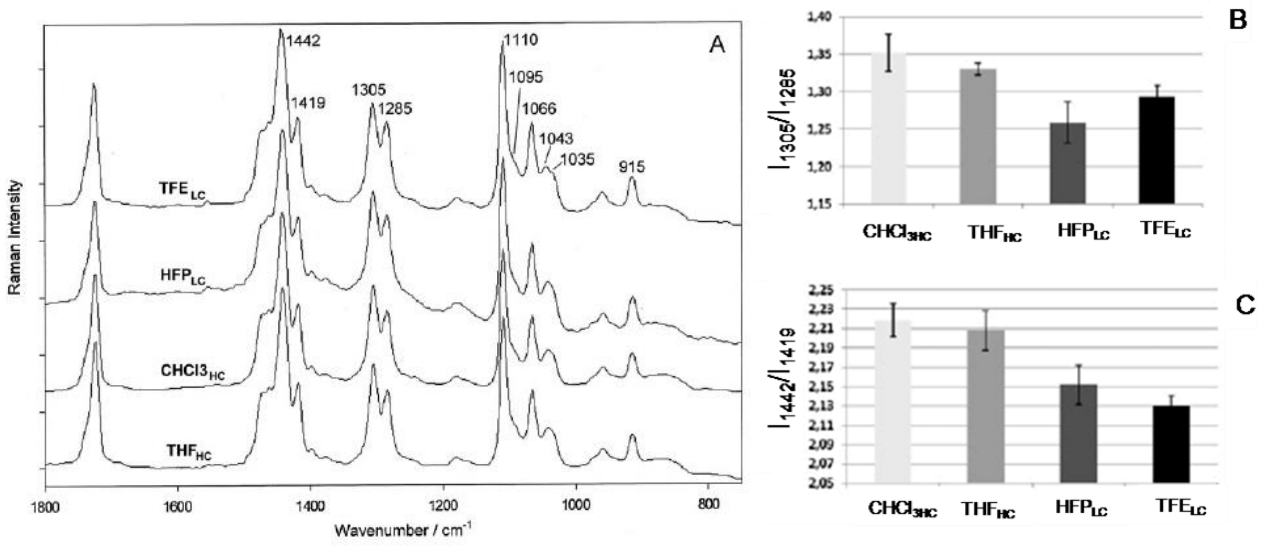

Figure 2.4: Raman spectroscopy of PCL micro- and nanofibers: A) Average Raman spectra; B) I_{1305}/I_{1285}; C) I_{1442}/I_{1419} intensity ratio obtained from $CHCl_{3HC}$, THF_{HC}, HFP_{LC} and TFE_{LC} solutions.

IR analysis generally confirmed the Raman data, although some discrepancies were observed between the results obtained by the two techniques. They can be explained by the fact that the two techniques are sensitive to different sampling areas. While the Raman spectrum gives information on the sample bulk, the IR spectrum recorded by the ATR technique is representative of the sample to a depth of 2 μm below the surface. The IR spectra reported in Figure 2.5 confirmed a general higher crystallinity of the samples obtained from fluorinated solvents. The 1100-1300 cm^{-1} spectral region (assignable to coupled modes variously associated with C-C-H and O-C-H bending vibrations, and C-C and C-O stretching vibrations) [16, 17] appeared to be the most sensitive to

morphology differences. Moving from non fluorinated to fluorinated solvents, the main band shifts from 1161 to 1166 cm^{-1}, that is, to wavenumber values closer to crystalline PCL [17]. This band (mainly due to amorphous PCL) [17] also progressively decreased in intensity with respect to the higher wavenumber component at 1184cm^{-1}, attributable to crystalline PCL [26]. The fibers obtained from fluorinated solvents showed higher intensity bands at 1293 and 1237 cm^{-1}, in agreement with literature reports [17]. In the C=O stretching region, the spectra of the fibers obtained from fluorinated solvents showed a less broad profile in the lower wavenumber region, with no significant difference in the position of the band maximum being observed. For a quantitative evaluation, the area of the band at 1293 cm^{-1} (A_{1293}) was calculated together with the I_{1160}/I_{1184} intensity ratio. The trend for these spectroscopic markers is shown in Figures 2.5 (B, C). The A_{1293} value, an established marker of PCL crystallinity [17, 18], was on average lower for the samples obtained from non fluorinated solvents. The fibers obtained from non fluorinated solvents also showed lower average I_{1160}/I_{1184} values than those obtained from fluorinated solvents, confirming the qualitative data reported above. It can be seen that, for samples obtained from $CHCl_3$ and THF, an increase in polymer concentration resulted in an increase in A_{1293} (i.e., in crystallinity), while Raman data showed that the opposite effect was observed for fibers obtained from TFE (Figure 2.2 D).

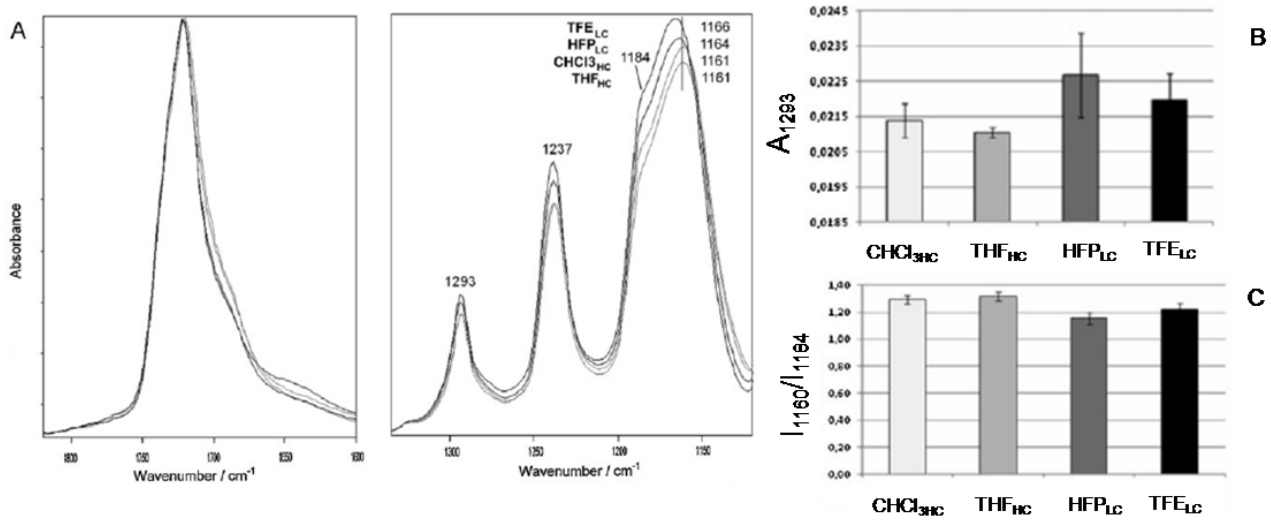

Figure 2.5: IR spectroscopy of PCL micro and nanofibers. A) Average IR spectra, B) A_{1293} band area and C) I_{1160}/I_{1184} intensity ratio obtained from $CHCl_{3HC}$, THF_{HC}, HFP_{LC} and TFE_{LC} solutions.

The spectroscopic data were confirmed by quantitative DSC studies on micro and nanofibers from HFP_{LC} and $CHCl_{3HC}$ solutions, respectively (Table 2.3). Fibers obtained from HFP_{LC} solutions showed a multi-component melting peak with maxima at about 55 and 62°C, indicating crystallites

of differing sizes. The fibers obtained from $CHCl_{3HC}$ showed a single melting peak at 54-56°C. After the second run, the latter sample showed a relatively broad crystallization peak at 39 °C, while fibers obtained from HFP_{LC} solution showed significantly higher crystallization temperatures (42-43°C) and significantly sharper peaks. They also showed the lowest CF % values, indicating that not all the molten crystallites in the 1st run were able to crystallize. In the 3rd run, as in the 2nd run, fibers from $CHCl_{3HC}$ solution showed a broad melting peak (at ~55-60°C), while fibers obtained from HFP showed a sharp peak at 55°C.

Table 2.3: Melting temperature (T_m), crystallinity degree (X_c), crystallization temperature (T_c) and crystallizable fraction (CF) as obtained from the DSC thermograms of micro- ($CHCl_{3HC}$) and nano-(HFP_{LC}) fibers.

Fiber type	T_m (°C)	X_c (%)	T_c (°C)	CF (%)
micro	56	46 ± 1	39	96 ± 1
nano	55/62	50 ± 2	43	94 ± 1

2.3.3 Biological Tests

The effect of PCL fiber size scale and crystallinity on the biocompatibility of electrospun fiber mats was investigated by hMSC adhesion and proliferation tests on micro and nanotextured PCL scaffolds with optimal fiber morphology, $CHCl_{3HC}$ and HFP_{LC}, respectively. SEM images of hMSC cultured after 4 and 24 h onto micro and nano electrospun fiber mats are reported in Figure 2.6 A. As can be clearly seen, cells contours were stretched in proximity to the fibers. hMSCs were dispersed and extended toward and along the lengths of the surface of both micro and nano-electrospun fiber mats of PCL surface structures. The spread and growth of hMSC on the membranes showed good biocompatibility, with some filopodia and higher numbers of intercellular connections maintained through the filopodia. A significant coverage and spreading of cells was preferentially detected on nanofiber scaffolds, in agreement with the quantitative adhesion assay reported in Figure 2.6 B. This shows the percentage of cells attached to PCL micro and nano electrospun fibers, calculated on the assumption of full cell attachment in the plastic control, after 4 h and 24 h of incubation. For nanofibers, after 24 h of cell culture, the percentage of adhered cells increased dramatically up to 90%. For microfiber electrospun mats, this value remained at ca. 70%, confirming the importance of the nanofiber morphology on hMSC interaction. Figure 2.6 C shows the absorbance of the MTT reagent reduction to (dark) formazan by viable cells on electrospun fiber mats of PCL. The absorbance data indicated that higher cell populations were formed over the same culture time on nanofiber mats compared to microfiber mats. All the data suggested good affinity and biocompatibility of the electrospun fibers mats of PCL for hMSC (p<0.05).

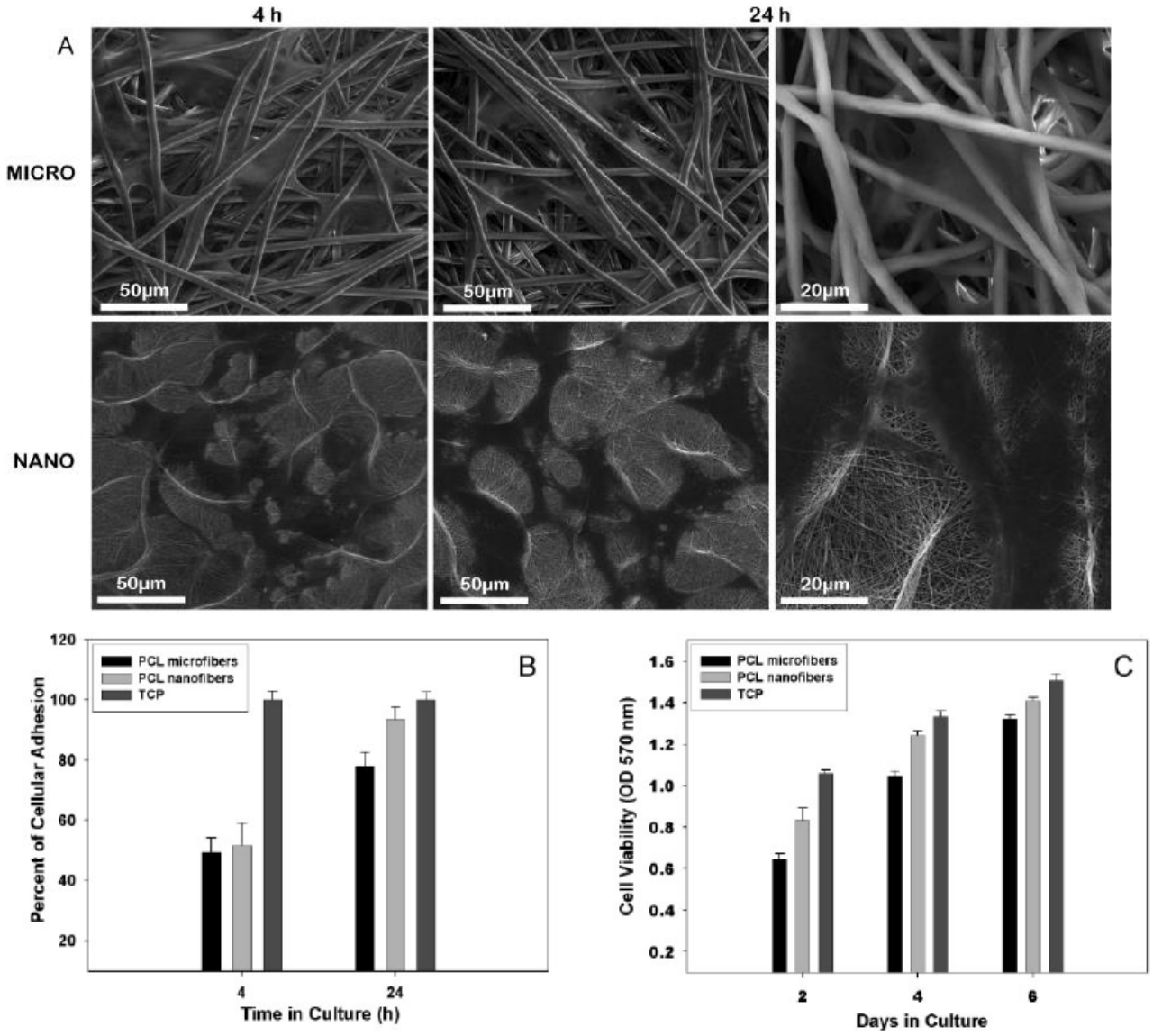

Figure 2.6: Effect of micro and nanostructure of fibers on the biological response of hMSC: A) SEM images of adherent hMSC after 24 h; B) attachment and C) hMSC viability essays on PCL micro and nanofibers, from $CHCl_{3HC}$ and HFP_{LC} solution, respectively.

2.4 DISCUSSION

A critical interpretation of solvent microscopic properties (i.e., density, boiling point, permittivity) is crucial to the understanding of how molecular properties directly affect the electrospinning mechanism and indirectly influence some basic macroscopic solution properties, such as viscosity, surface tension and conductivity, which are themselves able to affect the mechanism of jet formation during the electrospinning processes. Several researchers have recently investigated the role of materials and process parameters on the spinnability of polymer systems by an extensive evaluation of the morphological properties of the resultant electrospun fibers [19, 20]. It has been demonstrated that an increase in polymer concentration generally produces an average increase in

fiber diameter coupled with a reduction in fiber defects (e.g., beads) [21]. Several trends observed in previous investigations [22] have been verified in this study. For example, increases in fiber diameter and bead size were apparent as feed rate increased. Polymer concentration also affected fiber size (Figures 2.1 and 2.2), as confirmed by the evident reduction in fiber size as polymer concentration decreased. Beaded PCL fibers may be more apparent in solutions with lower concentration, where the higher level of solvent molecules both reduces the incidence of chain entanglements and promotes bead formation. These examples indicate the pivotal role of solvent mediated interactions during the electrospinning process, yet only a few investigations have to date provided an analytical study of the effects of solvent properties on the mechanism of electrospun fiber formation. In response to this, we have provided here a comparative study of PCL electrospun membranes obtained from solutions with different solvent permittivity ($CHCl_3$, THF, HFP and TFE). Quantitative image analysis on selected SEM images of identically processed PCL electrospun (Figures 2.1 and 2.2) clearly demonstrated a decrease in fiber size of up to an order of magnitude when moving from chloroform to fluorinated solvents, as the relative permittivity varies from 4.8 to 27.0 (at 25 °C). This may be directly ascribed to the relative permittivity, which is representative of the solvent polarity. Highly polar solvents, such as TFE and HFP, promote a higher net charge density in solution, producing enhanced stretching of fibers and therefore the formation of thinner fibers, as confirmed by SEM images (Figure 2.1). It is notable that, as the charges carried by the jet increased, higher elongation forces (i.e., electrostatic and Columbic forces) were produced by the electrical field forces during the jet formation, so increasing bending instability and the jet path [2]. As seen in previous studies [2], the use of polymer solutions with higher relative dielectric permittivity assures the creation of electrospun membranes with a narrower distribution of fiber diameters with an attendant reduction in bead formation (Figure 2.2). Fiber formation also involves a delicate balance of various physical parameters, such as solution density and boiling point, which may themselves influence concurrent physical phenomena including solvent evaporation and polymer phase crystallization. All these factors demand a well structured explanation, which has to take into account the interdependence among all the involved physical variables (Table 2.1). For example, low solvent density coupled with low permittivity (the THF solution case) promoted excessive chain mobility, limiting the occurrence of the chain interactions which guide the mechanism of fiber stretching. Fibers were therefore collected only with difficulty at lower flow rates and fibers (with several defects) were obtained only by imposing higher flow rates. The weak interactions among polymer chains also promoted the formation of secondary jets which erupted from the main jet during the electrospinning, explaining the wide fiber distribution observed (Figure 2.3). For chloroform and HFP solutions, higher solvent density

ensured more efficient packing of the polymer chains (the more viscous behavior of solution limiting chain sliding), thus drastically reducing the formation of beads along fibers. The high viscosity of the solution tended to discourage the breaking of the main jet into secondary jets, contributing to a more homogeneous distribution of fiber sizes. Chain mobility was also affected by polymer concentration, explaining the preferential occurrence of beads in less concentrated systems. In addition, the higher relative permittivity of HFP with respect to $CHCl_3$ significantly affected the efficiency of solvent mediated interaction among polymer chains, leading to thinner fibers at sub-micrometer scale (Figure 2.2). Finally, in the case of TFE solutions, the contribution of density and relative permittivity was also influenced by the solvent volatility and by the polymer/solvent thermodynamic affinity, expressed by the χ parameter (Table 2.2). In the case of TFE solutions, the higher boiling point prevented fast evaporation of solvent molecules which resided for a longer time, promoting the aggregation of free solvent molecules which tend to form beads during the electrospinning process. The tendency towards the partial demixing of the polymer solution due to sub-optimal thermodynamic coupling also catalyzed the formation of distributed defects along fibers. The modulation of fiber diameters as the polymer concentration changed (Figure 2.2) was also an indirect result of the variation of solution viscosity. Columbic and viscoelastic forces were also responsible for the formation of beads, supporting the thinning of the charged jet during its flight to the grounded target. Since the applied electrostatic field used to obtained PCL fibers was fixed (13 kV/14 cm), the increased viscoelastic force which characterized the more concentrated solution should prevent the jet segment stretching under the effect of the constant Coulomb force, resulting in fibers with larger diameters. This effect, coupled with the specific solvent mediated polymer macromolecular interactions due to the peculiar solvent microscopic properties (viz. permittivity) drastically affected the capability of polymer chains to fold and therefore influenced fiber crystallinity. It has been demonstrated that polar solvents with higher permittivity (i.e., TFE, HFP) in less concentrated solution (LC) promoted the formation of fibers with the lowest I_{1305}/I_{1285} and I_{1442}/I_{1419} band intensity ratios, confirming the more pronounced crystalline state of the fibers. In contrast, apolar/low polarity solvents with low permittivity (i.e., $CHCl_3$, THF) in more concentrated polymer solutions (HC) were able to form fibers with low crystallinity, confirmed by their high I_{1305}/I_{1285} and I_{1442}/I_{1419} values.

In this work, we have verified that differences in the biological response to the electrospun materials studied *in vitro* are directly ascribable to the differences in fiber size and crystallinity, which in turn arise from the dielectric properties of the polymer solution. Recent studies of non-fibrous substrates [23] report the heightened sensitivity of cell adhesion mechanisms to scaffold topography, also noting the adverse influence exerted by topological organization on proliferation,

due to the potential inhibition caused by other features of the materials (i.e., surface roughness, polymer crystallinity). In our biological study, a more drastic increase in cell attachment was detected after 24 h with nanofibers from HFP_{LC} compared to microfibers from $CHCl_{3HC}$ (Figure 2.6B). This is in complete agreement with several studies previously performed on micro and nano-structured fiber meshes, which showed a significant improvement of hMSC adhesion in the case of nanofibrous architecture [24-26]. The scaffold architecture is very important and affects cell binding (Figure 2.7). The cells binding to scaffolds with microscale architectures flatten and spread as if cultured on flat surfaces. The scaffolds with nanoscale architectures have bigger surface area for absorbing proteins and present more binding sites to cell membrane receptors. The adsorbed proteins further can change the conformations, exposing additional binding sites, expected to provide an edge over microscale architectures for tissue generation applications [27]. However, viability on nanofibers from HFP_{LC} solution did not show an equally significant rise after 2, 3 and 6 d in culture (Figure 2.6 C). This may depend upon the balance attained between two conflicting influences on cell behavior, namely the extent of fiber curvature and the degree of crystallinity. It is recognized that a high specific surface area is generally enable to be more reactive to the adhesion ligands [28].

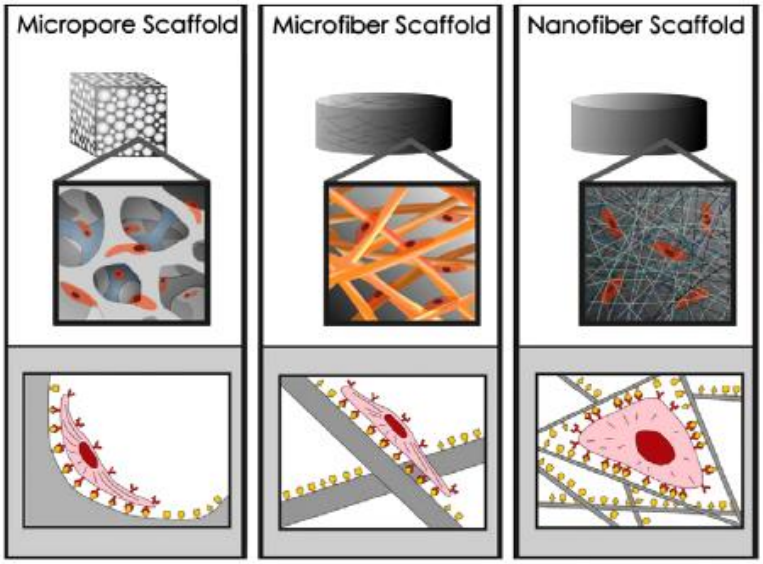

Figure 2.7: Scaffold architecture affects cell binding and spreading [27].

Other studies of poly(L-lactic acid) (PLLA) substrates indicated that cells proliferated more slowly on crystalline or smooth surfaces [29]. Our investigation here showed an evident improvement in cell adhesion ascribable to the nanoscale fiber recognition which is partially offset by the crystallinity contribution, as confirmed by proliferation data. It is therefore reasonable to conclude

that the choice of polymer solution with tailored dielectric properties allows the modulation of the influence upon the adhesion and/or proliferation kinetics of hMSC due to the effect of solvent permittivity on fiber morphology (i.e., size scale) and macromolecular assembly (i.e., crystallinity). It is also important to consider factors relating to the electrospinning process itself, which could further affect the macromolecular organization of polymer chains and therefore the final cell response. Besides, the investigation of biocompatibility provides only a preliminary indication of cell/material interaction mechanisms (adhesion and proliferation) pertaining to the early biological function of hMSCs.

2.5 CONCLUSION

The objective of this work was to examine the effect of solvent permittivity on the fiber morphology of PCL electrospun membranes for tissue engineering applications. We have presented a study oriented to predict the electrospinning mechanisms imposed by the proper selection of polymer/solvent coupling and process parameters in order to control the final morphology of membranes to be used for tissue engineering. Examination of the interplay between the various factors involved, including the dielectric constant and other solution properties (e.g., density, boiling point, solubility parameter) relating to the solvents used ($CHCl_3$, THF, HFP and TFE) indicated that the coupling of polymer and solvent components can drastically affect the final morphological appearance of electrospun fibers in terms of fiber size scale and bead formation. The results presented here suggest that solvents with different permittivity play an active role in polymer chain folding during the fiber deposition, thus affecting the fiber crystallinity. The responses of hMSC on PCL fibers with different fiber mesh scale and crystallinity ultimately confirmed that the dielectric properties of the polymer solution were fundamental to the design of PCL electrospun membranes. By adopting a particular fiber morphology (i.e., size scale) and mode of assembly of polymer chains (i.e., crystallinity), it is possible to influence the adhesion and/or proliferation kinetics of cells, ultimately determining the course of their differentiation process.

REFERENCES

[1] Fong H, Chun I, Reneker DH. Polymer. 1999; 40: 4585-4592.
[2] Son WK, Youk JH, Lee TS, Park WH. Polymer. 2004; 45: 2959-2966.
[3] Deitzel JM, Kleinmeyer J, Hirvonen JK, Beck Tan NC. Polymer. 2001; 42, 8163-8170.
[4] Megelski S, Stephens JS, Chase DB, Rabolt JF. Macromolecules. 2002; 35: 8456-8466.
[5] Wannatong L, Sirivat A, Supaphol P. Polym Int. 2004; 53: 1851-1859.
[6] Lee KH, HY Kim, La YM, Lee DR, J Polym Sci Pol Phys. 2002; 40: 2259-2268.
[7] Pattamaprom C, Hongrojjanawiwat W, Koombhongse P, Supaphol P, Jarusuwannapoo T, Rangkupan R. Macromol Mater Eng. 2006; 291: 840-847.
[8] Qian YF, Su Y, Li XQ, Wang HS, He CL. Iran Polym J. 2010; 19: 123-129.
[9] Sarac A, Ture A, Cankurtaran O, F Yilmaz. Polym Int. 2002; 51: 1285-1289.
[10] Ramakrishna S, Fujihara K, Teo WE, Lim TC, Ma Z. World Scientific. Singapore 2005.
[11] Kwon IK, Kidoaki S, Matsuda T. Biomaterials. 2005; 26: 3929-3939.
[12] Crescenzi V, Manzini G, Calzolari G, Borri C. Eur Polym J. 1972; 8: 449-463.
[13] Kister G, Cassanas G, Bergounhon M, Hoarau D, Vert M. Polymer. 2000; 41: 925-932.
[14] Taddei P, Di Foggia M, Causa F, Ambrosio L, Fagnano C. Int J Artif Organs. 2006; 29: 719-725.
[15] Guarino V, Taddei P, Di Foggia M, Fagnano C, Ciapetti G, Ambrosio L. Tissue Eng PT A. 2009; 15: 3655-3668.
[16] Snyder RG, Maroncelli M, Strauss HL, Hallmark VL. J Phys Chem. 1986; 90: 5623-5630.
[17] Coleman MM, Zarina J. J Polym Sci Pol Phys. 1979; 17: 837-850.
[18] Elzein T, Nasser-Eddine M, Delaite C, Bistac S, Dumas P. J Colloid Interf Sci. 2004; 273: 381-387.
[19] Shenoy SL, Bates WD, Frisch HL, Wnek GE. Polymer. 2005; 46: 3372-3384.
[20] Veleirinho B, Rei, Da Silva JL, J Polym Sci Pol Phys. 2008; 46: 460-471.
[21] Gupta P, Elkins C, Long TE, Wilkes GL. Polymer. 2005; 46: 4799-4810.
[22] Zhong XH, Kim KS, Fang DF, Ran SF, Hsiao BS, Chu B. Polymer. 2002; 43: 4403-4412.
[23] Washburn NR, Yamada KM, Simon CG Jr, Kennedy SB, Amis EJ. Biomaterials. 2004; 25: 1215-1224.
[24] Woo KM, Chen VJ, Ma PX. J Biomed Mater Res. 2003; 67A: 531-537.
[25] Smith LA, Liu X, Hu J, Ma PX. Biomaterials. 2009; 30: 2516-2522.
[26] He L, Li B, Xipeng G, Xie G, Liao S, Quan D, Cai D, Lu J, Ramakrishna S. Cell Mater. 2009; 18: 63-74.
[27] Agarwal S, Wendorff JH, Greiner A. Polymer. 2008; 49: 5603-5621.
[28] Flemming RG, Murphy CJ, Abrams GA, Goodman SL, Nealy PF. Biomaterials. 1999; 20: 573-588.
[29] Park A, Griffith LG. J Biomed Mater Res. 1996; 31: 117-130.

CHAPTER 3

Influence of Gelatin Cue in PCL Electrospun Membranes

3.1 INTRODUCTION

Tissues and human organs are usually composed of diverse cells types and extracellular components that provide specific tissue functions. The cells, together with the extracellular matrix (ECM), arrange and organize to form an elaborate and hierarchical structured order. The resultant structure is compatible with the execution of multi-scale functions, including regulation of cellular activity by soluble bioactive molecules, cell to cell direct contact, and cell-ECM interactions [1, 2]. The use of temporary platforms which are able to recapitulate all basic ECM functions allows the formation of a temporally coordinated and spatially organized structure [3] which simultaneously provides: (a) the required cell anchorage sites, (b) mechanical stability, and (c) structural guidance. It guarantees the availability of active interfaces which are able to respond to local physiological and biological changes, and to remodel the ECM in order to integrate with the surrounding native tissue [4].

The native ECM may be considered as a composite-like structure comprising proteoglycans and fibrous proteins, such as collagens, finely assembled to form multi-fibrillar structures which are highly organized into a mesoscopic 3D fiber network [5]. In the previous chapters it has been shown that by electrospinning technique it is possible to produce engineered platforms which afford effective biomimesis of the native ECM [6–9] exerting the architectural control (geometry, morphology, or topography) by a fine manipulation of system and process parameters. In particular, in Chapter 2, poly(ε-caprolactone) (PCL), a synthetic biodegradable aliphatic polyester with good chemical stability and mechanical performance [10, 11], was electrospun to develop of micro- and/or nanostructured systems and tested with hMSC cells.

However, it has been reported that, natural biopolymers show a higher cell affinity compared to synthetic polymers which have a relative lack of cell recognition sites on the surfaces [12]. This limits the control of scaffold morphology, imparting morphological features on the micro-scale, promoting specific events at the cellular and tissue levels, which are necessary to restore the lost functionality of diseased tissues [13]. On the other hand, biopolymers show some mechanical

inadequacies, due to the chemical modification of chain spatial conformation and fast degradation. For example, Zhang et al. [14] found that pure gelatin, when used as an electrospun scaffold, can rapidly dissolve and disappear under normal cell culture conditions. Several different methods have been explored to crosslink the electrospun gelatin fibers, using a variety of crosslinking agents (glyceradehyde [15], genepin [16] and glutaraldehyde [17]). However, this approach is limited due to the toxic effects of the crosslinking agents used [17]. Alternatively, the mixing of biopolymers with other synthetic polymers may offer a compromise solution for overcoming the main deficiencies of synthetic and natural polymers [18].

Thus, in order to get an improved cellular response, in the first part of this study, electrospun fibers have been produced with a fine tuning of system and process parameter by mixing a synthetic polymer, PCL, with a natural protein, gelatin. Membranes were then morphologically and physically characterized in order to verify the proper inclusion of the protein into the fibers.

In the second part, a comparative study about the contribution of gelatin to cell-material interaction was made in two different 2D substrates. PCL/Gelatin platforms, both as electrospun membranes and casted films, were investigated systematically to identify and define the contributions of individual morphological and biochemical cues on human mesenchymal stem cell (hMSC) response.

In the third part, the potential of the electrospinning process to create substrates for use as alternative scaffolds for nerve regeneration has been explored by investigating the interaction of PCL and PCL/Gelatin membranes with Rat adrenal pheochromocytoma (PC-12) cell line, extracted from a transplantable tumor arising from adrenal medulla [19, 20], able to develop neurite like processes [21-24]. The latter trait has been confirmed in several studies that use PC-12 cells as the standard model for studying the signaling regulation pathways of cell survival, proliferation, and neuronal differentiation [25-27]. In this work, scaffold biocompatibility and neuronal differentiation have been evaluated by neurite outgrowth, and the expression of neuronal markers by cells culturing on the electrospun scaffolds *in vitro* has been assessed to indicate the potential of these bicomponent membranes to be used as material for nerve repair.

3.2 MATERIALS AND METHODS

3.2.1 Materials

PCL pellets (M_w 65,000) and gelatin of type B (~ 225 Bloom) from bovine skin in powder form, were all purchased from Sigma–Aldrich (Italy). 2,2,2-Trifluoroethanol (TFE) and 1,1,1,3,3,3-hexafluoro-2-propanol (HFP) were supplied by Fluka (Italy). All products were used as received without further purifications.

3.2.2 Preparation of PCL/Gelatin Electrospun Membranes

PCL and gelatin were separately dissolved in HFP by magnetic stirring at 25°C overnight. After 24 h stirring, both solutions were then combined to form a single solution in HFP (0.1 g/ml) with a 1 : 1 PCL/Gelatin weight ratio.

The solution was dispensed from a 5 ml syringe (BD Pastipack) connected to a hypodermic needle (18 Ga). Different working parameters were selected to optimize the final morphology of fibers: a high voltage of 13 kV was applied to the needle (ES30-Gamma High Voltage Research, USA), capable of generating DC voltage in a range of 0-30 kV with a power of 5W and a maximum output current of 166 mA. The feed rate of the syringe pump was set at 0.5 ml/h to stabilize the mass flow, also minimizing all jet instabilities. An aluminum plate 120x120x3 mm was placed 140mm from the needle tip to collect the fibers. All the membranes were prepared by using a suitable deposition time to obtain membrane thickness ranging from 150 to 200 μm. In addition, electrospun membranes prepared from PCL solution in HFP (0.1 g/ml) were prepared as control. For degradation and biological test with hMSC, also solvent casted films were prepared as controls. PCL and gelatin were dissolved in TFE at 25°C overnight, to obtain a 7% (wt/v) solution, with a 1 : 1 PCL/Gelatin weight ratio. Solutions were poured into specially designed Teflon molds and kept overnight under the fume hood to allow the TFE to evaporate slowly. The surface morphology of films was investigated by SEM.

3.2.3 Electrospun Scaffold Characterization

The morphology of fibrous scaffolds was studied by scanning electron microscopy (SEM; Quanta FEG 200, FEI, The Netherlands) under high vacuum conditions (~10^{-5} Mbar) using an accelerating voltage of 14 kV. To improve the sample conductivity, scaffolds received a preliminary coating of a Pd-Au nanolayer, using a sputter coater (Emitech K550, Italy). The diameter of the fibers was measured from selected SEM micrographs (n = 5) by using open source image analysis software (Image J v.3.7; National Institutes of Health, U.S.A.).

For the determination of scaffolds wettability, the contact angle of electrospun scaffolds was measured by a water contact angle system (WCA) supported by videocam equipment (OCA20 Dataphysics, Italy). Five measurements with a single droplet (volume, 5 μl) were used for each test. All measurements were performed at time zero to eliminate any influence of subsequent perfusion flow through the membrane. Contact angle size was reported as mean ± standard deviation. Furthermore, thermogravimetric (TG) analyses (TA Instruments, Q500, U.S.A.) were performed on the PCL/Gelatin membranes to estimate the blending ratio in comparison with PCL and gelatin used as controls. The samples were preliminary dried under vacuum condition for 2 h at 37 °C. Weight loss measurements were performed under a nitrogen atmosphere from 40 to 600 °C at 10 °C/min.

The gelatin content in PCL/Gelatin membranes was detected as the weight loss ratio occurring around 300 and 400 °C, respectively, related to the thermal degradation of gelatin and PCL, respectively.

3.2.4 Degradation Studies

Films and electrospun nanofiber mats of PCL and PCL/Gelatin scaffolds were incubated in Eagle's alpha minimum essential medium (α-MEM). The morphology changes were followed by SEM after 1, 3, and 6 days of incubation. The films and nanofibrous mats of PCL and PCL/Gelatin were characterized by infrared (IR) spectroscopy (Spectrum 100, PerkinElmer, Italy). All spectra were taken in the range between 3800 and 1000 cm^{-1} at 4 cm^{-1} resolution, averaging 144 scans.

For gelatin protein detection in the films and nanofibers, the membranes were incubated at 4°C overnight in a 1 : 300 dilution of rabbit (IgG) polyclonal antibody against collagen type I in phosphate buffer saline (PBS) containing 2 mg/ml of bovine serum albumin. The scaffolds were then washed twice with ice-cold PBS plus 0.01% Triton X-100 for 10 min and incubated for 1 h with goat-anti-rabbit immunoglobulin secondary antibodies conjugated with fluorescein isothiocyanate (3 mg/ml, Sigma Chemical, St. Louis, MO), diluted 1 : 50 in PBS, and rinsed with PBS plus 0.01% Triton X-100; the immunostaining was visualized by laser scanning confocal microscopy (LSCM; LSM510, Carl Zeiss).

3.2.5 hMSC Cells Cultures

Samples were cut into a dish shape for biological characterization. Prior to the biological assays, PCL and PCL/gelatin electrospun scaffolds and films were sterilized by immersion in 70% of ethanol (v/v) with antibiotic solution (streptomycin 100 μg/ml and penicillin 100 U/ml) for 30 min, washed with phosphate-buffered saline (PBS) three times, and air dried.

Biological assays were performed using hMSC line obtained from LONZA. The hMSCs were cultured in 75 cm^2 cell culture flask in α-MEM supplemented with 10% fetal bovine serum, antibiotic solution (streptomycin 100 μg/ml and penicillin 100 U/ml, Sigma-Aldrich, Italy) and 2mM L-glutamin. The hMSC (4-6 passages) were used for all the experimental procedures and incubated at 37°C in a humidified atmosphere with 5% CO_2 and 95% air.

3.2.6 hMSC Cells Adhesion

The hMSCs were seeded ($1x10^5$) onto films and electrospun nanofiber scaffolds of PCL and PCL/Gelatin, placed in 24-cell culture plates, and allowed to adhere in standard cell culture for 4 and 24 h. After the specific time periods, substrates were rinsed three times using PBS to remove the unattached cells. Evaluation of cell attachment was performed according to Hayman et al. [28]. The adherent cells were fixed with 4% paraformaldehyde and incubated with 0.1% toluidine blue

for 3 h. The dye was extracted with 0.1% of sodium dodecyl sulfate and the optical absorption was quantified by spectrophotometry at 600 nm (Wallac Victor3 1420, PerkinElmer, Boston, MA). Conventional polystyrene 24-well culture plates were used as a control. Cell adhesion experiments were conducted in triplicate and repeated at least three times.

3.2.7 hMSC Cells Morphology

The spreading pattern interaction of the hMSC onto films and electrospun nanofiber scaffolds of PCL and PCL/Gelatin was evaluated by LSCM after 24 h of cell culture. The hMSC cultures onto films and nanofibers membrane scaffolds were fixed with 4% paraformaldehyde, rendered permeable with PBS containing 0.1% Triton X-100. For actin cytoskeleton, the cells were incubated for 30 min at room temperature with 1 : 1000 dilution of tetramethyl rhodamine iso-thiocyanate-conjugated phalloidin. The scaffolds were then washed with PBS to remove unbound phalloidin conjugate and visualized by LSCM. For SEM analysis, the scaffolds were washed three times with PBS, fixed with 4% formaldehyde for 1 h and then dehydrated with a graded series of ethanol (25–100%) and air dried. The samples without chromium sputter-coating were examined by FESEM under low vacuum conditions.

3.2.8 hMSC Cells Viability

For cell viability, the hMSC ($1x10^4$) were plated in triplicate onto films and electrospun nanofibers of PCL and PCL/Gelatin and 3-(4,5-dimethylthiazol-2-yl)-2,5-diphenyl tetrazolium bromide (MTT) assayed after 2, 4, and 6 days of culture. This assay is based on the ability of mitochondrial dehydrogenases of living cells to oxidize a tetrazolium salt (3-[4, 5-dimethylthiazolyl-2-y]-2,5-diphenyltetrazolium bromide) to an insoluble blue formazan product. The concentration of the blue formazan product is directly proportional to the number of metabolically active cells. The hMSCs seeded onto films and electrospun nanofiber mats of PCL and PCL/Gelatin were washed with PBS and incubated with fresh cultured medium containing 0.5 mg/ml of MTT for 4 h at 37°C in the dark. The culture medium during experimental time was daily changed with fresh media. The supernatant then was removed and dimethyl sulfoxide (DMSO) was added to each well. After 60 min of slow shaking, the absorbance was quantified by spectrophotometry at 570 nm with a plate reader. Cell viability experiments were conducted in triplicate and repeated at least three times.

3.2.9 PC-12 Cells Culture

Following a preliminary screening of polymeric substrates with hMSC cells, the interaction of rat pheochromocytoma PC-12 cells with electrospun membranes has been evaluated. PC-12 cells were kindly donated by the group of Dr. Cerchia Laura (Istituto per l'Endocrinologia e l'Oncologia Sperimentale del CNR Gaetano Salvatore, Naples, Italy). The cells were cultured in a 75 cm^2 cell

culture flask in RPMI 1640 medium, supplemented with 10% horse serum, 5% fetal bovine serum, antibiotic solution (streptomycin, 100 μg/ml, and penicillin, 100 U/ml, Sigma Chem. Co), and 2 mM L-glutamin and incubated at 37°C in a humidified atmosphere with 5% CO_2 and 95% air. PC-12 cells in culture were obtained by 10-12 passages for all the experiments.

3.2.10 PC-12 Cells Adhesion

PC-12 cells were seeded at $2x10^4$ onto PCL and PCL/Gelatin nanofiber scaffolds, placed in 24-well culture plates and allowed to adhere in standard cell culture for 4 and 24 h. After the prescribed time period, substrates were treated as described in par. 3.2.6. Conventional polystyrene 24-well culture plates were used as a control. Cell adhesion experiments were conducted in triplicate and repeated at least three times.

3.2.11 PC-12 Cells Viability

Cell viability of PC-12 cells plated at a concentration of $2x10^4$ onto PCL and PCL/Gelatin nanofiber scaffolds were checked by the MTT assay at 2, 4, and 6 days of culture as described for hMSC cells culture. During the experiment, the culture medium was changed every two days with fresh media and all viability experiments were conducted in triplicate and repeated at least three times.

3.2.12 PC-12 Cells Differentiation

For an *in vitro* differentiation assay, PC-12 cells at a concentration of $2x10^4$ were seeded onto PCL and PCL/Gelatin nanofiber scaffolds, placed in 24-well culture plates, and cultured with RPMI 1640 medium with 1% of horse serum and 50 ng/ml of neuronal growth factor. Control culture scaffolds were grown in RPMI 1640 medium with 1% of horse serum in the absence of neurotrophic factor. Cells on nanofiber scaffolds were assayed as described below.

3.2.13 Detection of the Neurite Marker

PC-12 cell differentiation cultures on nanofiber scaffolds grown in the presence of NGF and control medium for 6 days were characterized by reverse transcription polymerase chain reaction (RT-PCR) for gene expression of neurite marker. Total RNA was isolated from cell scaffolds using TRI reagent (SIGMA). The RNA was precipitated with isopropyl alcohol and the final pellet resuspended in DEPC-water and DNase I digested (Invitrogen Carlsbad, CA) to remove contamination of the genomic DNA. The absorbency at 260/280 nm was measured to determine the RNA concentration. An aliquot of 1 μg of total RNA was used to perform a one-step RT-PCR reaction (Invitrogen Carlsbad, CA) according to the manufacturer's protocol. In summary, the cDNA synthesis program was 1 cycle at 60 °C for 30 min followed by a denaturation cycle of 94 °C for 2 min. cDNA was amplified at 94 °C for 30 s, 60 °C for 1 min, and 72 °C for 1 min for 35

cycles in a thermal cycler (Applied, Biosystem). We used previously published neuronal growth-associated protein (GAP-43) primer sequences that result in a PCR product of 708 base pair (bp); that covers the entire coding region of rat GAP-43 [29]. The primers were as follows: upstream, 5′-tgctgtgctgtatgagaagaacc-3′, and downstream, 5′-ggcaacgtggaaagccgtttcttaaagt- 3′. Rat glyceraldheyde-3-phosphate dehydrogenase (GAPDH) primers used as positive controls were as follows: upstream, 5′- tccaccaccctgttgctgta-3′, and downstream, 5′-accacagtccatgccatcac-3′. Reaction products were separated using gel electrophoresis on 1.2% agarose gel, stained with ethidium-bromide. Bands were visualized using ultraviolet illumination and captured with BioRad Imaging System (BIORAD). Image density of amplified GAP-43 marker products was quantified and was represented as a ratio of the respective PCR product/GAPDH PCR product.

3.2.14 Immunostaining of Neurite Outgrowth Marker GAP-43

PC-12 cell cultures on nanofiber scaffolds grown in the presence of nerve growth factors (NGF) for 6 days were fixed with 4% paraformaldehyde and permeabilized with PBS containing 0.5% Triton X-100. Cells were incubated at 4 °C overnight in a 1:300 dilution of the rabbit (IgG) polyclonal antibody against rat GAP-43 in PBS containing 2 mg/ml of bovine serum albumin (BSA). Nanofiber scaffolds were washed with ice-cold PBS for 10 min at room temperature and incubated for 1 h at 4 °C with goat-antirabbit immunoglobulin secondary antibody conjugated with FITC (3 mg/ml, Sigma Chemical, St. Louis, MO), diluted 1:50 in PBS. Nanofiber scaffolds were rinsed with PBS plus 0.1% Triton X-100 and coverslipped in glycerol-PBS (1:9 v/v) containing 20 mg/ml of 1,2-diazabycyclo (2.2.2) octane (DABCO; thriethylenediamine). Immunoassaying was visualized by confocal laser scanning microscopy (LSM510, Carl Zeiss). Nanofiber scaffolds incubated in the absence of the first antibody were used as negative controls. The number of differentiated PC-12 cells was determined by visual examination of three fields per sample and counting cells that had at least one neurite with a length equal to cell body diameter and expressed as a percentage of the total PC-12 cells in the field. Neurite outgrowth was studied from selected LSCM micrographs. All the neurite extensions with a length equal to cell diameter were considered, and the neurite length was calculated as a linear distance that connects the neurite end part and the cell body in the neurite junction.

3.2.15 Statistical Analysis

All numerical data are presented as mean ± standard deviation. All results were subjected to statistical evaluation using an unpaired Student's t-test to determine significant differences between two groups. The significance level was set at $p < 0.05$.

3.3 RESULTS

Figure 3.1 shows the SEM micrographs of random electrospun PCL and PCL/Gelatin membranes. Several differences in terms of fiber morphologies have been detected. Membranes from PCL solution exhibited a fibrous morphology with the presence of few beads along the fibers on the submicrometric scale (Figures 3.1 A and C).

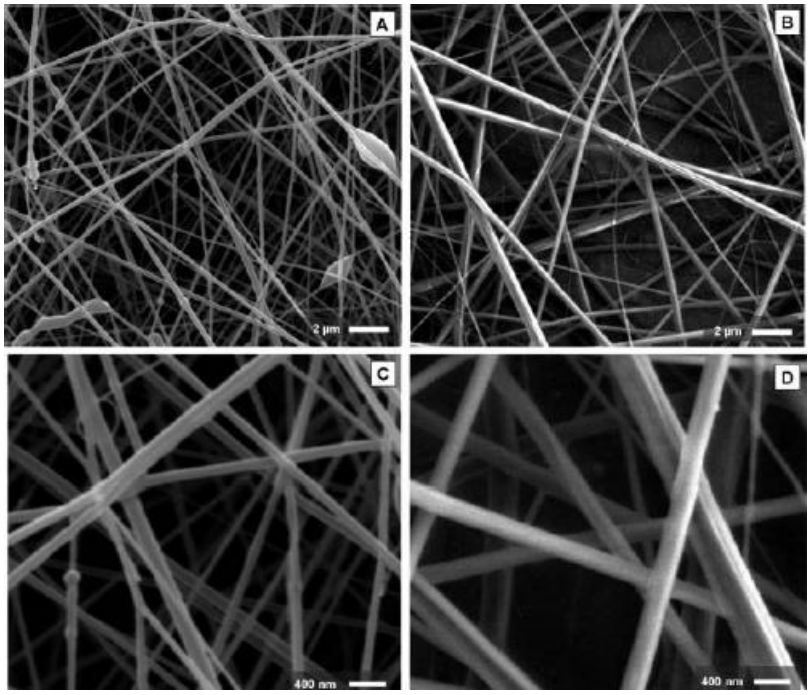

Figure 3.1: SEM images of PCL (A-C) and PCL/Gelatin (B-D) at different magnification, scale bars 2 µm (A, B) and 400 nm (C, D).

This has been confirmed by the estimation via image analysis, which gives a fiber diameter equal to 0.114 ± 0.028 μm. In contrast, membranes from PCL and Gelatin solution at the same concentration, obtained by the same process parameters, show defect-free, randomly oriented nanofibers (Figures 3.1 B-D) characterized by a higher fiber diameter of 0.548 ± 0.140 μm.

Measurements of the contact angle by water droplet have been performed to estimate the wettability of proposed membranes because wettability is a prerequisite for proper material recognition by cells and, thus, effective adhesion to the substrate. Figure 3.2 shows the droplet profiles at zero time on PCL (left) and PCL/Gelatin (right) electrospun nanofibers with optimal morphology. As it is clearly shown in Figure 3.2, PCL/Gelatin materials show a lower contact angle, 55.0 ± 7.7°, than that for PCL-only samples, 103.0 ± 7.8°. This confirms the higher hydrophilic behavior of the PCL/Gelatin membranes, directly ascribable to the presence of protein cue.

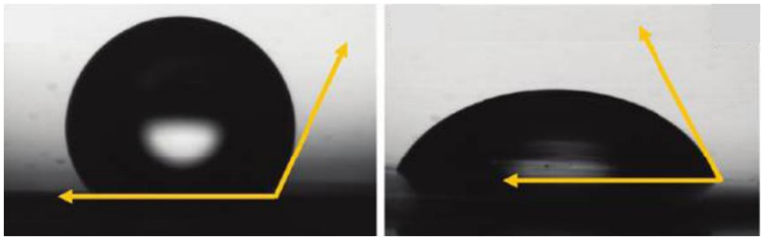

Figure 3.2: Wettability measurements on (left) PCL and (right) PCL/Gelatin membranes: droplet profiles and contact angle evaluation (marked by yellow arrows).

Therefore, TG measurements (Figure 3.3) were carried out to verify the gelatin content after the electrospinning process. By the evaluation of the weight loss with respect to the total weight of the sample, a gelatin amount of 40% has been estimated. This value is also affected by the presence of residual products related to the gelatin degradation over 600 °C, about 10 wt %, which proves the preservation of the theoretical PCL/Gelatin weight ratios (50/50 w/w) after the electrospinning process. This is also in agreement with the evaluation of weight losses at 100 °C due to the bound water molecules. In the case of PCL/Gelatin membranes (plain line), the water content loss is down by half in comparison with the gelatin control (dotted line), therefore, confirming the presence of about 50 wt % of gelatin into the bicomponent membrane.

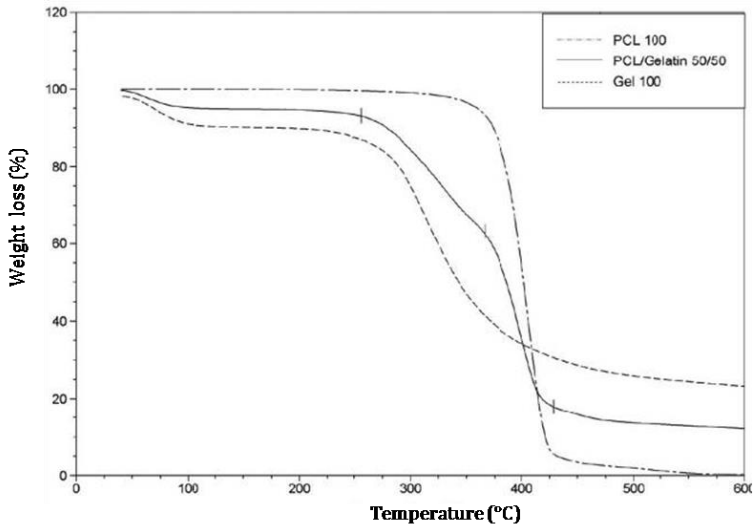

Figure 3.3: Evaluation of gelatin content by thermogravimetric analysis: thermograms of PCL/Gelatin membrane (plain line), PCL (dotted line), and gelatin (point-dot line) controls.

Once optimized the morphology of PCL/Gelatin electrospun membranes and verified the presence of the protein cue inside fibers, a comparative study with PCL and PCL/Gelatin casted film has been performed in terms of degradation kinetics and cells response in order to highlight the different contributions due to topographical and biological signals.

The SEM micrographs of PCL films and fiber electrospun membranes are shown in Figure 3.4. The PCL films have circular closed pores with an average size of 12.57 ± 1.80 µm, homogenously distributed on the surface (Figure 3.4 A). Smaller pores are detectable along the inner pore surface as well as in the intra-porous domains (Figure 3.4 C). This regular organization of pore architecture was ascribable to the evaporation mechanism, which in turn was affected by a combination of the polymer concentration and solvent evaporation properties. PCL electrospun fibers have been shown in (Figure 3.4 B) and in the images at higher magnification (Figure 3.4 D).

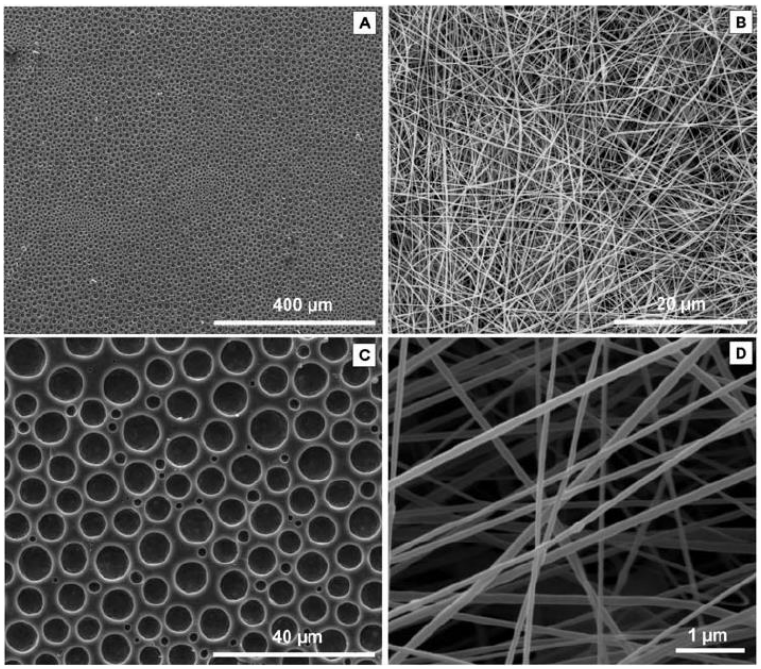

Figure 3.4: SEM images of PCL films (A–C) and nanofiber sheets (B–D).

SEM micrographs of PCL/Gelatin films and fibrous electrospun membranes are shown in Figure 3.5. In PCL/Gelatin films, porous PCL-rich domains coexist with the non-porous domains that contain bulk gelatin. The PCL/Gelatin films have smaller pores – average size of 5.19 ± 1.67 µm (Figure 3.5 C) – than the PCL films, due to the gelatin on the removal of TFE from the PCL matrix during the evaporation. The PCL and gelatin fibers membranes are reported in Figures 3.5 B-D.

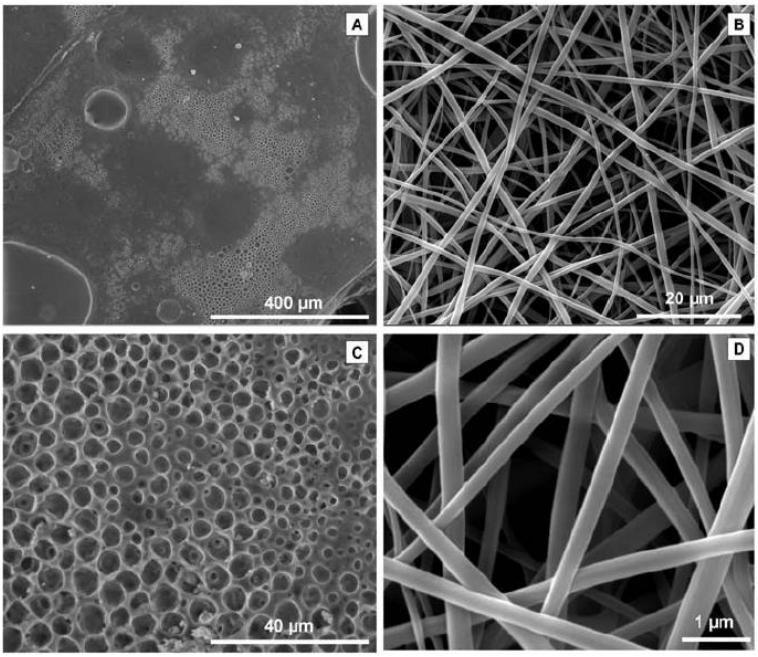

Figure 3.5: SEM images of PCL/Gelatin films (A–C) and nanofiber sheets (B–D).

Films and fiber sheets of PCL/Gelatin were cultured for 6 days to study the effect of degradation of gelatin in aqueous medium on the morphology of proposed systems. The SEM images of the morphological evolution of films (up) and fibers (down) at different incubation times are shown in Figure 3.6. A rapid depletion of gelatin from the films with the formation of crossing pores was observed after 3 days. In contrast, the morphology of the fiber network did not appear to be altered after 6 days of incubation. After 1 day, by increasing the roughness of the fiber surface, a slight degradation of gelatin was detected on the fibers at higher magnification.

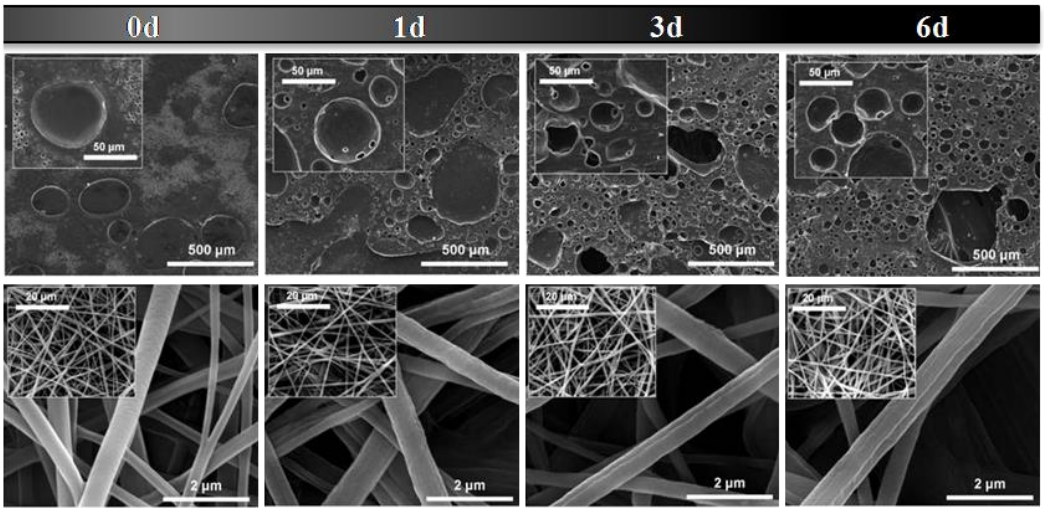

Figure 3.6: SEM images of PCL/Gelatin films (up) and fiber sheets (down) after incubation in α-MEM up to 6 days.

These results were validated by estimating the gelatin content in the films and fiber sheets during the incubation in α-MEM for 0, 1, 3 and 6 days by ATR-FTIR (Figure 3.7). At day 0, IR spectra (Figure 3.7 (a) and (e)) show all the main characteristic peaks of the protein – at ca. 1650 cm^{-1} (amide I) and 1540 cm^{-1} (amide II) – corresponding to the stretching vibrations of C=O bond, the bending of N–H bond and the stretching of C–N bonds, respectively [30]. Other characteristic bands of amide groups of gelatin, N–H stretching at 3310 cm^{-1} (amide A) and C–H stretching at 3068 cm^{-1} (amide B), were detected. After day 1, the peaks had almost disappeared in the case of films, while in the case of fibers, the peaks were only partially reduced, even after 6 days.

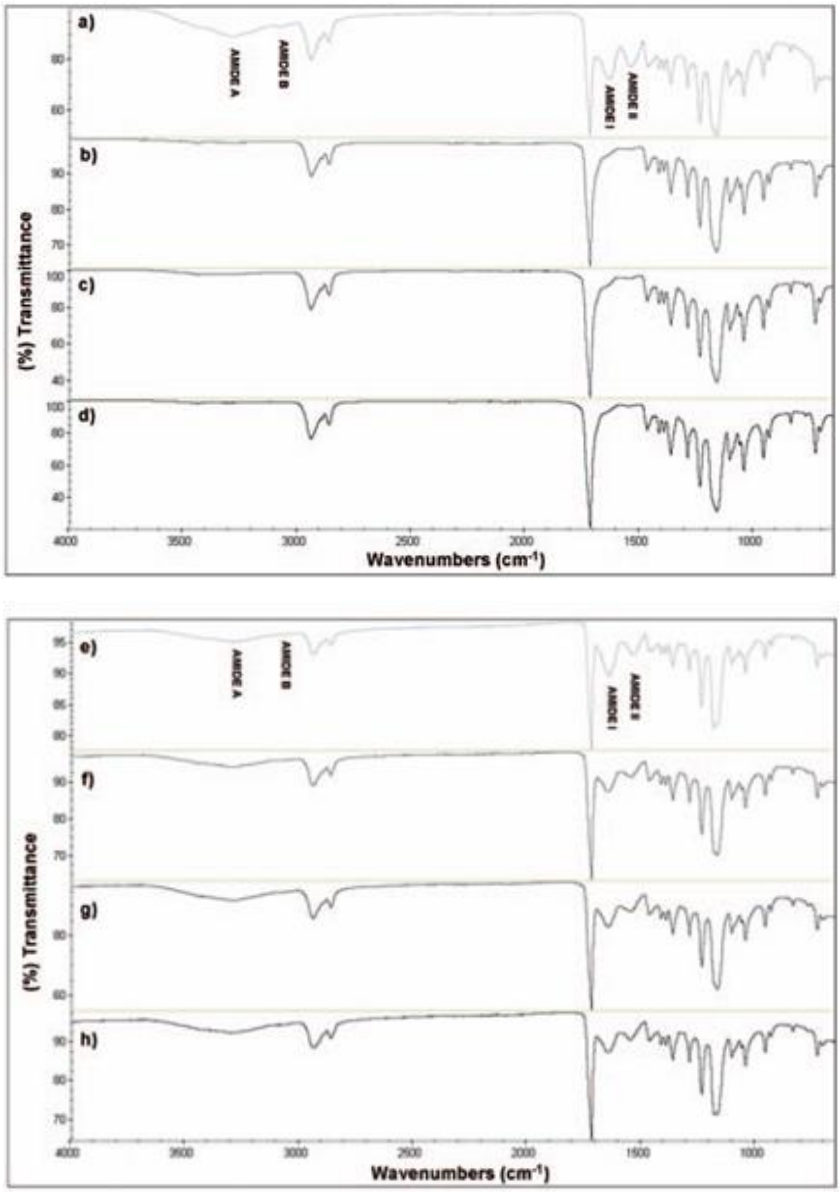

Figure 3.7: IR spectra of PCL/Gelatin films (a-d) and fiber sheets (e-h) after (a, e) 0, (b, f) 1, (c, g) 3 and (d, h) 6 days of incubation in α-MEM.

The presence of gelatin molecules, after conditioning in protein-free medium, was confirmed by the detection of protein using a polyclonal antibody against collagen type I. The LSCM images (Figure 3.8) clearly show the gradual degradation of the gelatin during incubation by the progressive decrease in the fluorescence signal produced; this was observed for bicomponent films and nanofibers during the first 6 days of culture. A drastic decay of the fluorescent signal was detected in those films where it was possible to clearly recognize the reduction in size of gelatin domains as the incubation proceeded. In contrast, only a slight reduction of signal was observed in the case of PCL/Gelatin nanofibers, thus confirming that a large amount of gelatin was still present in the membrane at day 6. The evaluation of the cross-reaction of the antibody performed on films and nanofiber sheets of PCL, as negative controls, showed no signal, confirming that gelatin was the source of the fluorescent signal.

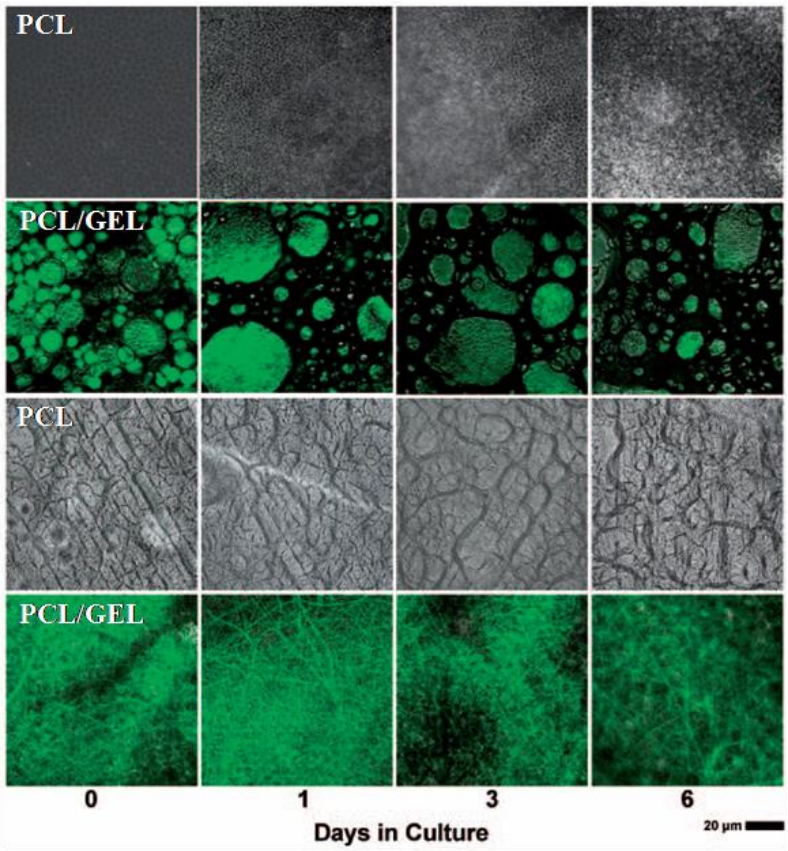

Figure 3.8: Detection of gelatin labeled by polyclonal antibody: LSCM images at different incubation times.

The effect of gelatin degradation was also analyzed in terms of biocompatibility and bioactivity response. A quantitative cell-binding measurement of cell adhesion was performed by colorimetric assay. Different propensities were exhibited by hMSCs to adhere to films and to electrospun membranes (Figure 3.9 A). After incubating for 4 and 24 h, the PCL/Gelatin platforms had a greater

MSC attachment in comparison with PCL platforms (p<0.05), with fiber sheets showing better adhesion than films in both cases. The adhesion of mesenchymal cells was similarly affected by chemical and morphological signals, although the more significant contribution may be ascribed to the platform fiber nanotexturing. Greater hMSC spreading on the PCL/Gelatin nanofibrous scaffold was detected after 24 h by SEM, in comparison with PCL, PCL/Gelatin and PCL films, respectively, in Figure 3.9 B. The hMSC cells had an elongation of shape after 24 h on PCL membranes, similar to the cells on PCL films. In contrast, cells with typically spindle or star-like shapes have been observed in the case of hMSC seeded onto PCL/Gelatin scaffolds. After 24 h, the hMSCs formed focal contacts and spread well on all the proposed materials, extending actin fiber to varying degrees (Figure 3.9 C). hMSCs had a more globular shape and less cell spreading on PCL films compared with the more elongated shape of the hMSCs on PCL/Gelatin film. On the other hand, on nanofiber scaffolds, hMSCs were significantly flattened, and typically spread with a spindle or star-like shape morphology. The extension of actin to form microfilament bundles could be clearly distinguished on bicomponent nanofibers.

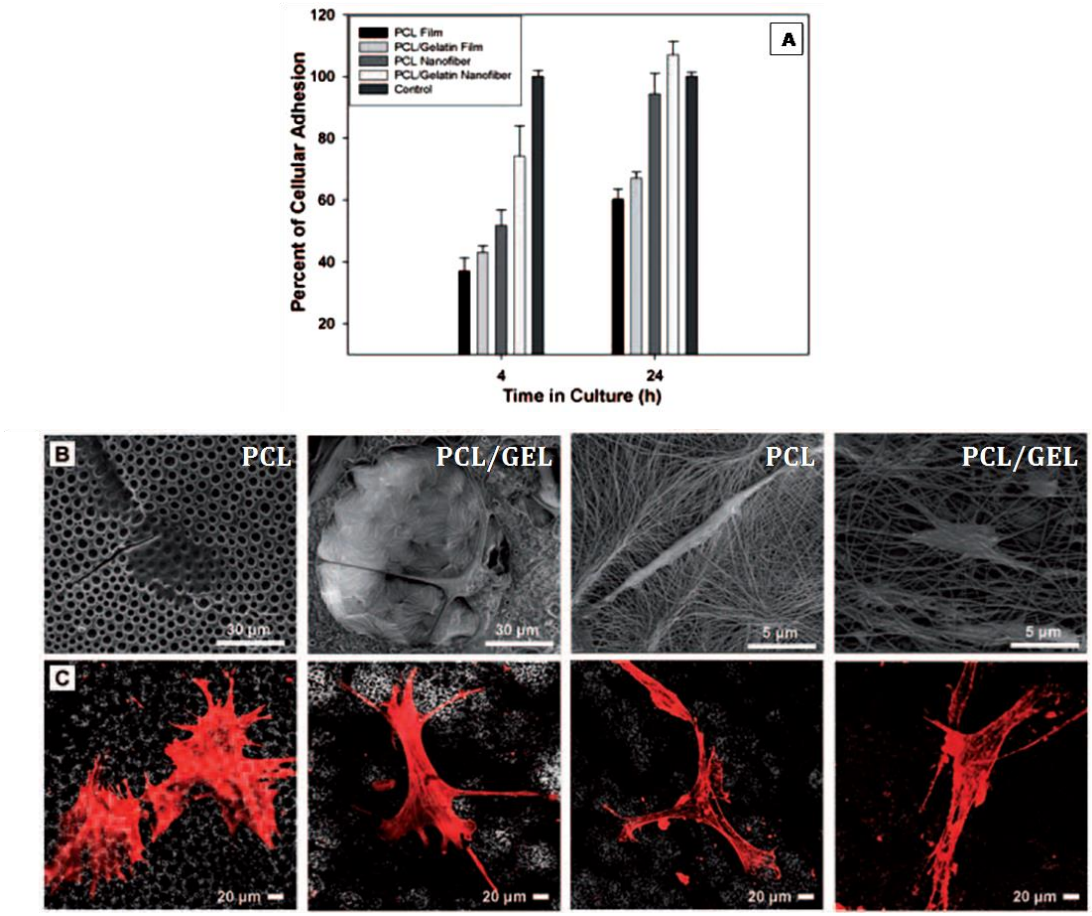

Figure 3.9: hMSCs attachment on PCL and PCL/Gelatin films and fiber sheets: (A) adhesion via colorimetric assay; cell morphologies obtained by FESEM (B) and LSCM (C) images after 24 h for films (left) and electrospun fibers (right);

The mesenchymal cells viability on all platforms after 2, 4, and 6 days of culture were evaluated by the MTT assay. The formazan absorbance confirmed hMSC growth, on films and nanofibers of PCL and PCL/Gelatin scaffolds, indicating good proliferation without any cytotoxic response (Figure 3.10). At day 2, a higher growth rate was observed for the bicomponent samples compared to PCL alone (p<0.05) in both architectures. Since the level of reduction of MTT to formazan is directly proportional to the cell number, the cell density on the surfaces increased with time. A greater increase was noted in the case of electrospun nanofibers of PCL and PCL/Gelatin mats compared to films, confirming the synergistic contribution of chemical cues from gelatin and the previously noted tendency of nanoscale fibers to favor the replicating capacity of hMSC.

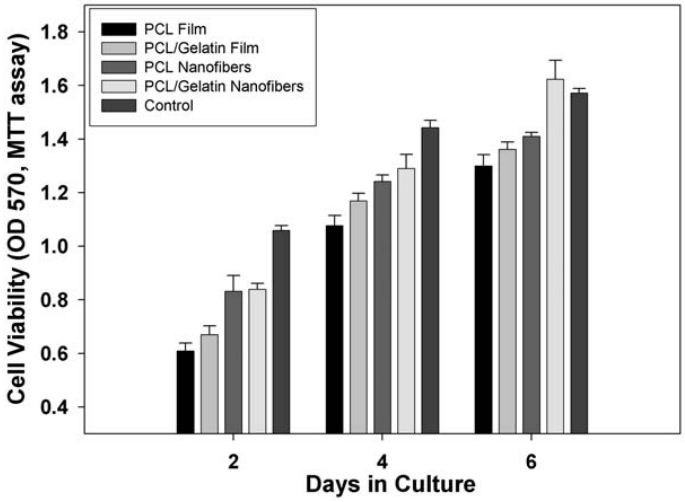

Figure 3.10: hMSC viability on PCL and PCL/Gelatin films and fiber sheets.

All reported data confirmed the slower degradation kinetics and the better biological response for both PCL and PCL/Gelatin electrospun membranes in comparison with casted films. Hence further investigation on the interaction with PC-12 cells was carried out only by using electrospun membranes in order to develop and optimize promising platforms for peripheral nerve regeneration.
Figure 3.11 shows the results of the colorimetric adhesion assay expressed as percentage of adherent PC-12 pheochromocytoma cells onto the PCL and PCL/Gelatin electrospun membranes nanofiber surface, determined at 4 and 24 h of culture with respect to the positive control. PC-12 cells were found to attach more readily and efficiently to the PCL/Gelatin than PCL electrospun membranes (p < 0.05), suggesting that the presence of gelatin help to improve the response of the PC-12 cells to the nanofiber membranes (Figure 3.11). For the PCL/Gelatin nanofiber membranes surface the cellular attachment is clearly enhanced attaining up to 57 and 130% more cells than control. Meanwhile for PCL nanofiber membranes surface the cellular attachment of PC-12 cell remains around 40 and 100%.

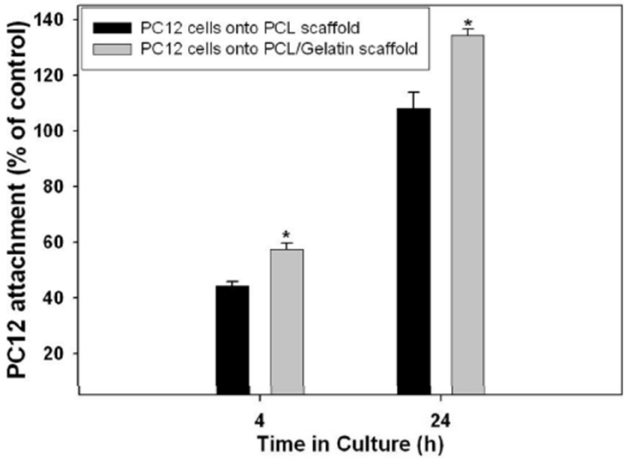

Figure 3.11: Quantitative cell adhesion of PC-12 pheochromocytoma cells seeded onto PCL and PCL/Gelatin electrospun membranes after 4 and 24 h of culture; expressed as the percentage of attached cells in comparison with the plastic-positive control. Asterisk denotes significant differences ($p < 0.05$) from PCL/Gelatin scaffold as compared to PCL as determined by Student's *t*-test.

Optical images highlight the spatial distribution of PC12 over the PCL (Figure 3.12 A) and PCL/Gelatin (Figure 3.12 B) membranes while SEM images provide to show size and cell shape. In particular, PC-12 cells on PCL nanofiber membranes tend to form aggregates (Figure 3.12 A) with rounded shape, indicating a not complete adhesion of cells. Otherwise, PC-12 cells on the PCL/Gelatin electrospun membranes appear more homogeneously distributed, showing a more flattened morphology with visible filopodia and focal adhesion points (Figure 3.12 B), which confirm the highest tendency of cells to adhere and to spread on the substrate.

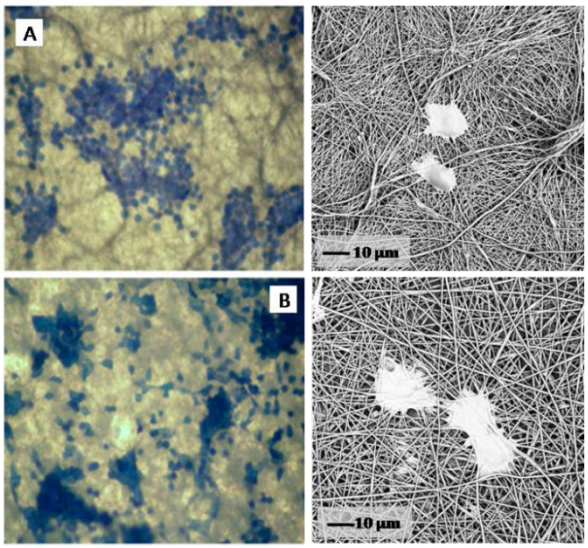

Figure 3.12: Optical micrographs of the distributions of PC-12 pheochromocytoma cells after 24 h of cell culture staining with toluidine blue onto PCL (A) electrospun membranes and onto PCL/Gelatin (B) electrospun samples. SEM images of the morphological appearance of PC-12 cells after 24 h of cell culture on PCL (up) and PCL/Gelatin (down) membranes.

MTT assay was carried out to evaluate the viability of PC-12 pheochromocytoma cells onto the PCL and PCL/Gelatin electrospun membranes nanofiber surface. MTT assay involves a reduction reaction that reduces MTT reagent to formazan when incubated with viable cells; providing information about cell growth and metabolic activity of cells. Thus, the level of reduction of MTT to formazan can reflect the level of cell metabolism. Figure 3.13 shows the time course of formazan accumulation for PC-12 cells proliferation on PCL and PCL/Gelatin electrospun membranes after 2, 4, and 6 days of culture. We found a high level of MTT conversion, indicating that the PC-12 cells' viability rate was significantly ($p < 0.05$) greater in PCL/Gelatin electrospun membranes nanofiber surface than in PCL electrospun membranes. Although the MTT conversion of cells cultured on PCL electrospun membranes also showed an increase in cell viability throughout the culture time, that increase was significantly lower. These results showed that PCL and PCL/Gelatin electrospun membranes nanofiber surface did not induce any cytotoxicity effects on PC-12 pheochromocytoma cells.

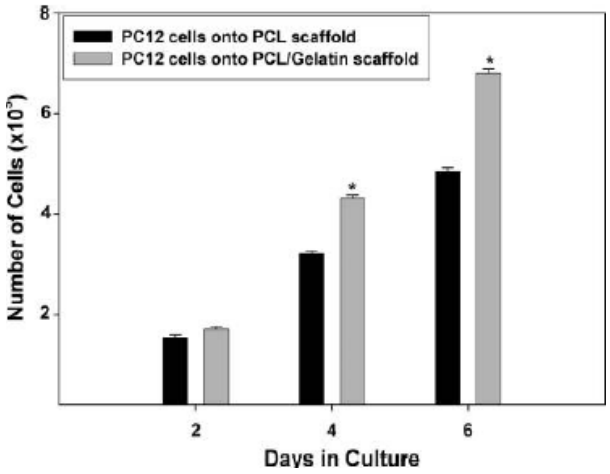

Figure 3.13: Cell viability determined by MTT assay expressed as number of PC-12 pheochromocytoma cells as a function of mitochondrial activity of reduction reaction of MTT to formazan product after 2, 4, and 6 days of cell culture onto PCL and PCL/Gelatin electrospun nanofiber scaffolds. Error bars represent mean ± SD, $n = 3$ cultures under each conditions. Asterisk denotes significant differences ($p < 0.05$) from PCL/Gelatin scaffold as compared to PCL as determined by Student's *t*-test.

Figure 3.14 illustrates the RT-PCR of GAP-43 mRNA expression on PC-12 pheochromocytoma cells cultured onto PCL and PCL/Gelatin electrospun membranes nanofiber surface after 6 days of *in vitro* differentiation. The results of the RT-PCR gel electrophoresis indicate the absence of a detectable product of GAP-43 from mRNA extracted from PC-12 pheochromocytoma cells cultured on both PCL and PCL/Gelatin electrospun membranes nanofiber surface without the addition of neurotrophic factor (NGF) in comparison with NGF treatment cultures where an amplified GAP-43

signal was detected from mRNA extracted from differentiated PC-12 cells (Figure 3.14 A). The GAP-43 product was approximately 700 bp in length, as previously reported using identical primers [29]. GAPDH was used as a housekeeping positive control for the RT-PCR assay. For semi quantitative analysis of the RT-PCR assay, the densitometry values of the amplified product of GAP-43, normalized to those of GAPDH, were obtained (Figure 3.14 B). Our data show no amplified or faint product obtained from PC- 12 cells culture in the absence of neurotrophic factor. However, PC-12 cells cultured on PCL/Gelatin electrospun membranes nanofiber surface showed an up regulation of GAP-43 mRNA with a relative expression about of 1 fold increase in GAP-43 amplified product when compared to PC-12 cells culture onto PCL electrospun membranes after 6 days of *in vitro* differentiation to sympathetic neurons ($p < 0.05$).

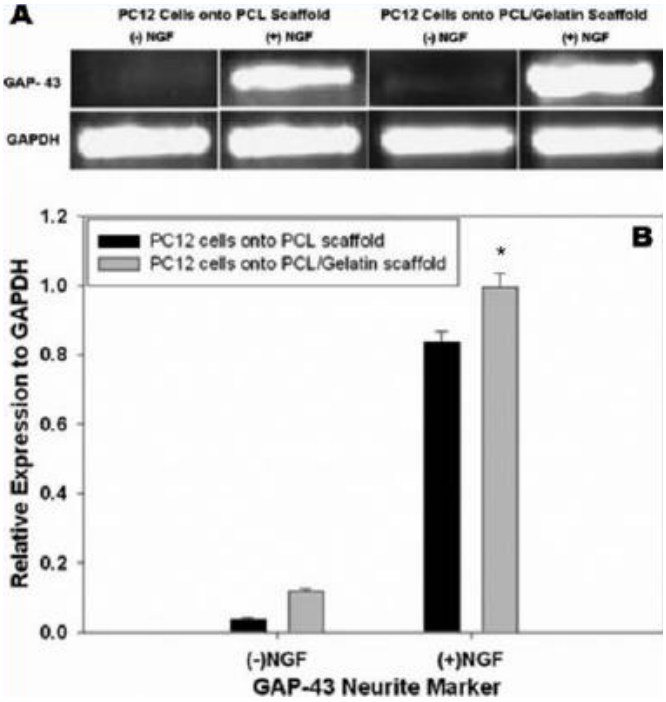

Figure 3.14: Representative gel electrophoresis bands stained with ethidium bromide of the gene expression of GAP-43 mRNA detected by RT-PCR from PC-12 pheochromocytoma cells cultured onto PCL and PCL/Gelatin electrospun nanofiber scaffolds in presence and absence of 50 ng/ml of NGF after 6 day of culture (A). Changes in gene expression of GAP-43 mRNA levels obtained of densitometric data of bands image products, represented as a ratio of GAP-43 product/GAPDH product of PC-12 cells cultured for 6 days with or without stimulation of 50 ng/ml of NGF in the medium onto PCL and PCL/Gelatin electrospun nanofiber scaffolds (B). The housekeeping GAPDH mRNA was used as internal gene control.

The neurite outgrowth of PC-12 cells was used to elucidate the bioactivity of PC-12 cells cultured on PCL (Figure 3.15 A, B) and PCL/Gelatin nanofiber (Figure 3.15 C, D) scaffolds with 50 ng/ml of NGF stimulation. Figure 3.15 shows typical immunofluorescence images of PC-12 cells sending

out neurite extension on PCL and PCL/Gelatin nanofiber scaffolds by immunodetection of the membrane protein of growth cone GAP-43 neurite marker.

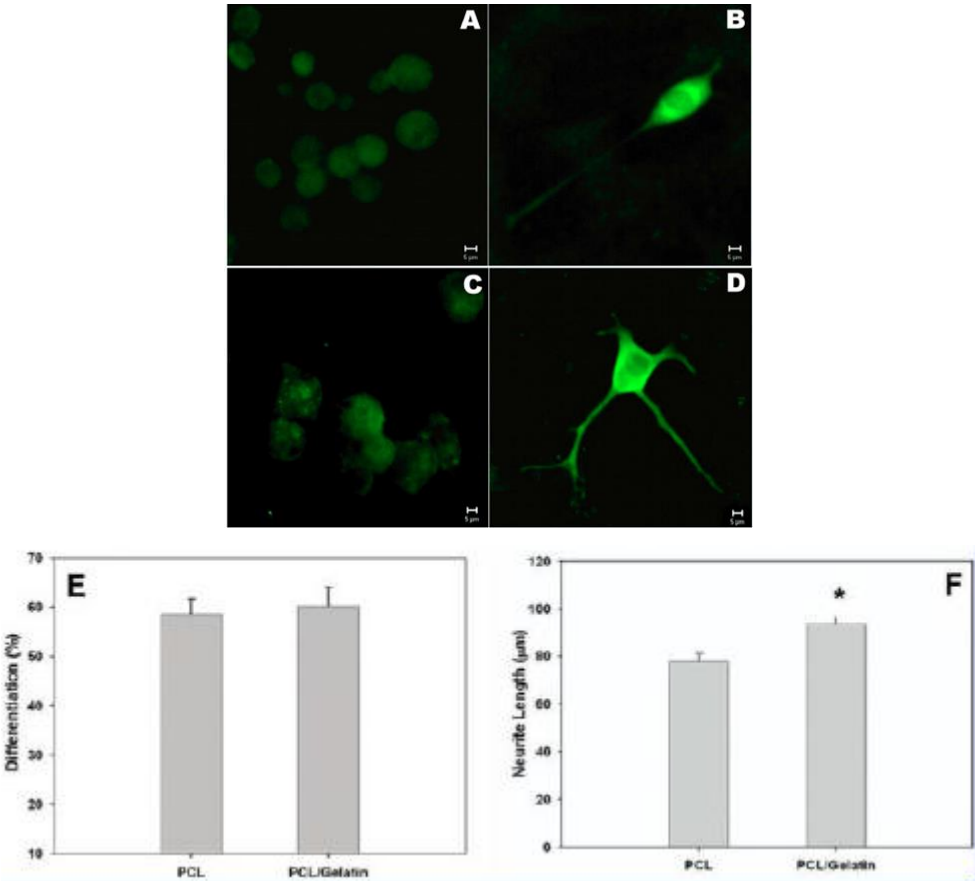

Figure 3.15: Representative confocal laser micrograph images of neurites outgrowth of PC-12 pheochromocytoma cells cultured for 6 days stimulated with 50 ng/ml of exogenous NGF in the medium onto PCL (B) and PCL/Gelatin (D) electrospun nanofiber scaffolds by immunoassay staining against the growth cone neurite marker GAP-43. Micrograph images of no extension of neurites prior to the onset of differentiation by the exposure to NGF of PC-12 cell cultured onto PCL (A) and PCL/Gelatin (C). Scale bar = 5 μm. Evaluation of percentage of differentiation (E) and neurite length (F) after 6 days of culture in NGF (50 ng/ml) loaded medium of PC-12 cells. Asterisk indicates a statistically significant ($p < 0.05$) increase in length on neuritis.

When the morphological appearance of the neurites outgrowth of PC-12 cells was compared, it was observed that neurites on PCL/Gelatin extend more prominently than those on PCL. On PCL/Gelatin, there is a growth cone with some microspikes protruding from them, and the outgrowth appears to be stapling the neurite to the nanofiber surface only at those points where the directions change (Figure 3.15 D). In comparison, on PCL, the neurites were slender and rectilinear with a growth cone at the end of the tip (Figure 3.15 B). However, the continuous and curvilinear appearance of neurites on both blends reflected their close association with the nanofiber surface. The percentage of differentiation related to the presence of neurite-like processes was about 60.2%

for PC-12 cells on PCL/Gelatin compared to 58.6% of PC-12 cells on PCL scaffolds (neurite growth after 6 days of culturing, Figure 3.15 E). The average neurite length of PC-12 cultured on PCL/Gelatin nanofiber was calculated as 93.55 ± 3.93 μm (Figure 3.15 F). This was significantly longer than the extension of neurite-like processes of PC-12 cells cultured on PCL (78.13 ± 3.05 μm). However, the extension of neurite-like processes of PC-12 cells cultured on PCL/Gelatin was greater and more vigorous on this scaffold, as determined by immunoassay.

3.4 DISCUSSION

After trauma or nerve injury, current clinical treatments involve the use of autograft or allograft. This has many limitations, including donor scarcity, multiple surgeries, donor site morbidity, scarring, and the need for an allograft patient to take immunosuppressant indefinitely post surgery to avoid rejection [31, 32]. The development of synthetic material for use in the engineering of nerve grafts is a promising alternative, which obviates the need for immunosuppression or surgery involving autografts or allografts [33, 34]. Our approach proposes the use of polymeric platforms, realized by electrospinning technology, as artificial grafts for nerve tissue regeneration. Here, a mixture of synthetic and natural polymers has been selected to satisfy all the basic requirements of biomaterials for tissue engineering. PCL is a bioresorbable and biocompatible polyester, approved by the FDA for several medical devices [35, 36] and widely used as a biomaterial scaffold with slow degrading behavior. Furthermore, gelatin is a natural biopolymer derived from collagen by controlled hydrolysis, widely used clinically because of its non antigenicity and having many advantages, such as its biological origin, biodegradability, biocompatibility, and commercial availability at relatively low cost [14, 37]. In comparison with other structural proteins (i.e., collagen), gelatin does not show any denaturation phenomena due to the interaction with the applied electric field during the electrospinning process [38] and it is less expensive so incentivizing its use for a large-scale production of electrospun membranes in clinical surgery.

This chapter is aimed to evaluate the role played by gelatin in promoting nerve regeneration. Firstly, mixing gelatin with PCL improves the morphology of the fibrous systems by influencing the interaction of the polymer solution with the electric field. In this case, the higher density of the protein (1.46 g/cm^3) than PCL (1.13 g/cm^3) allows preservation of optimum viscous behavior, which helps to prevent capillary instabilities of the jet occurring at the tip of the electrode needle during the fiber deposition, therefore, minimizing bead formation (Figure 3.1). Also, the protein drastically alters the hydrophobic behavior of PCL, as indicated by the differences in contact angles (Figure 3.2) and confirmed by experimental evidence in other work [30]. This enhanced

hydrophilicity arises from the presence of an amine and a carboxylic functional group (absent from PCL) in the gelatin structure.

Moreover, in this chapter, a comparative evaluation of the biological response of bicomponent films and electrospun membranes was done to determine the contribution of fiber nanopatterning on basic cell mechanisms in the tissue regeneration. The solvent casted PCL films showed a microporous surface due to a tailored evaporation of solvent. During this process, the film phases can vary in size within a micrometric range (Figures 3.4 A-C), to form a patterned template that influences cell attachment [39]. In contrast, electrospun nanofibers were arranged in a random manner, forming an interconnected fiber network with open porosity (Figure 3.4 B) that assures fluid transport, cell penetration, and tissue ingrowth. The homogeneous distribution of fiber sizes (Figure 3.4 D) on a nanometric scale enables the exposure of an ordered nanotextured surface that interacts more effectively with cells, due to the higher exposed scaffold surface. Based on the hMSCs' biocompatibility results (Figure 3.9), the nanofibrous scaffolds provide some signals to able cells to promote cell growth and functionality. The nanoscale fiber assembly also contributed to the mechanical properties and better biodegradation control to mimic a natural cellular remodeling process [11]. A more elaborate model of biological recognition and signaling function of the extracellular milieu is needed that requires a nanofibrous scaffolds to induce a precise recapitulation and spatiotemporal control of the cell living environment *in vitro* and *in vivo* [40]. Native proteins, such as collagen and gelatin, have been selected as candidate materials for reproducing the morphological and biochemical functionalities of natural ECM [41]. Unlike traditional engineering composites with inorganic components (e.g., carbon and glass fibers) used as reinforcement systems, the encoding role of natural biopolymers allows the imparting of bioactive cues to the biologically passive synthetic polymers. However, the main shortcoming of collagen is its inadequate mechanical properties and the changes in structure during scaffold manufacturing; both of which make it unsuitable for long-term applications [38]. Some researchers have proposed the use of crosslinking strategies (e.g., glutaraldehyde) to minimize the protein dissolution in aqueous media [42]. However, crosslinking agents above critical concentrations may affect the electrospinning parameters as well as the fiber morphology [43] and the release of unreacted highly cytotoxic products [44]. A mix of natural and synthetic polymers may overcome the deficiencies of single polymers to produce new platforms with excellent biocompatibility and enhanced cell–scaffold interactions that retain their structural integrity.

In this study, gelatin (denatured collage) was embedded in PCL for enhanced biodegradability with respect to the natural collagen. PCL/Gelatin electrospun membranes show a progressive slowing of the hydrolytic degradation of proteins, with some preservation of chemical functionality for up to 6

days of *in vitro* culture (Figures 3.6-3.8). Some gelatin was still present in the fiber sheets at day 6 as confirmed by the IR spectrum in Figure 3.5. The fibers display irregular topographical features which probably arise from partial gelatin loss along the fiber surface during water conditioning (Figure 3.6).

This was confirmed by a comparison with the smooth surface of pure PCL electrospun fibers. The film degradation studies (Figures 3.6-3.8) indicate the complete disappearance of gelatin after only 24 h, confirming that the phase separation occurring during processing can affect degradation kinetics. In particular, the electric field applied during electrospinning promoted the formation of finely dispersed and strictly embedded phases, which slow down the dissolution of the gelatin. This was also reported by Zeugolis et al. [38], who showed that the presence of extensive protein phases promoted rapid membrane dissolution. The surface roughness of the fibers and the hydrophilic signal of protein [45] improved the cell–surface recognition and enhanced cell spreading. The hMSC cells on PCL/Gelatin membranes show a more marked interaction, with the formation of filopodia which follows the morphological pattern of the tracks formed along the fiber surface. In contrast, in the case of bicomponent films, cells recognize the substrate only in the neighborhood of the gelatin phases forming specific contact over the surface. The enhanced biocompatibility of the bicomponent substrates may be explained by the presence of the gelatin amino acids, such as arginine, glycine, aspartic acid, which provide a positive signal of surface recognition confirming favorable conditions for cellular response [17, 18]. The cell adhesion represents the first aspect of cell-material interaction which may drastically determine the response of cell physiological and biological functions, thus compromising the potential fate of the biohybrid system (material and cells) [46]. PCL/Gelatin samples had the best biocompatibility followed by PCL fibrous membranes. Therefore, further investigations on electrospun scaffolds as guide for nerve regeneration were pursued with more specific cells (i.e., PC-12 cells).

Differences in the chemistry and morphology of PCL and PCL/Gelatin nanofiber significantly contribute to characterizing the biological response assessed by *in vitro* cell model based on rat pheochromocytoma PC-12 cell line. As a first step, both short and medium term bioassays have been performed to determine the adhesion and cytotoxicity of the different scaffolds.

It is recognized that adhesion is an important process, not only for attachment, but also for enabling nerve growth cone to move during the neurite-like process. All the results reported here showed an enhanced cellular adhesion, related to a favorable interaction of PC-12 cells, and proliferation, related to viability of PC-12 cells, when cultured onto a PCL/Gelatin scaffold compared with PCL alone, demonstrating the better biocompatibility of electrospun membranes with gelatin content (Figures 3.11-3.15). Despite the higher diameter of PCL/Gelatin fibers that evidently limits the

surface/volume ratio and fiber density so negatively concurring to influence cell recognition, the enhanced biocompatibility of the bicomponent scaffold demonstrates the main role of gelatin cue, which significantly improves cell affinity compared to synthetic polyester fibers of PCL with hydrophobic behavior and lack of surface cell recognition sites [47]. Furthermore, many cells types, including neural cells, are sensitive to chemical cues that support the advance of the basic mechanisms, namely, cell growth and differentiation, involved during the regeneration of the nerve [48]. In this case, the inclusion of gelatin exposes many integrin sites for cell adhesion and differentiation, which mimic the structural features of the natural extracellular matrix, creating a favorable environment for PC-12 cell attachment and proliferation [14, 30, 49, 50]. These results are in agreement with similar studies on PC-12 cells response onto electrospun scaffold. Ghasemi-Mobarakeh et al. reported that the proliferation of C17.2 neuronal cells on gelatin-containing PCL electrospun scaffold was higher than PCL scaffolds [30], while Chong et al. observed significant cell adhesion, growth, and proliferation of human dermal fibroblasts on electrospun PCL/Gelatin scaffold [45]. Prabhakaran et al. found good adhesion and higher cell viability of mesenchymal stem cells induced to differentiate into neuronal cells on engineering nanofibrous scaffolds of poly(L-lactic acid)-*co*-poly(3-caprolactone)/collagen [51], and Koh et al. found that poly(L-lactic acid) (PLLA) nanofiber scaffolds functionalized with laminin by different methods supported better PC-12 cells viability and adhesion compared with unmodified PLLA nanofiber [52]. Results from the analysis of PC-12 cell differentiation indicated the active role of gelatin as a biological cue on neurite outgrowth and on the expression of the membrane protein of growth cone GAP-43 neurite marker after exposure to 50 ng/ml of NGF. Recently, the PC-12 pheochromocytoma cell line has been extensively used as a model for studying neuronal differentiation in the presence of neurotrophic factors. In particular, PC-12 cells in the NGF-conditioned environment show an enhancement in the direction of outgrowing axons of sensory and sympathetic neurites along the factor concentration gradient and increased the tendency to start sprouting neurite like process [53, 54]. Also, NGF dependence has been confirmed by reported experimental evidence, indicating that, after 6 days of culture, PC-12 cells in the absence of NGF are rounded in shape, exhibiting no extension (Figure 3.15). The behavior of PC-12 cells in terms of neuronal differentiation shows that PC-12 cells preferably differentiate in the presence of PCL and gelatin nanofiber (Figure 3.14-3.15). The recognition of the growth cone GAP-43 by immunoassay and by estimation of the average neurite length shows that differentiation is related to the presence of neurite-like processes and that gelatin considerably contributes to the stabilization of the neurite outgrowth process. This promotes stronger and more prominent sprouting of neurites from cell bodies to the nanofiber surface. Additionally, several *in vitro* studies of the role of cell-substratum adhesion in neurite evolution

report a strong correlation between neuron-substratum adhesion strength and quality of neuronal morphogenesis in terms of neurite outgrowth [55-58]. The results obtained in the current work are in agreement with all previous literature, showing that the adhesive interaction between PC-12 cells and PCL/Gelatin nanofiber scaffolds and their surrounding microenvironment plays a crucial role in the initiation, elongation, and fasciculation of neurites.

Regarding assessment of neuronal differentiation, many neurotypic proteins may be used as markers of differentiation *in vitro* of PC-12 cells into the neuronal phenotype [59], including growth-associated protein 43 (GAP-43) and presynaptic membrane-associated proteins, such as synpatophysin and synapsin. Results from this study on the gene expression of GAP-43 after NGF exposure showed high levels of GAP-43 expression on PCL/Gelatin as compared to levels observed on PCL alone (Figure 3.14), directly indicating an increase of differentiated cells and neurite outgrowth length. These data are supported by the literature, where GAP-43 is implicated as a neuron-specific phosphoprotein whose gene expression has been used as an indicator of the early events in neurite outgrowth [60-62]. Also, it has to be noted that neurite outgrowth is a dynamic and complex process, guided by the interaction of the neuron with the substrate as well as by local environment, requiring multiple cycles of attachment and release and extension and retraction of the sprout nerve growth cones. The current challenge moves toward a control of the up regulation of GAP-43 by interactions between individual neurons. These interactions may be certainly carried by morphological cues offered by nanotextured membranes. Mainly, biochemical cues offered by gelatin enable concerted promotion of cell adhesion and migration, as well as supplementing the effect of NGF on cell differentiation while it progressively dissolves during cell culture [14]. This entails the creation of free volume within the microenvironment, which not only promotes motility and accessibility of the PC-12 cells but also improves the diffusion of NGF, enhancing the bioactivity of the scaffold. In particular, NGF stimulates the tyrosine kinase (TrkA) receptor to activate distinct intracellular signaling pathways, which could crosstalk with signaling pathways of the gelatin biopolymer mediated by integrin receptor ($\alpha 1\beta 1$), supporting the fate of progenitor-like PC-12 cells to sympathetic neurons. Also, GAP-43 is enriched at the interface by receptors and cytoskeleton at the growth cone tip. Its phosphorylation state influences cytoskeletal dynamics, including actin polymerization playing a pivotal role in the guidance of neurite outgrowth [63-65].

All these promising results show the way toward a new approach based upon the use of signal-inducing scaffolds in neural tissue regeneration, with significant benefits relevant to the traditional procedures of peripheral nerve repair.

3.5 CONCLUSION

Based on the results reported here, we can conclude that natural polymers such as gelatin integrated into PCL nanofibers may act as biological cues for promoting nerve repair. Although electrospun fibrous scaffolds have already been proven feasible as favorable substrates for nerve cell culture, the results of cell attachment, viability, and neurite outgrowth studies reported here demonstrated that the integration of gelatin with PCL nanofibers significantly improves the biointeraction of PC-12 pheochromocytoma nerve cells with the substrate. This improved bioactivity is related to the synergistic contribution of scaffold material topography, that is fiber diameter on the nanoscale, and biochemical signals offered by gelatin biopolymer, as confirmed also by the comparative study with casted films.

Immunostaining and RT-PCR results confirm that gelatin cue also support neuronal differentiation and changes in gene expression during *in vitro* differentiation, directly related to neurite outgrowth. These data suggest that stimulation of neurite outgrowth requires GAP-43 function, which can be guided by the fine design of signal-inducing scaffold, paving the way toward a renewed role of the substrate to assist neuronal pathfinding during nerve repairs or regeneration.

REFERENCES

[1] Stahl A, Wenger A, Weber H, Stark GB, Augustin HG and Finkenzeller G. Biochem Biophys Res Commun. 2004; 322: 684-692.
[2] Schwartz JD, Monea S, Marcus SG, Patel S, Eng K, Galloway AC, Mignatti P, Shamamian P. J Surg Res. 1998; 76(1): 79-85.
[3] Causa F, Netti PA, Ambrosio L. Biomaterials. 2007; 28: 5093-5099.
[4] Rose FR, Oreffo RO. Biochem Biophys Res Commun. 2002; 22(292): 1-7.
[5] Kadler KE, Holmes DF, Trotter JA, Chapman JA. Biochem J. 1996; 316: 1-11.
[6] Suri S, Schmidt CE. Acta Biomater. 2009; 5(7): 2385-2397.
[7] Puppi D, Piras AM, Detta N, Ylikauppila H, Nikkola L, Ashammakhi N, Chiellini F, Chiellini E. J Bioact Compat Polym. 2011; 26: 20-34.
[8] Stoilova O, Manolova N, Gabrovska K, Marinov I, Godjevargova T, Mita DG, Rashkov I. J Bioact Compat Polym. 2010; 25: 40-57.
[9] Spasova M, Stoilova O, Manolova N, Rashkov I, Altankov G. J Bioact Compat Polym. 2007; 22(1): 62-76.
[10] Matthews JA, Wnek GE, Simpson DG, Bowlin GL. Biomacromolecules. 2002; 3: 232-238.
[11] Agarwal S, Wendorff JH, Greiner A. Polymer. 2008; 49: 5603-5621.
[12] Cai Q, Yang J, Bei J, Wang S. Biomaterials. 2002; 23: 4483-4492.
[13] Tsang VL, Bhatia SN. Adv Drug Delivery Rev. 2004; 56: 1635-1647.
[14] Zhang YZ, Ouyang HW, Lim CT, Ramakrishna S, Huang ZM. J Biomed Mater Res B. 2005; 72: 156-165.
[15] Vandelli MA, Rivasi F, Guerra P, Forni F, Arletti R. Int J Pharm. 2001; 215: 175-184.
[16] Bigi A, Cojazzi G, Panzavolta S, Roveri N, Rubini K. Biomaterials. 2002; 23: 4827-4832.
[17] Sisson K, Zhang C, Farach-Carson MC, Chase DB, Rabolt JF. Biomacromolecules. 2009; 10(7): 1675-1680.
[18] Venugopal JR, Low S, Choon AT, Kumar AB, Ramakrishna S. Artif Organs. 2008; 32(5): 388-397.
[19] Green LA, Tischler AS. Proc Natl Acad Sci. U.S.A. 1976; 73: 2424-2428.
[20] Green SH. Methods Enzymol. 1995; 7: 222-237.
[21] Attiah DG, Kopher RA, Desai TA. J Mater Sci Mater Med. 2003; 14: 1005-1009.
[22] Das KP, Freudenrich TM, Mundy WR. Neurotoxicol Teratol. 2004; 26: 397-406.
[23] Ohnuma K, Hayashi Y, Furue M, Kaneko K, Asashima M. J Neurosci Methods. 2006; 151, 250-261.
[24] Cappelletti G, Galbiati M, Ronchi C, Maggioni MG, Onesto E, Poletti A. J Neurosci Res. 2007; 85: 2702-2713.
[25] Fujita K, Lazarovici P, Guroff G. EnViron Health Perspect. 1989; 80: 127-142.
[26] Pantera B, Bini C, Cirri P, Paoli P, Camici G, Manao G, Caselli A. J Neurochem. 2009; 110: 194-207.
[27] Qu Z, Wolfraim LA, Svaren J, Ehrengruber MU, Davidson N, Mildbrant J. J Cell Biol. 1998; 142: 1075-1082.
[28] Hayman EG, Engvall E, A'Hearn E, Barnes D, Pierschbacher M, Ruoslahti E. J Cell Biol 1982; 95(1): 20-23.
[29] Baetge EE, Haammang JP. Neuron. 1991; 6: 21-30.

[30] Ghasemi-Mobarakeh, L.; Prabhakaran, M. P.; Morshed, M.; Nasr- Esfahani, M. H.; Ramakrishna, S. Biomaterials 2008, 29, 4532–4539.
[31] Wilberg M, Terenghi G. Surg Technol Int. 2003; 11: 303-310.
[32] Chalfound CT, Wirth GA, Evens GR. J Cell Mol Med. 2006; 10: 309-317.
[33] Harley BA, Hastings AZ, Yannas IV, Sannino A. Biomaterials. 2006; 27: 866-874.
[34] Madaghiele M, Sannino A, Yannas IV, Spector M. J Biomed Mater Res Part A. 2008; 85: 757-767.
[35] Pok SW, Wallace KN, Madihally SV. Acta Biomater. 2010; 6 (3): 1061-1068.
[36] Chiona V, Vozzi G, Vozzi F, Salvadori C, Dini F, Carlucci F, Arispici M, Burchielli S, Di Scipio F, Geuna S, Fornaro M, Tos P, Nicolino S, Audisio C, Perroteau I, Chiaravalloti A, Domenici C, Giusti P, Ciardelli G. Biomed MicrodeV. 2009; 11: 1037-1050.
[37] Zang S, Huang Y, Yang X, Mei F, Ma Q, Chen G, Ryu S, Deng X. J Biomed Mater Res Part A. 2009; 90: 671-679.
[38] Zeugolis DI, Khew ST, Yew ES, Ekaputra AK, Tong YW, Yung LY, Hutmacher DW, Sheppard C, Raghunath M. Biomaterials. 2008; 29: 2293-2305.
[39] Tang ZG, Black RA, Curran JM, Hunt JA, Rhodes NP, Williams DF. Biomaterials. 2004; 25(19): 4741-4748.
[40] Zhang YZ, Su B, Venugopal J, Ramakrishna S, Lim CT. Int J Nanomed. 2007; 2(4): 623-638.
[41] Matthews JA, Boland ED, Wnek GE, Simpson DG, Bowlin GL. J Bioact Compat Polym. 2003; 18: 2125-2134.
[42] Zhang YZ, Venugopal J, Huang ZM, Lim CT, Ramakrishna S. Polymer. 2006; 47: 2911-2917.
[43] Han B, Jaurequi J, Tang BW, Nimni ME. J Biomed Mater Res. 2003; 65A: 118-124.
[44] Drumheller P, Hubbell J. Boca Raton, FL: CRC Press LLC, 2000.
[45] Chong EJ, Phan TT, Lim IJ, Zhang YZ, Bay BH, Ramakrishna S, Lim CT. Acta Biomater. 2007; 3(3): 321-330.
[46] Luan XY, Wang Y, Duan X, Duan QY, Li MZ, Lu SZ, Zhang HX, Zhang XG. Biomed Mater. 2006; 1: 181-187.
[47] Cheng M, Deng J, Yang F, Gong Y, Zhao N, Zhang X. Biomaterials. 2003; 24: 2871-80.
[48] Gunn JW, Turner SD, Mann BK. J Biomed Mater Res. 2005; 72: 91-97.
[49] Lee J, Tae G, Kim YH, Park IS, Kim SH. Biomaterials. 2008; 29: 1872-1879.
[50] Yao L, O'Brien N, Windebank A, Pandit A. J Biomed Mater Res Part B. 2009; 90: 483-491.
[51] Prabhakaran MP, Venugopal JR, Ramakrishna S. Biomaterials. 2009; 30: 4996-5003.
[52] Koh HS, Yong T, Chan CK, Ramakrishna S. Biomaterials. 2008; 29: 3574-3582.
[53] Arien-Zakay H, Lecht S, Perets A, Roszell B, Lelkes PI, Lazarovici P. J Mol Neurosci. 2009; 37: 225-237.
[54] Hondermarck H. Am J Phatol. 2008; 172: 865-867.
[55] Kofron CM, Fong VJ, Hoffman-Kim DJ. Neural Eng. 2009; 6: 1-12.
[56] Vogelezang M, Forster UB, Han J, Ginsberg MH, French- Constant C. BMC Neurosci. 2007; 8: 44.
[57] Nisbet DR, Pattanawong S, Ritchie NE, Shen W, Finkelstein DI, Horne MK, Forsythe JS. J Neural Eng. 2007; 4: 35-41.
[58] Tai HC, Buettner HM. Biotechnol Prog. 1998; 14: 364-370.

[59] Jap Tjoen San SE, Schmidt-Michels MH, Oestreicher AB, Schotman P, Gispen WH. J Mol Neurosci. 1992; 3: 189-195.

[60] Aigner L, Caroni P. J Cell Biol. 1995; 128: 647-660.

[61] Mingorance-Le Meur A, Mohebiany AN, O'Connor TP. PLoS ONE. 2009; 4: e4344.

[62] Paden CM, Watt JA, Selong TH, Paterson CL, Cranston H. J Endocrinology. 2006; 147: 952-958.

[63] Stritmatter SM, Fankhauser C, Huang PL, Mashimo H, Fishman MC. Cell. 1995; 80: 445-453.

[64] Aigner L, Arber S, Kapfhammer JP, Laux T, Schneider C, Botteri F, Brenner HR, Caroni P. Cell. 1995; 83: 269-278.

[65] Denny JB. Curr Neuropharm. 2006; 4: 293-304.

CHAPTER 4

Design and Characterization of PCL and PCL/Gelatin Electrospun Conduits for Peripheral Nerve Regeneration

4.1. INTRODUCTION

Peripheral nerve injuries are very common in clinical practice and often lead to permanent disability. Once the adult nerve tissue is injured, it is hard to regenerate especially as a nerve defect or gap is too long [1-3]. Currently, nerve autografts are considered as the "*gold standard*" for the structural and functional restoration of nerves. However, several drawbacks are related to the use of autografts, including extended surgery, donor site morbidity, limited availability, size mismatch, and painful neuroma formation. Nerve conduits represent a promising alternative for the regeneration of the damaged or transected nerve tissue. In this context, three-dimensional structures, namely conduits, may act as bridge, providing directional guidance as well as support to nerve regeneration [4].

The use of hollow conduits was originally proposed for nerve repair in 1881 with the first successful application occurring in 1882, a tube was used to bridge a 30 mm nerve gap in a dog [5, 6]. Today, the use of this synthetic implant is the clinically approved alternative to autograft repair, presenting several advantages, such as limited myofibroblast infiltration, reduced neuroma and scar formation, reduction in collateral sprouting and no associated donor site morbidity [7].

In ensuring the success of neural tissue engineering strategies, material choice plays a crucial role. Tailored material degradation rates and mechanical properties allow minimizing inflammatory response, thus providing the required support and guidance to sustain the regeneration of axons [8]. A large body of research has been conducted to investigate different kinds of biomaterials for neural tissue engineering, as reported in Figure 4.1, including synthetic materials such as poly(glycolic acid) (PGA) [9], poly(L-lactide-co-glycolide) (PLGA) [10, 11], poly(3-hydroxybutyrate) (PHB) [12, 13] and natural biopolymers such as gelatin [14-16], collagen [3, 10, 17-20], chitosan [9, 21-24] and silk [25, 26]. Biocompatible synthetic materials are attractive as neural tissue engineering scaffolds because of the ease in tailoring the degradation rate and mechanical properties of these materials to suit the application, while natural materials offer biomolecular recognition site [27].

product	company	composition	degradation time	max length
Neurogen	Integra Neurosciences, Plainsboru, NJ, USA	collagen type I	4 years	3 cm
NeuraWrap	Integra Neurosciences, Plainsboru, NJ, USA	collagen type I	4 years	4 cm
Neuromend	Collagen Matrix, Inc., Franklin Lakes, NJ, USA	collagen type I	4–8 months	2.5 cm
Neuromatrix/Neuroflex	Collagen Matrix, Inc., Franklin Lakes, NJ, USA	collagen type I	4–8 months	2.5 cm
Neurotube	Synovis Micro Companies Alliance, Birmingham, AL, USA	woven polyglycolic acid (PGA)	6–12 months	3 cm
Neurolac	Polyganics Inc., The Netherlands	poly(DL-lactic-co-ε-caprolactone) (PLCL)	2–3 years	3 cm
Salubridge/Hydrosheath or Salutunnel	Salumedica LLC, Atlanta, GA, USA	Salubria—polyvinyl alcohol (PVA) hydrogel	non-biodegradable	6.35 cm
Surgisis Nerve Cuff/ Axoguard	Cook Biotech Products, West Lafayette, IN, USA	porcine small intestinal submucosa (SIS) matrix	not reported	4 cm
AxonScaff/Cellscaff/ StemScaff (filing for CE and FDA approval)	Axongen, Umeå, Sweden	polyhydroxybuturate (PHB)	not reported	not reported

Figure 4.1: Current clinically approved and upcoming nerve guidance conduits [5].

Despite some success in nerve repair, these hollow conduits fail to match the regenerative levels of autograft and show poor functional recovery [5, 28]. Therefore, there is still an active area of intense research to find new biomaterials, able to better interact with cells, more flexible and processed by less expensive methods to create new conduits for peripheral nerve repair [26].

An attractive feature of electrospinning process is the ability to fabricate fibrous tubular assemblies with tunable three-dimensional (3D) microarchitecture [29] obtained by direct deposition of nanofibers onto a rotating mandrel [29-32]. According to other studies [33, 34], the investigation of cell/materials interaction (see Chapter 3), has revealed that even the combined contribution of biochemical cues may support the main cellular events triggering cell adhesion and neurite out-growth over the fiber architecture.

Consequently, this study is aimed to design and fabricate nerve conduits with interconnected pores and able to resist structural collapse during implantation by using electrospinning technique [35].

Poly(ε-caprolactone) (PCL) and PCL/Gelatin electrospun tubular conduits are proposed as a nerve guidance channel for complex motor nerve regeneration. We previously investigated the biocompatibility of nanofibers, so demonstrating their non-cytotoxic response and their ability to provide a favorable environment that supports the growth of cell lines [34, 36, 37]. Here, we identify the optimal process parameters to fabricate electrospun conduits and investigate morphological (i.e., fiber size scale, porosity) and functional (i.e., stiffness, interaction with primary cells) properties of the best prototypes.

4.2. EXPERIMENTAL SECTION

4.2.1 Materials

PCL pellets (M_n 45 kDa) and Gelatin of type B (~225 Bloom), from bovine skin in powder form, were all purchased from Sigma-Aldrich (Italy), while 1,1,1,3,3,3-hexafluoro-2-propanol (HFP) was supplied by Fluka (Italy) and chloroform ($CHCl_3$) by J.T. Baker (Italy). All products were used as received without further purifications.

A 1:1 (weight ratio) polymer solution of PCL and Gelatin was prepared by firstly dissolving the polymers separately in HFP for 24 h under magnetic stirring and then mixing them in order to obtain a solution with a final polymer concentration of 0.1 g/ml.

Alternatively, PCL was dissolved in chloroform at a concentration of 0.33 g/ml. The solution was kept under magnetic stirring at room temperature until a clear solution was obtained.

4.2.2 Preparation of electrospun conduits

Electrospun fibers were obtained by using a commercially available electrospinning setup (Nanon01, MECC, Japan). The polymer solution was placed in a 5 ml plastic syringe connected to a needle with a tip diameter of 18 Gauge. At the first stage, fibers were randomly collected over a grounded aluminium foil target in order to obtain flat membranes. Different process parameters were selected to optimize the final fiber morphology: in particular for PCL/Gelatin platforms a distance of 8 cm, a voltage of 13 kV and a flow rate of 0.5 ml/h were set while for PCL fibers the selected parameters were 15 cm, 20 kV, 0.5ml/h. The process was carried out in a vertical configuration, and the deposition time was adequate to obtain the proper thickness (~ 150 μm) to remove the membranes from the grid. Tubular nerve conduits were developed by collecting fibers onto a 1.5 mm diameter metal mandrel, with an imposed rotating rate of 50 rpm.

4.2.3 Morphological characterization

Qualitative evaluation of fibers morphology of the electrospun PCL and PCL/Gelatin membranes/tubes was performed by field emission scanning electron microscopy (FESEM, QUANTA200, FEI, The Netherlands). Samples were dried in the fume hood at least for 24 h in order to remove any residual solvent, mounted on metal stubs and sputter-coated with gold-palladium for about 20 sec in order to get a 19 nm thick conductive layer. SEM images were taken under high vacuum conditions (10^{-7} torr) at 10 kV, using the secondary electron detector (SED). On selected SEM images, the fiber diameter distribution, the mean total porous area and the % porosity were determined by using freeware image analysis software (NIH Image J 1.37).

4.2.4 Mechanical testing

Mechanical characterization was achieved by applying tensile test loads to specimens prepared from the electrospun non-woven fiber mats. Sufficient care must be taken in preparing and then gripping the tensile specimens in order to avoid severe damage of the membranes. After the aluminum foil was carefully peeled off, specimens (n=10/group) were cut fixing the following dimensions of width and length: (0.5x3) cm. Specimen thicknesses were measured using a digital micrometer in 4 points in each samples and averaged. Finally, tapes were applied onto the gripping areas as end-tabs and samples were hydrated with distilled water.

The tensile testing was performed by using a dynamometric machine (Instron 5566, Germany) with a load cell of 2.5 N. Cross-head speed of 3 mm/min was used for all of the specimens tested. The machine-recorded data were used to process the tensile stress–strain curves of the specimens.

Transverse compression testing of PCL and PCL/Gelatin tubes was performed by using again a dynamometric machine (Instron 5566). The length of samples (n=5/group) was 7 mm and the tube wall thickness was measured before testing. All the tubes were hydrated before testing by soaking them in deionized water. The crosshead speed was maintained at 1 mm/min. The compressive strengths of PCL and PCL/Gelatin tubes were reported against the displacement values. Results are expressed as means ± standard deviations on five different samples (n =5).

4.2.5 Biological response in vitro

The flat membranes were cut into 6 mm discs and placed into 96-well tissue culture plates for biological characterization. Prior to the biological assays, PCL and PCL/Gelatin electrospun scaffolds were sterilized by immersion in 70% of ethanol (v/v) with antibiotic solution (streptomycin 100 μg/mL and penicillin 100 U/mL) for 30 min, washed three times with phosphate-buffered saline (PBS) and air dried.

All sterilized samples were immersed in Dulbecco's Modified Essential Medium (DMEM) for 24 h prior to plating undissociated lumbar Dorsal Root Ganglion (DRG), dissected from E15 chick embryos incubated at 37°C. After 24 and 72 h of seeding, cells were fixed with 4% paraformaldehyde (PFA) and stained with NF-200 antibody in order to observe the neurite extension by fluorescence microscopy. All experiments were run in triplicate.

4.3 RESULTS

In this study, PCL and PCL/Gelatin platforms were fabricated by electrospinning technique to explore their application as nerve guidance substrates. A flat aluminum target and a rotating mandrel were used to produce flat membranes and tubes, respectively (Figures 4.2 A and 4.3 A).

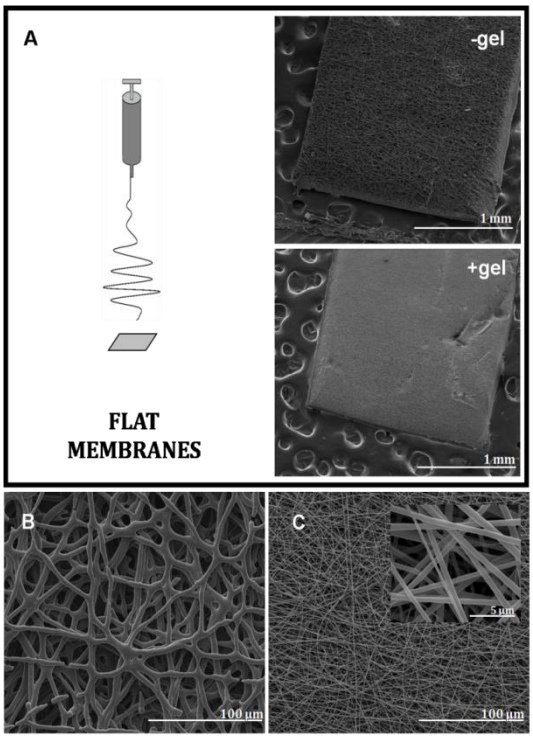

Figure 4.2: A) Electrospinning setup for flat membranes production; SEM images of PCL (B) and PCL/Gelatin (C) flat membranes.

Micrometer size PCL fibers with average diameter of (5.61 ± 0.8) µm were produced from a 0.33 g/ml solution of PCL in chloroform - solvent with low polarity (Figure 4.2 B). PCL/Gelatin fibers (Figure 4.2 C) obtained from a solution in HFP - higher polarity solvent - showed characteristic sizes in a submicrometric range with an average diameter of (0.59 ± 0.15) µm, confirming that polymer concentration and solvent polarity significantly influenced the fiber diameter as introduced in Chapter 2. Figures 4.3 B and C show SEM images of PCL and PCL/Gelatin fibers along the surface of the electrospun tube. The use of rotating collectors did not evidently influence fiber morphology.

The distribution of fiber diameter was assessed by using image analysis as shown in Figure 4.4 A. PCL/Gelatin fibers were shown to have a narrower diameter distribution in comparison to PCL samples, by statistical modes of 0.70 and 4.75 µm and skewness of 0.26 and 0.40. Mesh porosity (%) and the mean total porous area (μm^2), plotted in Figure 4.3 D were calculated by using an inverse contrast tool (Figures 4.4 B-C) on SEM images. Porosity was comparable for PCL (35.47 ± 3.66) % and PCL/Gelatin, (36.05 ± 2.86) % electrospun conduits, but the mean area was much greater for PCL (76562.0 ± 7861.3) μm^2 as compared to the bicomponent scaffold (776.33 ± 62.76) μm^2.

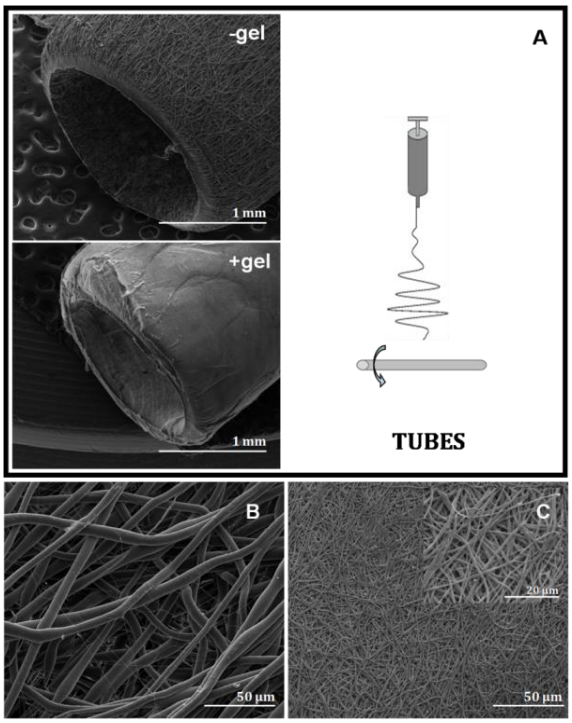

Figure 4.3: A) Electrospinning setup for nerve conduits production; SEM images of PCL (B) and PCL/Gelatin (C) tubes.

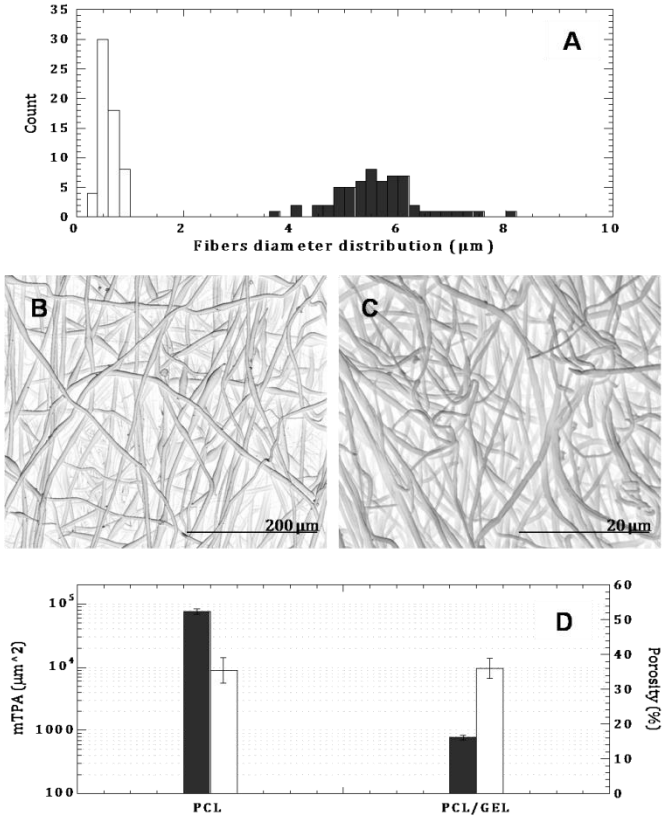

Figure 4.4: Image analysis data: A) fibers diameters distribution for PCL (■) and PCL/Gel samples (□); SEM images with inverse contrast of PCL (B) and PCL/gel (C) samples; D) Mean Total Porous Area (mTPA, ■) and porosity (□) for PCL and PCL/Gelatin fibers.

The tensile stress-strain curves of electrospun PCL and PCL/Gelatin membranes are shown in Figure 4.5. The averaged tensile modulus and the ultimate tensile strain and stress are summarized in Table 4.1

As evident from tensile stress-strain curves PCL membranes presented higher elastic modulus and stress at break but lower strain at break comparing to PCL/Gelatin membranes.

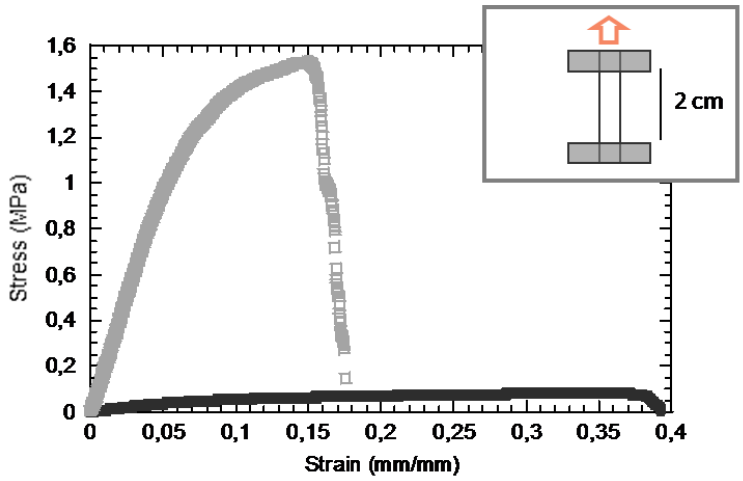

Figure 4.5.: Representative tensile stress-strain curves of PCL (■) and PCL/Gelatin (■) membranes

Table 4.1.: Averaged tensile modulus, ultimate tensile strain and stress.

	Elastic Modulus (MPa)	**Strain at break (mm/mm)**	**Stress at break (MPa)**
PCL	18.71 ± 6.85	0.17 ± 0.05	1.45 ± 0.24
PCL/GEL	0.79 ± 0.28	0.39 ± 0.16	0.10 ± 0.02

The transverse compressive strengths of electrospun tubes were measured by applying a transverse displacement to the longitudinal axis (Figure 4.6 A) and analyzing the resulting load. Analysis of the load-displacement curves in Figure 4.6 B, showed that PCL/Gelatin tubes possessed lower load-bearing ability and compressive strength than PCL tubes for displacement values up to 50%. This difference was evident mainly for low displacement (< 0.1) as reported in Figure 4.6 C.

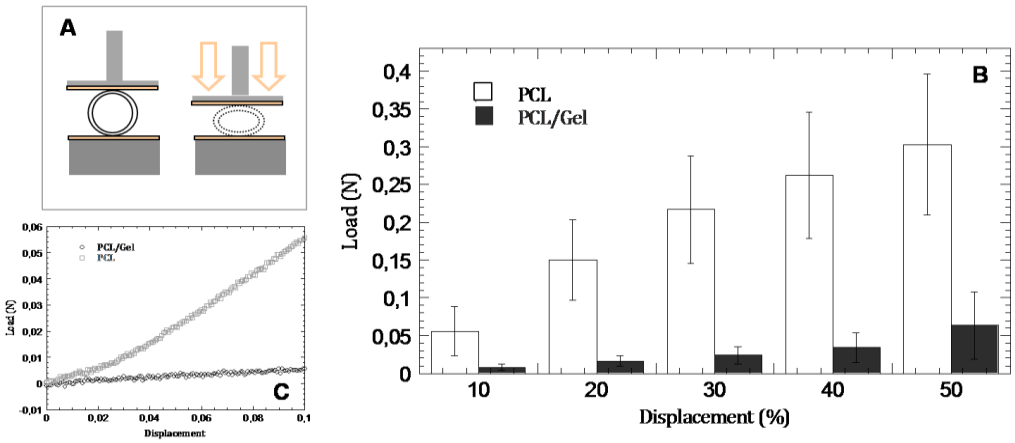

Figure 4.6: Transverse compressive tests on PCL and PCL/Gelatin conduits: A) Scheme of the mechanical test; B) load vs displacement comparative histogram; C) load-displacement curve for small displacement (< 0.1).

Before evaluating artificial nerve conduits *in vivo*, the biocompatibility of electrospun PCL and PCL/Gelatin fibrous substrates was tested *in vitro* with primary cells using Dorsal Root Ganglia (DRGs). DRGs were seeded on the electrospun fibers and on tissue culture plates (TCP) coated with laminin. DRGs were fixed at two time points (24h and 72h) to evaluate neurite extension by fluorescence microscopy. After 24 h, DRGs adhered on all the examined samples (Figure 4.7-top row), but neurite extension was mainly observed in PCL/Gelatin membranes (Figure 4.7 C) and TCP controls (Figure 4.7 E). After 72 h, neurites appeared to have extended along the fiber axes outward from the main DRG body without any directional preference, therefore exhibiting a circular appearance (Figure 4.7-bottom row). Neuritis have preferentially grown in the case of PCL/Gelatin membranes (Figure 4.7 D) and TCP laminin coated (Figure 4.7 F), less for PCL scaffolds (Figure 4.7 B).

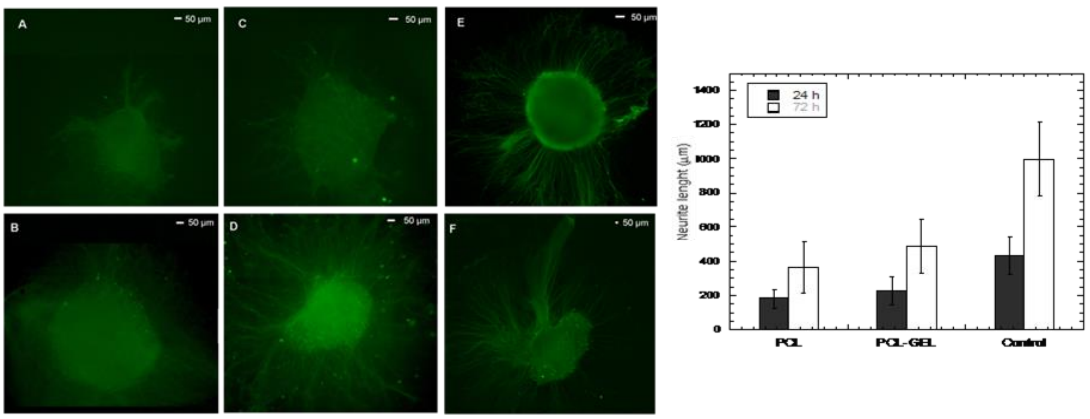

Figure 4.7: Biological validation *in vitro*: DRG's confocal images after seeding 24h (A-C-E) and 72h (B-D-F) on PCL (A-B), PLC/Gelatin (C-D) substrates and on the control (E-F).

4.4 DISCUSSION

Electrospinning currently represents a good choice to develop scaffolds made of nano or micrometric fibers by using different kind of materials, as supporting device for nerve regeneration. In particular PCL, an aliphatic and degradable polyester, has good tensile properties and slow degradation kinetics, suitable characteristics to make a scaffold for peripheral nerve repair. Unfortunately, its bioinert and hydrophobic properties limit its use as a biomedical material [38]. In Chapter 3, it has been demonstrated that mixing PCL with a natural protein, i.e. gelatin, to produce electrospun membranes, induced increased adhesion, proliferation, viability and differentiation of rat pheochromocytoma PC-12 cells [34].

According to previous promising results, here, PCL and PCL/Gelatin fibers were collected on a rotating mandrel in order to produce conduits as graft for nerve repair. Tubes morphology has been investigated in terms of fiber size and porosity and compared with fibers from 2D electrospun membranes.

From SEM analysis, no significant change in terms of fibers morphology has been observed in electrospun conduits compared to 2D fibrous membranes confirming that diameter and morphology of electrospun fibers are controlled mostly empirically, as a function of solution concentration, molecular weight of the polymer and of different polymers ratios [39].

In our case, the interaction of the polymer solution with the electric field has been altered by changing the polymer/solvent system, i.e., switching from PCL/Gelatin/HFP solution to PCL/chloroform – thus affecting the final morphology of fibers. Moving from high polarity fluorinated solvents, as HFP, to apolar solvent, as chloroform, higher net charge density in solution is promoted. This is ascribable to the enhanced stretching of the jet and therefore the formation of thinner fibers [40]. We demonstrate that higher concentration of PCL/chloroform solutions prevent the jet segment stretching under the effect of the constant Coulomb force, due to an increased viscoelastic force, so fibers with larger diameters, up to an order of magnitude, are obtained.

Hence, a narrower fiber diameter distribution was detected by image analysis in the case of PCL/Gelatin/HFP solution. According to Chapter 2 data on fiber size, the use of polymer solutions with higher relative dielectric permittivity leads to the creation of electrospun membranes with a narrower distribution of fiber diameters [40-41]. As consequence of different fibers size scale, the mean total porous area (μm^2) is greater for PCL micrometric scaffolds respect to PCL/Gelatin, without any noticeable difference in terms of total mesh porosity (%) as expected.

Moreover it was essential to explore the mechanical behavior of nerve conduits. Indeed, good flexibility and tailored degradation rate are also important factors for a tissue-engineered conduit to resist tearing and stretching forces and retain stable shape during nerve regeneration process [42]. If

nerve conduits show large rigidity, it might exert chronic compression to regenerated nerves. Besides, an excessive softness of device does not assure an adequate mechanical support, also limiting the handling during implant surgery. Consequently, the conduits do not bear forces, thus collapsing *in vivo*.

The combination of PCL and gelatin with ratio of 50/50 by weight gave rise to loose and weak structure compared to pure PCL [43]. Indeed, tensile test made on electrospun membranes confirmed that PCL/Gelatin samples had a low elastic modulus and stress at break, in comparison with PCL. All tests were performed on hydrated samples in order to mimic *in vitro* and *in vivo* conditions.

Furthermore, to verify the ability of electrospun conduits to withstand the compression exerted by the surrounding tissues, transverse compressive test were carried out and PCL/Gelatin conduits showed lower load bearing ability respect to PCL tubes, appearing less suitable for stand stresses during the surgical procedure and implantation time.

On the other hand, biological tests showed that the neurite extension of DRGs seeded on electrospun membranes was more pronounced on PCL/Gelatin substrates than PCL scaffolds, in agreement with PC-12 cells interactions results on electrospun PCL and PCL/Gelatin fibers [34]. This is probably due to the fact that gelatin is a natural biopolymer derived from collagen by controlled hydrolysis and has structural similarity to collagen. Therefore, the inclusion of gelatin into PCL enhances the interaction of the cells with the scaffolds by engaging cell-adhesion molecules which then permit the cells to exert/generate higher interaction forces [43].

4.5 CONCLUSION

Here, our objective was the design and characterization of PCL and PCL/Gelatin conduits produced via electrospinning for peripheral nerve regeneration.

Results demonstrated that the use of rotating mandrel does not affect fibers morphology in both cases - PCL and PCL/Gelatin. Only mechanical properties of the electrospun conduits were strongly influenced by the amount of gelatin in the fibers (PCL-Gelatin ratio is 50:50).

Further *in vitro* characterization with primary cells, i.e. DRGs, also confirmed that the fibrous scaffolds are able to support cell attachment and neurite extension, in particular PCL/Gelatin substrates improved neurite outgrowt from DRGs principal body.

Present findings represent an encouraging knowledge on which to base the evaluation of *in vivo* regeneration process in rat sciatic nerve model.

REFERENCES

[1] Bian YZ, Wang Y, Aibaidoula G, Chen GQ, Wu Q. Biomaterials. 2009; 30: 217-225.

[2] Nakayama K, Takakuda K, Koyama Y, Soichiro I, Wei W, Tomokazu M, Noriaki S. Artif Organs. 2007; 31: 500-508.

[3] Schnell E, Klinkhammer K, Balzer S, Gary B, Doris K, Paul D, Mey J. Biomaterials. 2007; 28: 3012-3025.

[4] de Boer R, Knight AM, Borntraeger A, Hebert-Blouin MN, Spinner RJ, Malessy MJA, Yaszemski MJ, Windebank AJ. Microsurgery. 2011; 31(4): 293-302.

[5] Daly W, Yao L, Zeugolis D, Windebank A, Pandit A. *J R Soc Interface.* 2012; **9**: 202-221.

[6] Ijpma FFA, Van De Graaf RC, Meek MF. J Hand Surg. 2008; 33: 581-586.

[7] Lundborg G. J Hand Surg. 2000; 25: 391-414.

[8] Cao H, Liu T, Chew SY. Adv Drug Deliver Rev. 2009; 61: 1055-1064.

[9] Wang XD, Hu W, Cao Y, Yao J, Wu J, Gu XS. Brain. 2005; 128: 1897-1910.

[10] Liu B, Cai SX, Ma KW, Xu ZL, Dai XZ, Yang L, Lin C, Fu XB, Sung KL, Li XK. J Mater Sci Mater Med. 2008; 19: 1127-1132.

[11] Oh SH, Kim JH, Song KS, Jeon BH, Yoon JH, Seo TB, Namgung U, Lee IW, Lee JH. Biomaterials. 2008; 29: 1601-1609.

[12] Mohanna PN, Terenghi G, Wiberg M. Scand J Plast Recons. 2005; 39: 129-137.

[13] Young RC, Wiberg M, Terenghi G.Br J Plast Surg. 2002; 55: 235-240.

[14] Lu MC, Hsiang SW, Lai TY, Yao CH, Lin LY, Chen YS. J Biomater Sci Polym Ed. 2007; 18: 843-863.

[15] Chen YS, Chang JY, Cheng CY, Tsai FJ, Yao CH, Liu BS. Biomaterials 2005; 26: 3911-3918.

[16] Chen MH, Chen PR, Chen MH, Hsieh ST, Huang JS, Lin FH. J Biomed Mater Res Part B Appl Biomater. 2006; 77B: 89-97.

[17] Kim SW, Bae HK, Nam HS, Chung DJ, Choung PH. Macromol Res. 2006; 14: 94-100.

[18] Ahmed MR, Vairamuthu S, Shafiuzama M, Basha SH, Jayakumar R. Brain Res. 2005; 1046: 55-67.

[19] Li WS, Guo Y, Wang H, Shi DJ, Liang CF, Ye ZP, Qing F, Gong J. J Mater Sci Mater Med. 2008; 19: 847-854.

[20] Waitayawinyu T, Parisi DM, Miller B, Shai L, Holly JM, Simon HC, et al. J Hand Surg Am Vol 2007;32A:1521–9.

[21] Lu GY, Kong LJ, Sheng BY, Wang G, Gong YD, Zhang XF. Eur Polym J. 2007; 43: 3807-3818.

[22] Wang AJ, Ao Q, Cao WL, Yu MZ, He Q, Kong LJ, Zhang L, Gong YD, Zhang XF. J Biomed Mater Res Part A. 2006; 79A: 36-46.

[23] Zhang P, Xu H, Zhang D, Fu Z, Zhang H, Jiang B. Artif Cells Blood Substit Immobil Biotechnol. 2006; 34: 89-97.

[24] Wang AJ, Ao Q, Wei YJ, Gong K, Liu XS, Zhao NN, Gong YD, Zhang XF. Biotechnol Lett. 2007; 29: 1697-1702.

[25] Uebersax L, Mattotti M, Papaloizos M, Merkle HP, Gander B, Meinel L. Biomaterials. 2007; 28: 4449-4460.

[26] Yang Y, Ding F, Wu H, Hu W, LiuW, Liu H, et al. Biomaterials. 2007; 28: 5526-5535.

[27] Willerth SM, Sakiyama-Elbert SE. Adv Drug Deliv Rev. 2007; 59: 325-338.

[28] Ribeiro-Resende VT, Koenig B, Nichterwitz S, Oberhoffner S, Schlosshauer B. Biomaterials. 2009; 30: 5251-5259.

[29] Zhang D, Chang J. Nano Letters. 2008; 8(10): 3283-3287.

[30] He W, Ma Z, Teo WE, Dong YX, Robless PA, Lim TC, Ramakrishna S. J Biomed Mater Res. 2009; 90A: 205-216.

[31] Inoguchi H, Kwon IK, Inoue E, Takamizawa K, Maehara Y, Matsuda T. Biomaterials. 2006; 27: 1470-1478.

[32] Williamson MR, Black R, Kielty C. Biomaterials. 2006; 27: 3608-3616.

[33] Neal RA, McClugage SG, Link MC, Sefcik LS, Ogle RC, Botchwey EA. Tissue Eng. 2009; 15 (1): 11-21.

[34] Alvarez-Perez MA, Guarino V, Cirillo V, Ambrosio L. *Biomacromolecules. 2010;* 11: 2238-2246.

[35] Bini TB, Gao S, Wang S, Ramakrishna S. *J Mater Sci Mater Med.* 2005; 16: 367-375.

[36] Subramanian A, Krishnan UM, Sethuraman S. *Journal of Biomedical Science.* 2009; **16**: 108-112.

[37] Guarino V, Alvarez-Perez MA, Cirillo V, Ambrosio L. J Bioact Comp Pol. 2011; 26(2): 144-160.

[38] Zhu Y, Wang A, Patel S, Kurpinski K, Diao E, Bao X, Kwong G, Young WL, Li S. Tissue Eng. 2011; 17(7): 705-715.

[39] Chew SY, Wen Y, Dzenis Y, Leong KW. *Curr Pharm Des. 2006;* 12(36): 4751-4770.

[40] Guarino V, Cirillo V, Taddei P, Alvarez-Perez MA, Ambrosio L. Macromol Biosci 2011; 12: 1694-1705.

[41] Son WK, Youk JH, Lee TS, Park WH. Polymer. 2004: 45: 2959-2966.

[42] Wang W, Itoh S, Matsuda A, Ichinose S, Shinomiya K, Hata Y, Tanaka J. *J Biomed Mater Res A.* 2008; 84(2): 557-566.

[43] Ghasemi-Mobarakeh L, Prabhakaran MP, Morshed M, Nasr-Esfahani MH, Ramakrishna S. Biomaterials. 2008; 29: 4532-4539.

CHAPTER 5

PCL and PCL/Gelatin Electrospun Conduits for *in Vivo* Implant in Rat Sciatic Nerve Model

5.1. INTRODUCTION

The incidence of nerve traumatic injuries is estimated to be more than 500000 new patients annually [1]. Once peripheral nerve is transected, Wallerian degeneration occurs in all of the axons distal to the injury site [2], as shown in Figure 5.1, whereby the axoplasmic microtubules and neurofilaments disintegrate due to a calcium dependent proteolytic process [3]. These rapid events occur as the axon is separated from its trophic (nutritive) source in the nerve cell body (located in the spinal cord, dorsal root ganglia, or autonomic ganglia) [4].

After injury, circumstanced regeneration may occur, resulting in partial or total loss of motor, sensory and autonomic functions in the involved segments of the body. However, regeneration across extended nerve gaps must be even surgically facilitated [5].

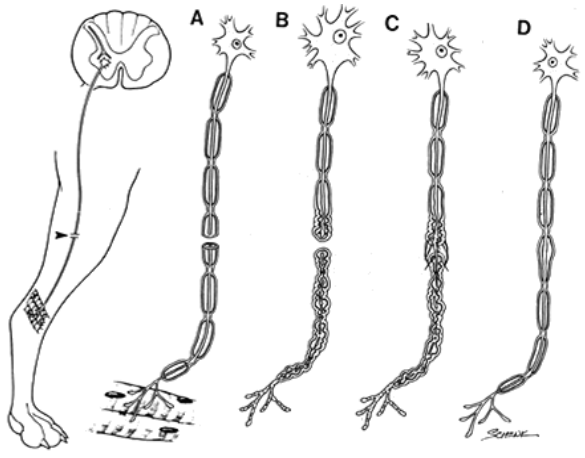

Figure 5.1: Schematic description of nerve injury. After transection of axons (A), morphologic hypertrophy of nerve cell body to aid in biosynthetic regeneration is demonstrated. All neural degenerate in the distal stump (B). Axoplasmic filaments arise from the proximal stump in an attempt to recannulate the distal Schwann cell tube (C). After proper recannulation, all axoplasmic migration is directed into the distal fragment for regeneration (D) [6].

Currently, there are a variety of microsurgical repair methods available, including direct repair, autograft/allograft transplantation and the use of hollow nerve guidance conduit repair [4-9]. Direct nerve repair (also known as end-to-end suturing, end-end repair, end-to-end neurorrhaphy or end-to-end coaptation) is the preferred method of treatment for peripheral nerve repair for gaps shorter than 5 mm [2]. Since it requires tension-free suturing of the injury site [10], for optimal regeneration, the nerve stumps must be correctly aligned and repaired with minimal tissue damage, using the minimal number of sutures. Since the nerve stumps sometimes cannot be directly coapted without producing tension, the gap must instead be bridged, most commonly by autografted nerve segments. However, autologous graft bridging is limited by deficiency of donor nerves and by several drawbacks, such as the need of a secondary surgery and the loss of donor site function. Furthermore, autografts show several drawbacks in the suturing practice, due to mismatch in dimension and modality between the injured and donor nerves [7-9]. Hence, engineered guidance channels have been explored as an alternative to autografts for the repair of nerve injury.

The understanding of the natural regenerative process in hollow silicon tube may be informative to design ideal artificial graft also supporting the interpretation of the *in vivo* results [2]. Briefly, this regenerative process can be divided into five main phases: (1) the fluid phase; (2) the matrix phase; (3) the cellular migration phase; (4) the axonal phase; and (5) the myelination phase (Figure 5.2) [11].

Belkas et al. reported spatial and temporal sequences in which various nerve regeneration events occurred across a 10 mm rat sciatic nerve gap within a silicone chamber [2, 12]. A clear tissue fluid containing neurotrophic factors and extracellular matrix (ECM) precursor molecules (e.g. fibrinogen and factor XIII) from the damaged nerve ends, fills the chamber by 3-6 hours. During the first week, acellular matrix, largely made of fibrin, is formed between the proximal and distal stumps [2, 12, 13].

During the second week of repair, Schwann cells (SC) from the proximal and distal nerve stumps, as well as some endothelial cells and fibroblasts, migrate along this fibrin cable [2, 14]. The formation of this fibrin matrix is critical for regeneration. If a matrix fails to form, as can happen when a tube is used to repair a long gap, no regeneration may occur [15]. These SC subsequently proliferate and align themselves, forming an aligned SC cable, i.e. glial bands of Büngner [11]. This formed biological tissue provides a trophic and topographical tissue cable for the axonal phase of repair. Axons appear inside the chamber by the second week, and even then only cover the first proximal 1-3 mm. Some non myelinated axons cross the 10 mm gap by the third week. By week 4, myelinated axons can be seen at the chamber midpoint. SC and fibroblasts advance ahead of the axons in the first few weeks and blood vessels lag behind them.

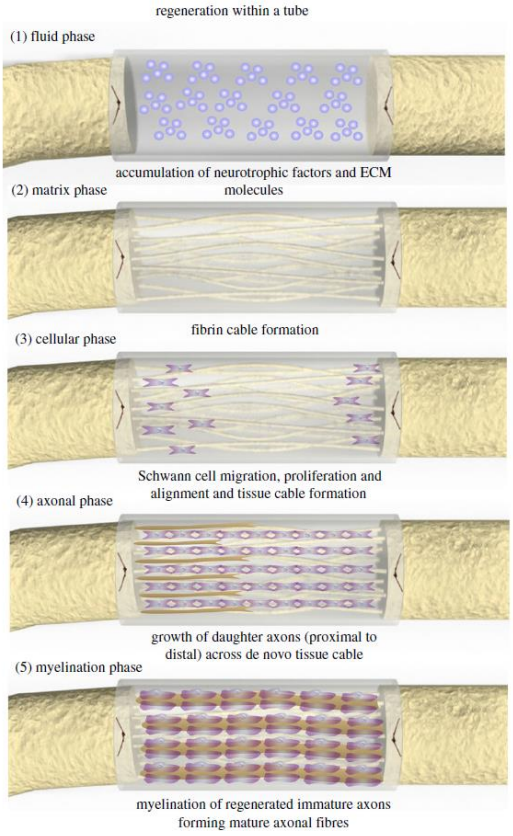

Figure 5.2: Regenerative sequence occurring within a hollow NGC. This regenerative process occurs in five main phases: (1) the fluid phase: plasma exudate fills the conduit resulting in accumulation of neurotrophic factors and ECM molecules; (2) the matrix phase: an acellular fibrin cable forms between the proximal and distal nerve stumps; (3) the cellular phase: Schwann cells, endothelial cells and fibroblasts migrate (from the proximal and distal nerve stumps), align and proliferate along the fibrin cable forming a biological tissue cable; (4) axonal phase: re-growing axons use this biological tissue cable to reach their distal targets; (5) myelination phase: Schwann cells switch to a myelinating phenotype and associated with regenerated axons forming mature myelinated axons [11].

Hence, a number of criteria for the ideal hollow conduit can be outlined, including: (i) limiting scar infiltration, while allowing diffusion of nutrients into the conduit and wastes to exit the conduit; (ii) providing sufficient mechanical properties for structural support; (iii) exhibiting a low immune response; and (iv) biodegradability, to remove the need for secondary surgery and to prevent chronic inflammation and pain caused by nerve compression due to the eventual collapse of implanted nerve conduits [16].

We previously developed a bicomponent tubular conduit by mixing poly(ε-caprolactone) (PCL) with gelatin using electrospinning technique. The electrospun PCL/Gelatin conduits are non-cytotoxic, porous, biodegradable and provide a favorable environment that supports the growth of cells, due to its interconnected porosity. We hypothesized that electrospun tubular conduit may be used as a nerve guidance channel for complex motor nerve regeneration. Hence, we compare the *in vivo* response of PCL and PCL/Gelatin conduits implanted in a 5 mm rat sciatic nerve defect until

18 weeks. We examined the levels of nerve function restoration using various assessment modalities, including electrophysiologic tests, muscle weights and histological evaluations.

5.2. EXPERIMENTAL SECTION

5.2.1 In vivo implants

In vivo study was performed at New Jersey Center for Biomaterials (USA) in collaboration with the group of Dr. J. Kohn. Eighteen female Lewis rats weighing 200 g were used for this study. Procedures were reviewed and approved by the Rutgers University Institutional Animal Care and Use Committee (IACUC). Rats were randomly assigned to one of three groups (n=6 rats/group). Prior to surgery, rats were anesthetized using an intraperitoneal injection of ketamine/xylazine cocktail.

A 3 cm incision was made along the left femoral axis on the left leg. Gluteal muscles were carefully split and the sciatic nerve was exposed. A 5 mm nerve segment was resected 5 mm distal to the tendon of the internal obturator muscle. 7 mm long nerve conduits were secured to nerve stumps with two 9-0 ethilon sutures (Ethicon, Somerville, NJ) on either side, leaving a 5 mm gap.

In the autologous graft group, a 5 mm nerve segment was resected, flipped 180° and subsequently sutured back into the nerve using four 9-0 ethilon sutures on either side.

Muscle and skin were then closed with 6-0 ethilon sutures, respectively using single, separate sutures. Rats received buprenex for one week postoperatively. For autotomy prevention, all rats were treated daily after surgery with chew guard for one week, in addiction they had chow and water available *ad libitum*.

5.2.2 Electrophysiological recordings

Compound muscle action potentials (CMAPs) were recorded using a Viking Quest EMG system (Care Fusion, San Diego, CA). All rats were anesthetized and microelectrodes were placed in the appropriate foot musculature following three different approaches: a distal recording (DR) of signals was obtained placing the ground electrode at the Achilles tendon, the reference electrode at the lateral side of the fifth digit of the foot and the recording electrode at the plantar or dorsal side of the foot for the tibial or peroneal nerve, respectively, while applying a supramaximal stimulus, using bipolar electrodes placed 4 mm apart, just posterior of the tibia, distal to the injury site (distal stimulation, DS). Further distal recordings were taken with supramaximal stimulus applied proximal to the injury site (proximal stimulation, PS). Moreover, potentials were also recorded proximally to the injury site (proximal recording, PR) by placing the recording electrodes directly into tibialis anterior and gastrocnemious muscles, respectively innervated by peroneal and tibial

nerve branches, while applying supramaximal stimulus proximal to the injury site. CMAPs were recorded starting 10 days postoperatively and at 4 week intervals for 18 weeks. Electrophysiological response was characterized by calculating the peak amplitude and latency and reported in three cases: proximal stimulation-proximal recording (PS-PR), proximal stimulation-distal recording (PS-DR), distal stimulation-distal recording (DS-DR), (Figure 5.3).

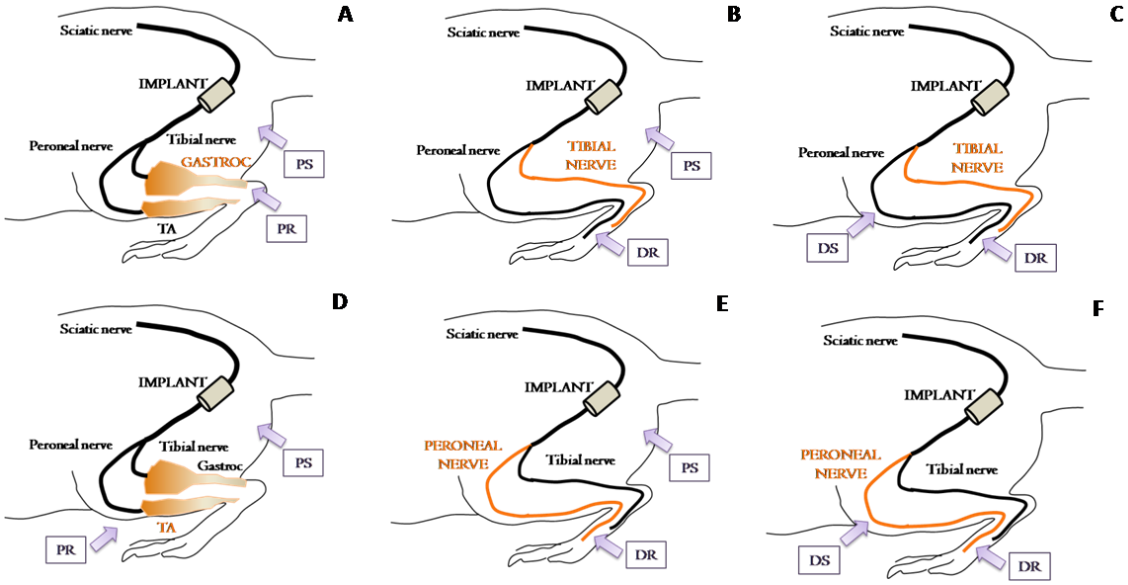

Figure 5.3: Tibial CMAP measured by placing the EMG electrodes in three different anatomical locations: A) Proximal stimulation (PS) - proximal recording (PR); B) Proximal stimulation (PS) - distal recording (DR); C) Distal stimulation (DS) - distal recording (DR). Peroneal CMAP measured by placing the EMG electrodes in three different anatomical locations: D) Proximal stimulation (PS) - proximal recording (PR); E) Proximal stimulation (PS) - distal recording (DR); F) Distal stimulation (DS) - distal recording (DR).

5.2.3 Nerve histology and muscle weight

After 18 weeks, rats were sacrificed and conduits harvested from animals were post-fixed in osmium tetroxide, and embedded in resin according to standard protocol. The mid tube segment of the nerve was embedded in resin and the proximal stump was transversely cut into 1 µm thick sections and stained with 1% toluidine blue/1% borax in distilled water. Images of sections were acquired using a camera connected to a microscope at a magnification of 50x and 100x. On selected images, total fiber diameter, axonal diameter and number of myelinated axons were measured. In addition, the ratio between axonal diameter and total fiber diameter, *G-ratio*, was calculated. For each type of implant, 9 random images were selected for quantification at 100x magnification.

Tibialis anterior and gastrocnemious muscles of both hind legs were also harvested during sacrifice and weighed to assess the recovery of the muscle weight after nerve regeneration and reinnervation.

5.3 RESULTS

The *in vivo* efficacy of electrospun nerve conduits was evaluated in a 5 mm rat sciatic nerve defect model (Figure 5.4). No mortalities occurred during the study but three rats (two from autologous group and one from PCL/Gelatin one) were sacrificed one day after surgery because of autophagia at the implant site.

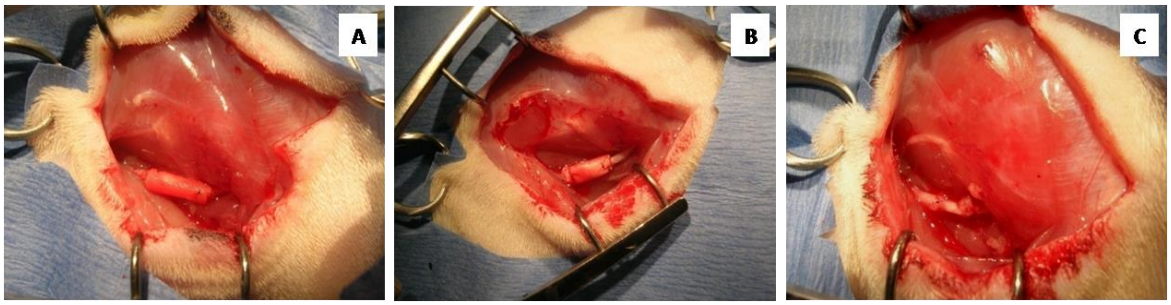

Figure 5.4: *In vivo* implants in rat sciatic nerve model: A) PCL implant; B) PCL/Gelatin implant; C) autologous graft.

CMAPs were measured in tibialis anterior and gastrocnemious muscles (PR) and at the dorsal and plantar foot muscles (DR) stimulating proximally and distally with respect to the injury site, every 4 weeks post-operatively. For PR measured from the gastrocnemius muscle belly (PS-PR), peaks with non-zero baseline amplitudes and greater latencies were measured after nerve transection (Figure 5.5 A). Increased amplitude and decreased latency were observed in all groups after 8 weeks.

As for distal recording from the distal foot muscle innervated by the tibial nerve, in case of proximal stimulation (PS-DR), signals completely disappeared after surgery (Figure 5.5 B). Potentials appeared again for the autograft group at 8 weeks, for PCL at 12 weeks and for PCL/Gelatin at 18 weeks. When distal stimulation and distal recording were considered (DS-DR), signals completely disappeared after surgery, but amplitude rose and latency decreased for the autograft group after 8 weeks and for PCL and PCL/Gelatin groups after 18 weeks (Figure 5.5 C).

For PR measured into the TA muscle (Figure 5.6 A) and for DR in the peroneal nerve in case of PS (Figure 5.6 B), measured potentials were analogous to the gastrocnemius and tibial nerve, respectively. When DS-DR was considered (Figure 5.6 C), again signals completely disappeared after surgery, but amplitude increased and latency decreased for the autograft group after 8 weeks, for PCL after 12 weeks and PCL/Gelatin after 18 weeks. However, in all cases, amplitudes at the 18-week endpoint were much smaller than their baseline levels while the latency values remain slightly above their baseline levels. The percentage of the amplitude at the endpoint with respect to the baseline levels for each group was calculated as the percent recovery of the CMAP amplitude and reported in Table 5.1 for both tibial and peroneal nerve.

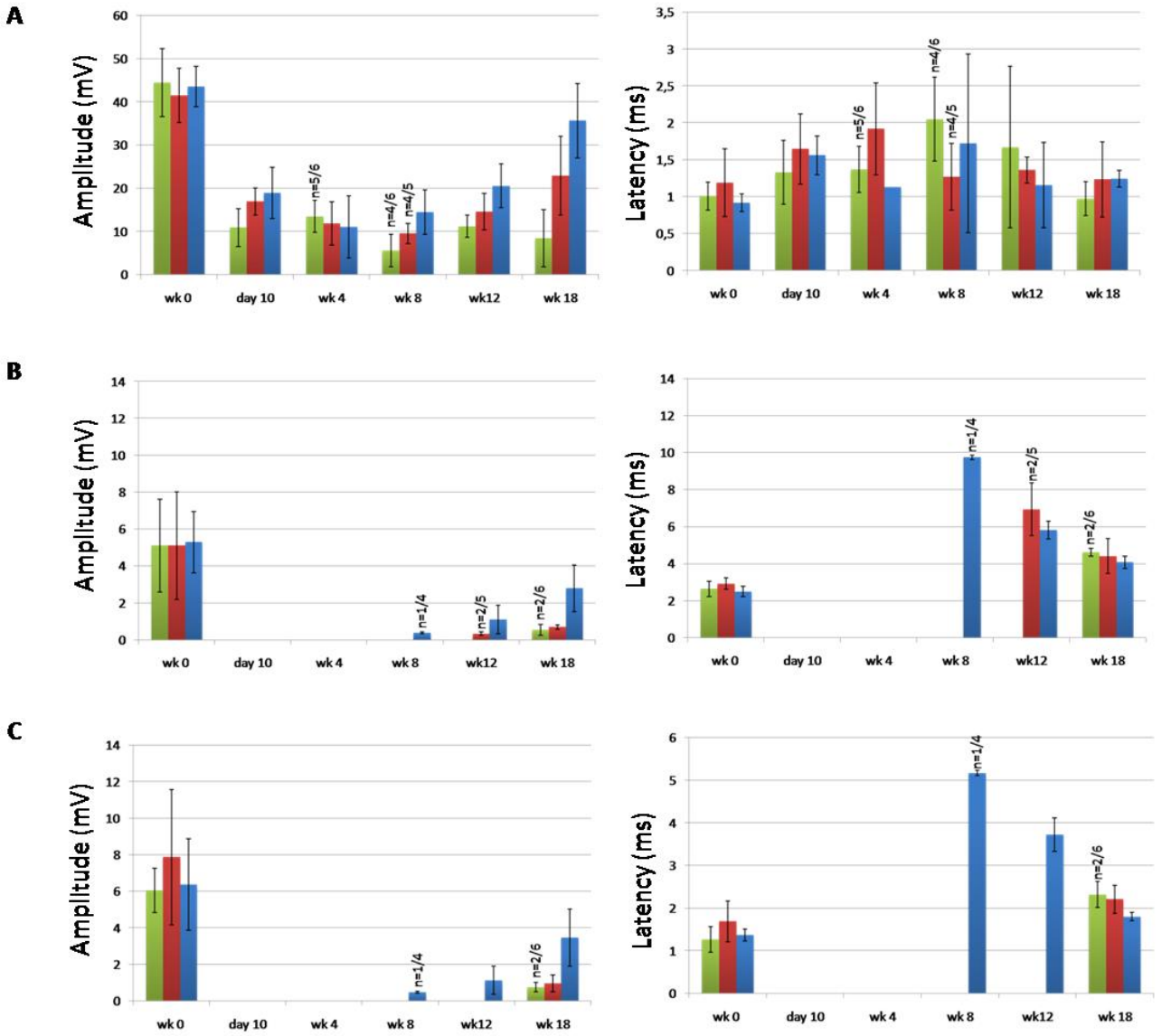

Figure 5.5: Electrophysiological recordings from the *in vivo* study. Tibial CMAP amplitude and latency, measured by placing the EMG electrodes in three different anatomical locations: A) Proximal stimulation (PS) - proximal recording (PR); B) Proximal stimulation (PS) - distal recording (DR); C) Distal stimulation (DS) - distal recording (DR). [PCL, n=5, ( ), PCL/Gelatin samples, n=6, ( ) and autograft, n=4, ( )]. The number of responding animals in each group is indicated above the bars, all animals are responding if not indicated.

The autograft group showed the best electrophysiological recovery, regaining 53-81% (tibial nerve) and 35-55% (peroneal nerve) of the baseline amplitude measured prior to injury. PCL and PCL/Gelatin groups were equivalent in the percentage of signal gain in distal recording modes while electrophysiological recovery was significantly greater in PCL grafts in the proximal recording mode for both tibial and peroneal nerve. Also when the number of responsive animals were taken into account, PCL and autograft groups with all animals responding with positive

CMAP amplitude were markedly better than the PCL/Gelatin group with only 2 out of 6 animals having a positive CMAP signal (4 out of 6 animals non-responsive by 18 weeks).

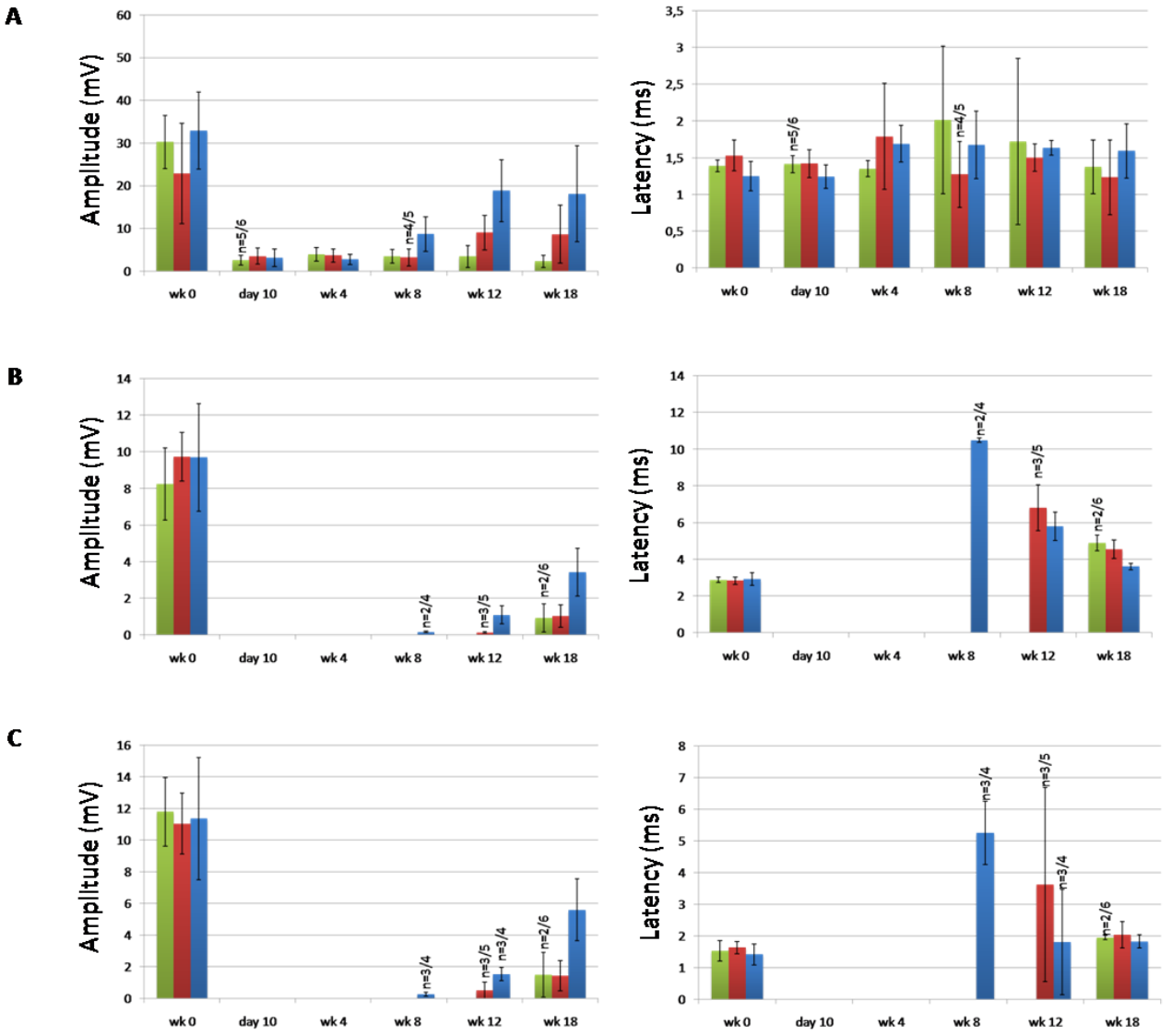

Figure 5.6: Electrophysiological recordings from the *in vivo* study. Peroneal CMAP amplitude and latency, measured by placing the EMG electrodes in three different anatomical locations: A) Proximal stimulation (PS) - proximal recording (PR); B) Proximal stimulation (PS) - distal recording (DR); C) Distal stimulation (DS) - distal recording (DR). [PCL, n=5, ( ), PCL/Gelatin samples, n=6, ( ) and autograft, n=4, ( )].

Table 5.1: Percent recovery of the CMAP amplitude for autograft, PCL and PCL/Gelatin implants measured at the study endpoint for tibial and peroneal nerve.

		AUTOGRAFT	PCL	PCL/GELATIN
TIBIAL NERVE	PS-PR	81	52	19
	PS-DR	53	13	10
	DS-DR	54	12	12
PERONEAL NERVE	PS-PR	55	36	8
	PS-DR	35	10	11
	DS-DR	49	13	13

TA and gastrocnemius muscle weights of the injured and healthy limbs were also measured at sacrifice and ratios of injured muscle weight to the healthy muscle weight are plotted in Figure 5.7. The autograft group had the highest degree of muscle weight recovery followed by the PCL group (Figure 5.7). The animals with the PCL/Gelatin implant had the worst muscle weight recovery, with both muscle groups greatly atrophied after 18 weeks of conduit repair.

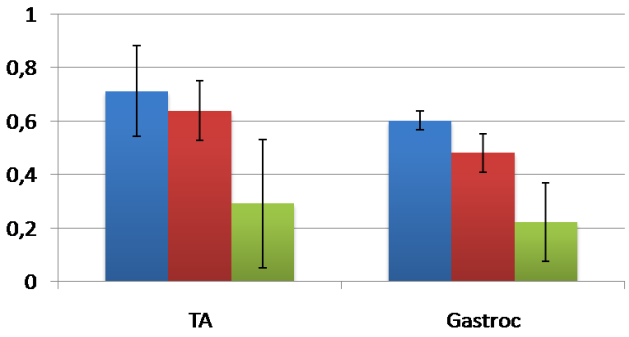

Figure 5.7: The ratio of the injured muscle weight to the healthy muscle weight in the tibialis anterior and gastrocnemius muscles 18 weeks post-op. [PCL, n=5, ( ), PCL/Gelatin samples, n=6, ( ) and autograft, n=4, ( )].

Histological and histomorphic analyses were performed to compare the morphology of the regenerated axons and the surrounding myelin sheet. Images of 1 μm thick toluidine-blue stained nerve mid-sections are shown in Figure 5.8, where rats implanted with PCL or autografts had robust nerve cables, while few myelinated axons and more inflammatory cells were present in PCL/Gelatin implants.

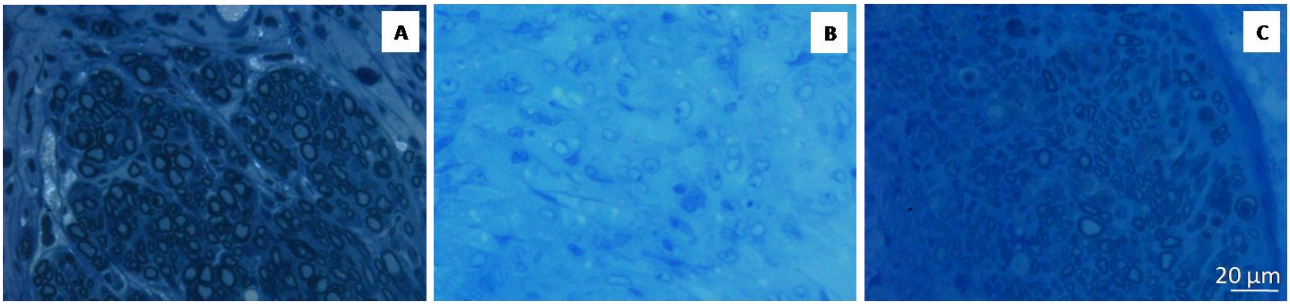

Figure 5.8: Images of 1 µm thick toluidine-blue stained nerve mid-sections of a) PCL implant; B)PCL/Gelatin implant, C) autograft (Magnification 50x).

A fibrous capsule layer, with a mean thickness of (71.53±28.43) µm, was formed on the outer surface of all PCL conduits (Figure 5.9 A, red arrows), while this layer was absent in the case of autografts and PCL/Gelatin implants (Figures 5.9 B-C).

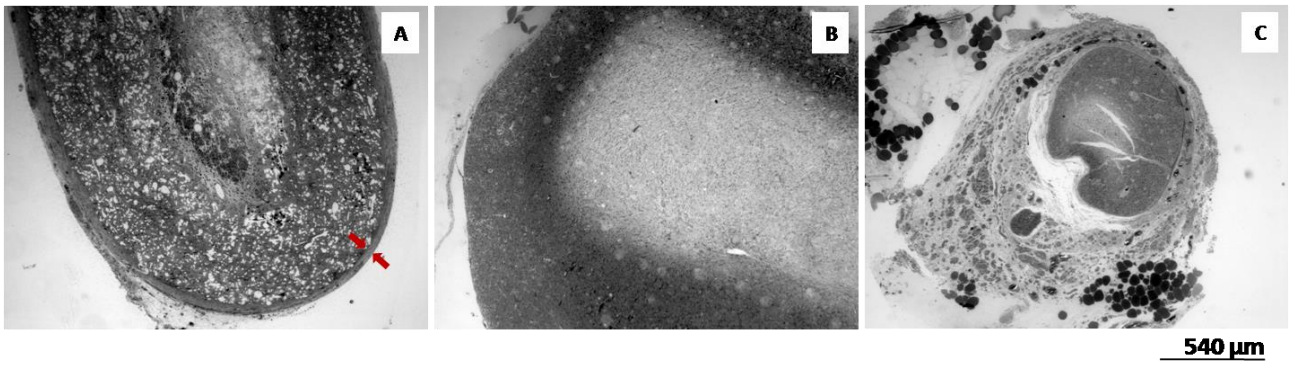

Figure 5.9: Images at low magnification (4x) of 1 µm thick toluidine-blue stained nerve mid-sections of a) PCL implant, red arrows indicate a fibrous capsule layer; B) PCL/Gelatin implant and C) autograft, absence of fibrous capsule.

The lumen of PCL tubes was also occupied with fibrous and connective tissue, which enclosed the axons and blood vessels (Figure 5.10 A) anyway myelinated axons are evident at higher magnification images (Figure 5.10 D). PCL/Gelatin implants induced a strong inflammatory response without any evident axonal regeneration, (Figures 5.10 B-E). For autologous graft the best regeneration process occurred as confirmed by histologies in Figures 5.10 C-F.

The mean G-ratio for PCL and autograft was 0.71 ± 0.07 and 0.66 ± 0.05, respectively (Figure 5.11). G-ratio could not be calculated in PCL/Gelatin implants due to the poor axonal regeneration and high degree of inflammation in this group. The mean myelinated fiber diameter was (4.77 ± 1.36) µm for nerve regenerated into PCL implant and (5.82 ± 1.18) µm for autograft group.

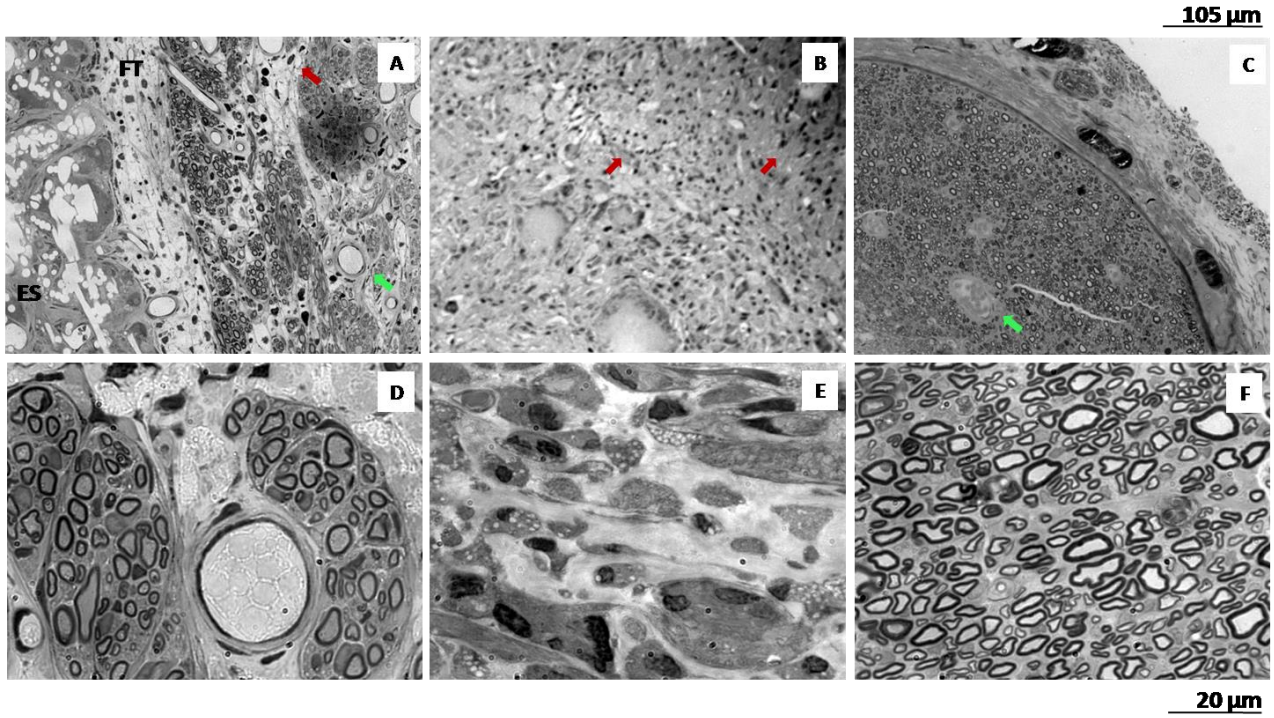

Figure 5.10: Images of 1 µm thick toluidine-blue stained nerve mid-sections of A) PCL implant; B) PCL/Gelatin implant; C) Autologous graft at low magnification (20x); D) PCL implant; E) PCL/Gelatin; F) Autologous graft at high magnification (100x). Red arrows point out the presence of inflammatory cells; green arrows signal the presence of blood vessels; FT indicates a fibrous layer that encloses axons; ES states the electrospun conduit.

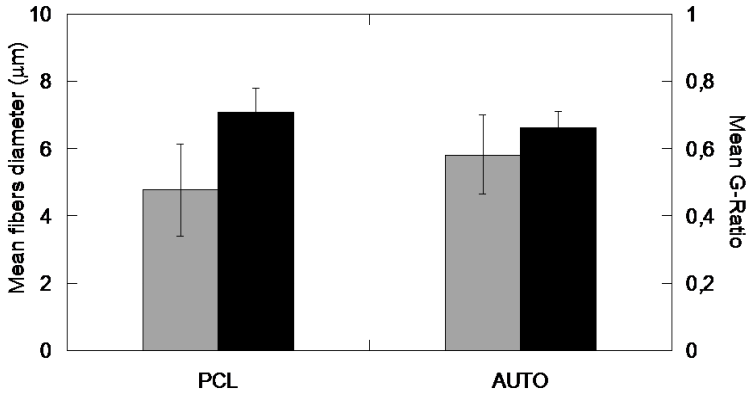

Figure 5.11: Image analysis data: mean value of myelinated fibers diameters ( ) and mean value of G-ratio ( ) for all examined samples.

5.4 DISCUSSION

For *in vivo* test, a 5 mm gap in rat sciatic nerve model was chosen instead of a critical size defect of 1 cm gap to preliminary evaluate materials suitability as a nerve guide. To assess axonal outgrowth and muscle reinnervation, a combination of traditional methods was used, including electrophysiology and muscle weights. For electrophysiological assessment, the amplitude of

CMAP is one commonly used parameter which indirectly reflects the numbers of regenerated motor nerve fibers and the extent of muscle reinnervation, while latency is an indirect parameter which refers to maturation of nerve fibers [17]. However three different approaches were used to measure CMAP: signals were recordered distally respect to the implant site by applying an electrical stimulus proximal and distal to the injury site and recordered proximally with a proximal stimulation. All the electrophysiological analysis demonstrated the superior capability of autograft and PCL nerve conduits in nerve regeneration when compared to PCL/Gelatin random nanofibrous nerve conduits, in fact based on the 18 weeks results, better functional recovery in terms of CMAP amplitude and latency was observed when the autograft and PCL tubes were implanted. These results were indirectly confirmed by muscles weight ratio: for PCL/Gelatin tubes, after 18 weeks of implant, the TA and Gastrocnemius muscles were almost entirely atrophied. The maintenance of muscle mass is controlled by a balance between protein synthesis and protein degradation pathways. When a muscle is denervated as a consequence of nerve injury, the balance is destroyed and shift to degradation tendency which leads to decreased muscle cell size, muscle weight loss and hyperplasia of connective tissues [18]. As the nerve regenerates into the muscle, it regains its mass proportional to the amount of reinnervation. This provides indirect evidence of nerve regeneration.

Histological analysis of explanted nerve samples showed myelinated axons and vasculature in both autograft and PCL nerve conduits. The presence of axons with myelin sheaths in PCL implants correlates with the higher CMAP amplitude measured in this group with respect to PCL/Gelatin implants, where the formation of fibrous tissue and inflammatory cells have been detected making impossible the quantification of axon diameter and G-ratio. The occurrence of a significant inflammatory response can be due to not adequate mechanical properties of PCL/Gelatin device comparing to PCL, as confirmed also in literature [19].

Cross sectional nerve areas images, quantified for axon, fiber diameter and G-ratio (axon diameter / myelinated fiber diameter) by image analysis software for autograft and PCL implant, show a higher value of G-ratio and lower mean fiber diameter for the polymeric graft comparing to the autologous, due to a reduced myelination process. The axons in the autologous group are more mature and the G-ratio approximate better to the theoretical value of 0.6, optimal for the spread of current from one node of Ranvier to the next, observed in most healthy nerves [9].

All the presented *in vivo* results are in agreement: PCL grafts performed well but not equivalent to the autograft, while PCL/Gelatin implants yielded consistently poor histology, electrophysiology and muscle weight data. PCL/Gelatin electrospun device failed as graft *in vivo* for peripheral nerve regeneration for lack in terms of mechanical response, despite the stronger cell/material interaction *in vitro* due to the materials chemistry and membrane submicrometric structure as confirmed by *in*

vitro test in our previous studies with DRGs and PC-12. In fact comparing with PCL, gelatin exposes many integrin sites for cell adhesion and differentiation, the presence of amine and carboxylic functional groups are responsible for the higher hydrophilicity and fiber size is smaller ensuring high surface/volume ratio for cells anchoring.

Since in the implementation of a 3D device as nerve graft *in vivo*, mechanical properties play an important role in the application success, PCL conduits represent a promising starting point that can be further optimized compensating the lack in terms of surface chemistry in order to improve peripheral nerve regeneration.

5.5 CONCLUSION

PCL and PCL/Gelatin solutions were processed by electrospinning to fabricate fibrous conduits as artificial grafts for sciatic nerve repair after transection.

Our animal experiment, electrophysiology and histological results showed that the PCL conduits gave good performance in resisting collapse and stretch forces *in vivo* and induced better recovery comparing to PCL/Gelatin conduits. Despite the submicrometric size scale of fibers and the better *in vitro* response with primary cells, PCL/Gelatin electrospun scaffolds are not capable of sustaining nerve regeneration *in vivo*, where the device mechanical response assumes greater importance.

REFERENCES

[1] Rodriguez FJ, Valero-Cabré A, Navarro X. Drug Discov Today: Dis Models. 2004; 1: 177-185.
[2] Belkas JS, Shoichet MS, Midha R. Neurol Res. 2004; 26: 1-10.
[3] Seckel BR. Enhancement of peripheral nerve regeneration. Muscle Nerve. 1990; 13: 785-800.
[4] Chaudhry V, Glass JD, Griffin JW. Wallerian degeneration in peripheral nerve disease. Neurol Clin 1992; 10: 613-627.
[5] Wong KH, Naidu M, David P, Abdulla MA, Abdullah N, Kuppusamy UR, Sabaratnam V. eCAM Advance Access. 2010; doi:10.1093/ecam/neq062.
[6] Newton CD, Nunamaker DM. Textbook of Small Animal Orthopaedics. J.B. Lippincott Company in 1985.
[7] Clements IP, Kim YT, English AW, Lu X, Chung A, Bellamkonda RV. Biomaterials. 2009; 30(23-24): 3834-3846.
[8] Nichols CM, Brenner MJ, Fox IK, Tung TH, Hunter DA, Rickman SR, Mackinnon SE. Exp Neurol. 2004; 190(2): 347-355.
[9] Matsuyama T, Mackay M, Midha R. Neurol Med-Chi. 2000; 40(4): 187-199.
[10] Pabari A, Yang SY, Seifalian AM, Mosahebi A. J Plast Reconstr Aesthet Surg. 2010; 63: 1941–1948.
[11] Daly W, Yao L, Zeugolis D, Windebank A, Pandit A. J R Soc Interface. 2012; 9: 202-221.
[12] Williams LR, Longo FM, Powell HC, Lundborg G, Varon S. J Comp Neurol.1983; 218: 460-470.
[13] de Ruiter GCW, Malessy MJA, Yaszemski MJ, Windebank AJ, Spinner RJ. Neurosurg. 2009; 26: E5. (doi:10.3171/FOC.2009.26.2.E5)
[14] Mukhatyar V, Karumbaiah L, Yeh J, Bellamkonda R. Adv Mat. 2009; 21: 4670-4679.
[15] Zhao Q, Dahlin LB, Kanje M, Lundborg G. Restorative Neurol Neurosci. 1993; **5**: 197-204.
[16] Park SC, Oh SH, Seo TB, Namgung U, Kim JM, Lee JH. J Biomed Mater Res B Appl Biomater. 2010; 94B: 359-366.
[17] Wolthers M, Moldovan M, Binderup T, Schmalbruch H, Krarup C. Microsurgery. 2005; 25(6): 508-519.
[18] Bodine SCLE, Baumhueter S, Lai VK, Nunez L, Clarke BA, Poueymirou WT, Panaro FJ, Dharmarajan K, Pan ZQ, Valenzuela DM, Stitt TN, Yancopoulos GD, Glass DJ. Science. 2001; 294: 1704-1708.
[19] Subramanian A, Krishnan UM, Sethuraman S. J Biomed Sci. 2009; 16:108-118.
[20] Xander Smit, A rat sciatic nerve study on fundamental problems of peripheral nerve injury.

CHAPTER 6

Moving Towards Anisotropic and Multilayers Structures

6.1 INTRODUCTION

Poly(ε-caprolactone) (PCL) and PCL/Gelatin electrospun conduits were used as artificial grafts for sciatic nerve repair after transection. Data reported previously demonstrated that PCL/Gelatin electrospun device failed in sustaining nerve regeneration *in vivo*, despite the better *in vitro* response of primary (DRGs) and cell lines (i.e., hMSC and PC-12). While characteristic size scale of fibers seems to evidently affect *in vitro* response, other factors such as mechanical properties may affect the *in vivo* behavior. Furthermore, in Chapter 5, we have demonstrated that PCL conduit alone does not represent the best choice, but the autologous graft still remains the gold standard in terms of regeneration.

Recently, alternative repair strategies include the use of intraluminal guidance structures and micro-grooved luminal designs [1] to provide additional structure support and topographical guidance to regenerating axons and migrating Schwann cells (SC) (Figure 6.1).

However, Ngo et al. [2] showed that the presence of fillers clustered in the centre of the conduit may reduce the axonal regeneration until a regeneration failure. This result highlights the need of a correct placement of intraluminal fillers within a hollow nerve conduit by the proper combination of material components. For instance, Stang et al. [3] demonstrated that the addition of a dense collagen sponge within a hollow nerve conduit also inhibits regeneration entirely.

A promising strategy in the conduit design consists in the use of multi-channel conduits to control axonal dispersion, as well nutrient exchange or external stimuli. Sometimes, these approaches are not efficacious alone but also require further surface functionalization to improve cell adhesion, migration, alignment and proliferation [1].

The electrospinning process currently represents a very interesting approach to realize ‘‘*bio-inspired*’’ scaffolds by the assembly of (micro or nano) textured layers with increasing complexity, by the stratification of fibers sheets with a distinct composition [4] and topographical pattern [5-7]. Hence, it is possible to design a scaffold with tunable chemical and structural features able to address different cell behaviors [8].

As consequence, bilayered electrospun conduits, made by the overlapping of a PCL/Gelatin nanotextured inner layer and PCL microfibers as outer layer are introduced in this chapter as innovative graft for peripheral nerve repair. By this new approach, the inner layer guarantees topographic and biochemical cues to improve cells activities while the outer mainly ensures the mechanical stability required to guide the regenerating nerve.

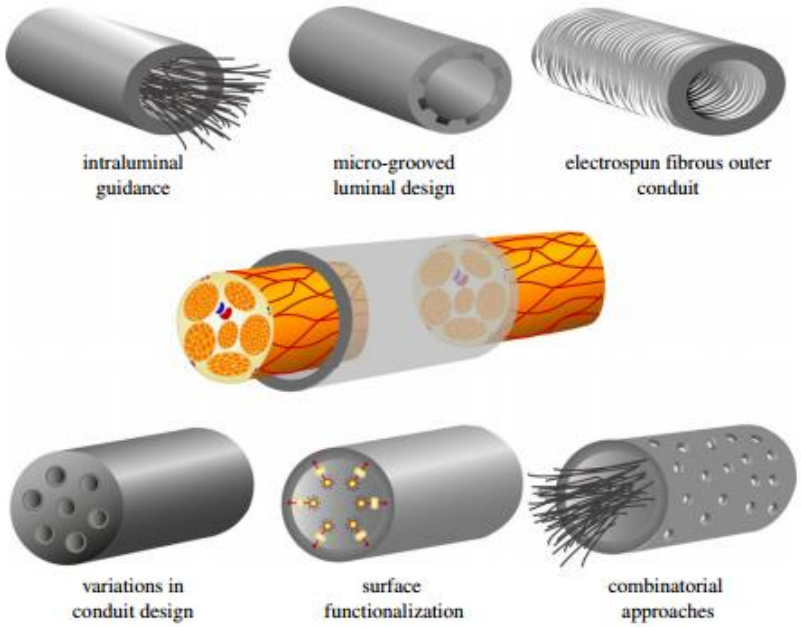

Figure 6.1: Summarized scheme of the structural repair strategies used for improving existing hollow nerve guidance conduits [1].

Since one of the biggest challenges with axonal regeneration is misdirected axonal growth, which results in inappropriately directed reinnervation between motor and sensory axons and their respective targets [9, 10], a possible approach to achieve directional axonal growth is the incorporation of contact guidance cues, whereby the topographical features of the biomaterial surface regulates the direction of cell growth [11]. Electrospun fibrous conduits are attractive for guidance because fibers may be aligned to orient axonal growth up to bridge large nerve gaps in both spinal cord regeneration [12, 13] and peripheral nerve [14, 15] cases.

Alternatively, an additional multilayer system with micro or nanotexture and pre-determined anisotropy may be conceived by the inner surface of PCL micrometric fibers tubes by PCL/Gelatin fibers highly oriented along the longitudinal axis with incremental changes in fiber alignment controlled by the mandrel rotation.

6.2 MATERIALS

PCL (M_n 45 kDa) and Gelatin (Type B from calf skin, ~225 Bloom) were purchased from Sigma-Aldrich (Italy). 1,1,1,3,3,3-hexafluoro-2-propanol (HFP), (Fluka, Italy), and chloroform ($CHCl_3$), from J.T. Baker (Italy), were used as received without further purification. PCL was dissolved in chloroform (0.33 g/ml) by magnetic stirring at room temperature overnight to attain a clear solution ready to be electrospun. PCL and Gelatin were separately dissolved in HFP at a concentration of 0.1 g/ml and kept under magnetic stirring at room temperature for 24 h. Then, polymer solutions were mixed to obtain a 50/50 wt/wt PCL/Gelatin solution.

6.3 METHODS

6.3.1 Electrospinning Process

Bilayered scaffolds were in both case - tubes with random inner layer (RILT) and tubes with aligned inner layer (AILT) - developed by a two-step electrospinning process.

The luminal layer made of random PCL/Gelatin fibers was obtained by deposition on a stainless steel mandrel rotating at 50 rpm. Later, it was coated with micrometric PCL fibers, which formed the outer layer of the tube, with mandrel rotating rate equal to 50 rpm.

The aligned fibrous nerve conduits comprised a luminal region of longitudinally aligned PCL/Gelatin fibers and an outer region of randomly oriented PCL fibers. Longitudinal alignment of PCL/Gelatin fibers was achieved through a drum rotating at high speed (3000 rpm). Once obtained the anisotropic membrane, it was cut and wrapped on the cylindric mandrel, ready for the subsequent deposition of PCL randomly oriented fibers. Upon completion of electrospinning, the nerve conduits were air-dried on the steel mandrel overnight to remove residual solvents.

6.3.2 Morphological Analysis

The morphology of fibrous devices was studied by scanning electron microscopy (SEM; QuantaFEG 200, FEI, The Netherlands) under high vacuum conditions (~10^{-5} Mbar). To improve the sample conductivity, specimens were preliminary coated with a Pd-Au nanolayer by using a sputter coater (Emitech K550, Italy). To analyze fiber alignment, SEM images of the nerve conduit luminar surfaces were imported into ImageJ software and transformed using the two-dimensional FFT function. This function converted the image into a spatial distribution corresponding to the changes in pixel intensity across the sample. Transformed images were rotated by 90° to match the alignment of the original images.

6.3.3. Cells Culture

PC-12 cell, a cell line derived from pheochromocytoma of the rat adrenal medulla, and human mesenchymal stem cells (hMSC) were again selected as the testing cell models (see Chapter 3).

PCL/Gelatin membranes scaffolds (random and aligned structured) were used as the experimental group. PC-12 cells were routinely cultured in tissue culture flask surfaces with High Glucose-Dulbecco´s Modified Eagle´s Medium (HG-DMEM), containing 100 units/ml penicillin, 100 µg/ml streptomycin sulfate (Sigma), 5% fetal bovine serum and 15% of horse serum.

hMSCs were cultured in Eagle's alpha minimum essential medium (α-MEM) supplemented with 10% fetal bovine serum, antibiotic solution (streptomycin 100 µg/ml and penicillin 100U/ml, Sigma Chem. Co) and 2 mM L-glutamin. Both cell lines were incubated at 37°C in a humidified atmosphere with 95% air and 5% CO_2. When the cells became almost confluent, they were released by treating with 0.25% trypsin-EDTA solution for 3 min at 37°C and resuspended in their respective medium with a final concentration of 2 x 10^5 cells/ml.

6.3.4 In vitro Neuronal Cell Differentiation assay

For *in vitro* differentiation assay, PC-12 cells were seeded onto PCL/Gelatin membranes scaffolds (random and aligned structured) placed in 24 cell culture plates and cultured with RPMI 1640 medium with 1% of horse serum and 50 ng/ml of neuronal growth factor (NGF) for 6 days. For neuronal induction, hMSCs were pre-treated with α-MEM containing 0.0001% β-mercaptoethanol, IBMX, DMSO, 10 ng/ml epidermal growth factor (EGF) and 10 ng/ml basic fibroblast growth factor (β-FGF) (Chemicon, Temecula, CA, USA) previously seeded onto electrospun membranes for 24 h. After pre-treatment, hMSCs were washed with PBS and then incubated with 50 ng/ml of NGF and 20 ng/ml of brain derived neurotrophic factor (BDNF) for 6 days. After induction, both PC-12 and hMSC cells cultures onto electrospun membranes scaffolds were fixed with 4% paraformaldehyde and permeabilized with PBS containing 0.5% Triton X-100. Cells were incubated at 4ºC overnight in a 1:300 dilution of the rabbit (IgG) polyclonal antibody against rat GAP-43 in PBS containing 2 mg/ml of bovine serum albumin (BSA). Scaffolds were washed with ice-cold PBS for 10 min at room temperature and incubated for 1 h at 4ºC with goat-anti-rabbit immunoglobulin secondary antibody conjugated with FITC for PC-12 and rhodamine for hMSC (3 mg/ml, Sigma Chemical, St. Louis, MO), diluted 1:50 in PBS. Immunoassaying was visualized by Laser Scanning Confocal Microscopy (Carl Zeiss) (LSCM).

6.4 RESULTS

Bilayered tubes surface appeared macroscopically smooth and without any coarse defects along fibers. They were cross-sectioned and imaged to view the electrospun layers interface. SEM clearly

evidenced the bilayered structure of the tubular scaffolds: an inner layer with nanometric random PCL/Gelatin fibers and an outer layer with micrometric PCL fibers (Figure 6.2). The measured thickness of the PCL/Gelatin layer was 30.02 ± 2.34 μm while the external PCL layer had thickness of 978.53 ± 47.84 μm. Layers are strictly adhered to each other and no visible delamination is recognized in both cases- RILT and AILT conduits.

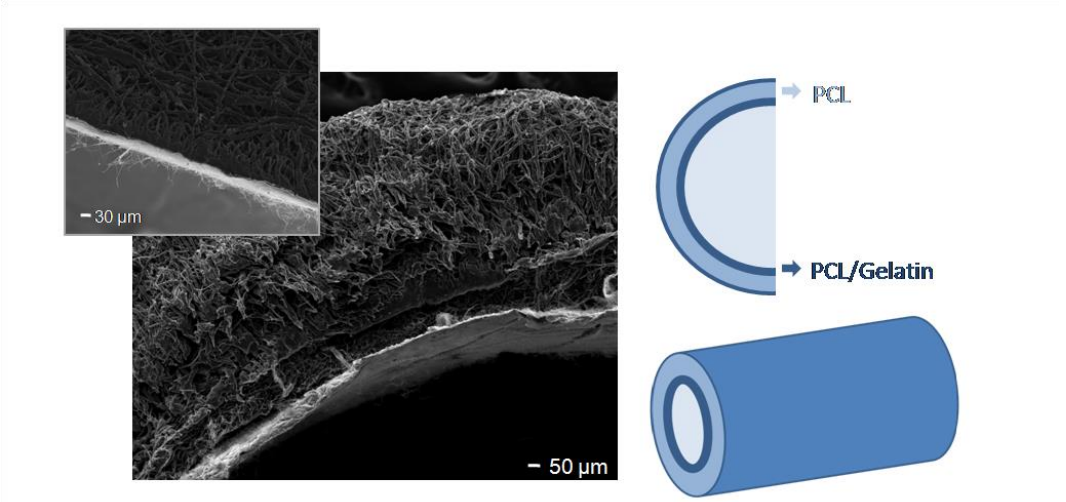

Figure 6.2: Bilayered electrospun conduit made of PCL micrometric fibres (outer layer) and random PCL/Gelatin fibers (inner layer).

Likewise, SEM image from sectioned AILT showed that PCL microfibers were randomly oriented on the external surface and PCL/Gelatin aligned fibers were on the internal surface (Figure 6.3).

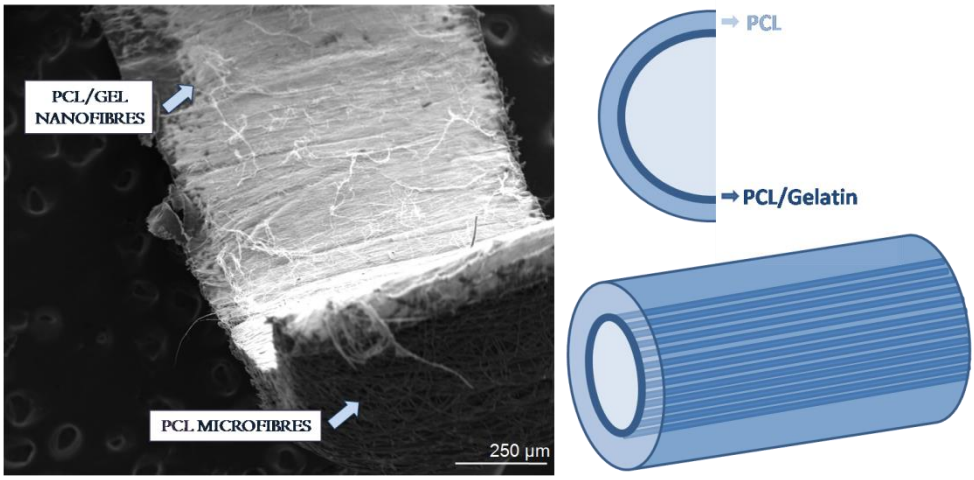

Figure 6.3: Bilayered electrospun conduit made of PCL micrometric fibers (outer layer) and aligned PCL/Gelatin fibers (inner layer).

SEM images of both luminal surfaces, i.e. random and aligned, were analyzed using the FFT function. The image containing randomly oriented fibers generated an output FFT image where the pixel intensities appeared to be uniformly distributed in a circular pattern (Figure 6.4 left). The image containing aligned fibers generated an output FFT image with a group of pixel intensities oriented in a preferential direction (Figure 6.4 right). Further analysis to calculate a quantitative value for fibers alignment is still ongoing.

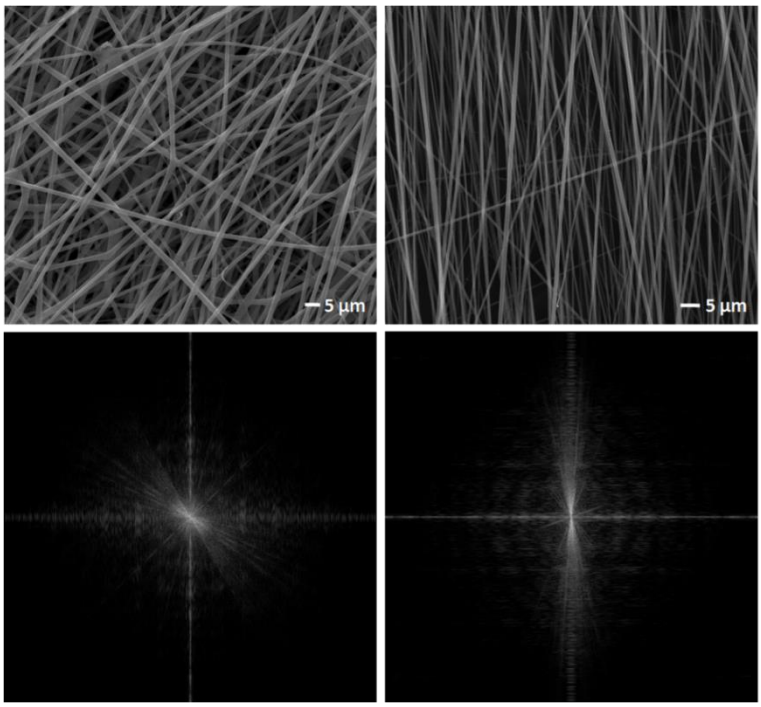

Figure 6.4: On the left random PCL/Gelatin and on the right aligned PCL/Gelatin SEM and relative FFT images, displayed in black and white for clarity.

Preliminary biological validation with PC-12 and hMSC cells was performed in order to qualitatively identify the effect of the different pattern due to fibers spatial disposition on cells behavior. SEM pictures showed the spreading and cell attachment of cells after neurnal induction media for hMSC (Figure 6.5 left column) and PC-12 (Figure 6.5 right column). After 6 days of hMSC and PC-12 cultures with NGF treatment, PC-12 and hMSC cells showed a good spreading and attachment to the substrate scaffold developing characteristic neuritis with growth conical ends for physical contact with the surface of the electrospun fibers. Cells seeded on randomly oriented fibers showed randomly oriented growth patterns (Figure 6.5, up-row), while cells elongated parallel growth on aligned fibers (Figure 6.5, down-row).

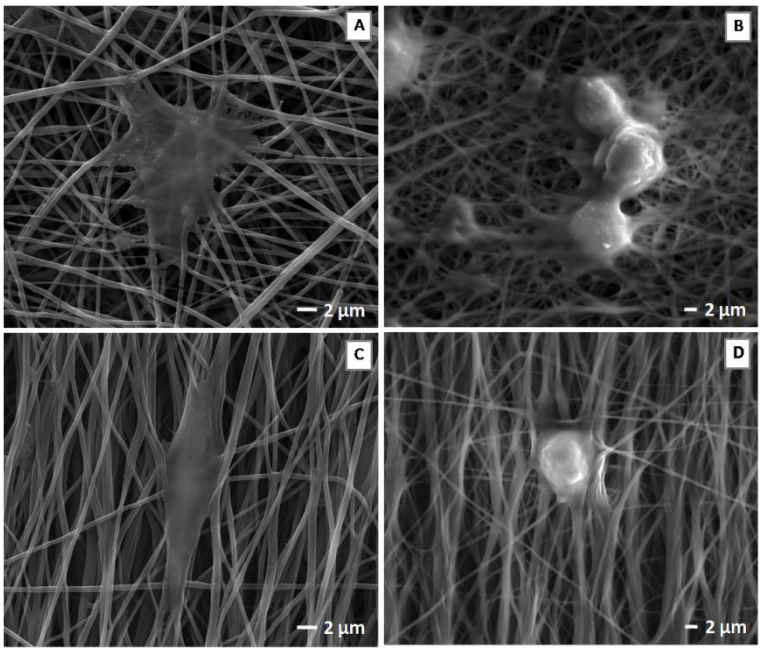

Figure 6.5: SEM images of hMSC (left) and PC-12 (right) cell morphology after 6 day culture with NGF addition on RILT (A-B) and AILT (C-D) device.

Confocal images obtained after immunostaining confirmed SEM results: they prove the preliminary differentiation of hMSC cells and PC-12 (Figure 6.6) culturing onto the random (up-rows) and aligned fibers (down-rows) scaffolds by detection of the membrane neurite marker growth associated protein GAP-43.

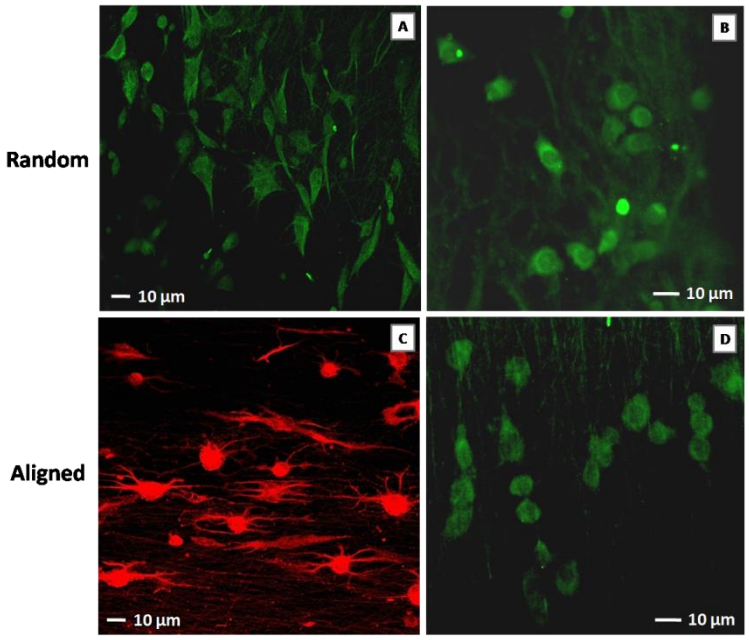

Figure 6.6: Confocal images of hMSC (A-C) and PC-12 (B-D) cells morphology after 6 day culture with NGF addition on RILT (up-row) and AILT (dow-row) device.

The morphological appearance of PC-12 and hMSC differentiation showed that cells were sending out neurites that extend and attach to the substratum with a growth cones which extended from them onto fibrous scaffolds after 6 days of using neuronal induction media. In the specific case of aligned fibers, neurites from hMSC and PC-12 cells followed a rectilinear direction parallel to the long axes of the conduits.

6.5 DISCUSSION

Various nerve conduits are often not able to facilitate growth over long gaps due to collapse, scar infiltration, and, as in the case of biodegradable materials, early resorption [16, 17]. In these multilayered devices, the fibrous micro-structure of PCL may confer the adequate mechanical strength to the three-dimensional structure until later neo-tissue formation. Meanwhile, gelatin cue may encourage cells recognition [18] and the nanostructure adds high exposed surface (per volume unit) for cell attachment.

Indeed, the homogeneous distribution of fiber diameter in the nanometric scale enables the exposure of an ordered nanotextured surface, interacting more effectively with cells, due to the higher exposed scaffold surface. The presence of the protein cue also provides specific signals to promote cell growth and functionality as confirmed by MSCs' biocompatibility experiments.

Here, PCL/Gelatin membranes were chosen as inner layer for the implementation of bilayered electrospun conduits. Gelatin integration directly inside the tubes guarantees favorable conditions for cellular adhesion, first aspect of cell-material interaction able to influence the response of cells' physiological and biological functions, proliferation and differentiation.

Schnell et al. [19, 20] reported that a biochemical interaction between cells and collagen exposed on the surface of the nanofibers is mediated by the ECM glycoprotein fibronectin, which binds to collagen I and to integrin receptors on cell membranes [20]. Gelatin is a natural biopolymer derived from collagen by controlled hydrolysis and has structural similarity to collagen. Therefore, it can be concluded that the inclusion of gelatin into PCL enhances the interaction of the cells with the scaffolds by engaging cell-adhesion molecules so permitting cells to exert/generate higher interaction forces as required for cell motility.

Moreover the direction of neurite elongation was preferentially extended along the aligned fibers and such contact guidance might enhance the rate and the extent of neurite elongation, affecting the nerve regeneration process, strictly dependent *in vivo* on the formation of bands of Bünger by the alignment of Schwann cells [21-24]. Hence, it can be concluded that the arrangement of cells in controlled architecture may have beneficial effects on nerve regeneration.

Additionally, the outer layer made of randomly disposed PCL micrometric fibers assured that the conduits was pliable enough to glide and bend with the animal's limb movements, yet stiff enough not to collapse *in vivo*.

Moreover, micrometric fibers size and micrometric porous area (see Chapter 4) allow the exchange of nutrient with the surrounding tissue, indeed porous conduits permeable to the surrounding tissue medium provide better nutritional support and improve regeneration as demonstrated by Midha et al. [25].

6.6 CONCLUSION

Based on the *in vivo* results reported in Chapter 5, the implementation of 3D electrospun structures with higher degree of complexity has been addressed here. Bilayered nerve conduits has been produced by covering a PCL/Gelatin nanotextured layer by PCL microfibers, in this way the luminal bicomponent layer can offer peculiar topographic and biochemical cues to improve cells activities while the outer synthetic layer mainly ensures the mechanical stability required to guide the regenerative nerve processes. Preliminary results, also suggested that the fibers alignment in the inner layer may further help regeneration avoiding misdirectional axonal growth.

REFERENCES

[1] Daly W, Yao L, Zeugolis D, Windebank A, Pandit A. J R Soc Interface. 2012; **9:** 202-221.

[2] Ngo TTB, Waggoner PJ, Romero AA, Nelson KD, Eberhart RC, Smith GM. J Neurosci Res. 2003; 72: 227-238.

[3] Stang F, Fansa H, Wolf G, Reppin M, Keilhoff G. Biomaterials. 2005; 26: 3083-3091.

[4] Tampieri A, Sandri M, Landi E, Pressato D, Francioli S, Quarto R, Martin I. Biomaterials. 2008; 29: 3539-3546.

[5] Papenburg BJ, Liu J, Higuera GA, Barradas A, de Boer J, van Blitterswijk CA, Wessling M, Stamatialis D. Biomaterials. 2009; 30(31): 6228-6239.

[6] Guarino V, Causa F, Salerno A, Ambrosio L, Netti PA. Mater Sci Technol. 2008; 24: 1111-1117.

[7] Guarino V, Causa F, Taddei P, Di Foggia M, Ciapetti G, Martini D, Fagnano C, Baldini N, Ambrosio L. Biomaterials. 2008; 29: 3662-3670.

[8] Guaccio A, Guarino V, Alvarez- Perez MA, Cirillo V, Netti PA, Ambrosio L. Biotechnol Bioeng. 2011; 108(8): 1965-1976.

[9] Yao L, O'Brien N, Windebank A, Pandit A. J Biomed Mater Res-A. 2009; 90B: 483-491.

[10] Leach JB. In: Metin Akay, editor. Encyclopedia of Biomedical Engineering, Hoboken, NJ: Wiley. 2006; 6: 3568-3578.

[11] Bashur CA, Dahlgren LA, Goldstein AS. Biomaterials. 2006; 27: 5681-5688.

[12] Yoshii S, Oka M, Shima M, Akagi M, Taniguchi A. Spine. 2003; 28: 2346-2351.

[13] Novikov LN, Novikova LN, Mosahebi A, Wiberg M, Terenghi G, Kellerth J-O. Biomaterials 2002; 23: 3369-3376.

[14] Lundborg G, Dahlin L, Dohi D, Kanje M, Terada N. J Hand Surg [Br]. 1997; 22: 299-303.

[15] Cai J, Peng X, Nelson KD, Eberhart R, Smith GM. J Biomed Mater Res A. 2005; 75: 374-386.

[16] Doolabh VB, Hertl MC. Rev Neurosci. 1996; 7: 47-84.

[17] Belkas JS, Munro CA, Shoichet MS, Johnstona M, Midha R. Biomaterials.2005; 26: 1741-1749.

[18] Guarino V, Alvarez-Perez MA, Cirillo V, Ambrosio L. J Bioact Comp Pol. 2011; 26(2): 144-60.

[19] Ghasemi-Mobarakeh L, Prabhakaran MP, Morshed M, Nasr-Esfahani MH, Ramakrishna S. Biomaterials. 2008; 29: 4532-4539.

[20] Schnell E, Klinkhammer K, Balzer S, Brook G, Kleeb D, Dalton P, Mey J. Biomaterials. 2007; 28: 3012-3025.

[21] Chew SY, Mi R, Hoke A, Leong KW. Biomaterials. 2008; 29: 653-661.

[22] Thompson DM, Buettner HM. Tissue Eng. 2001; 7(3): 247-265.

[23] Miller C, Shanks H, Witt A, Rutkowski G, Mallapragada S. Biomaterials. 2001; 22: 1263-1269.

[24] Schmalenberg KE, Uhrich KE. Biomaterials. 2005; 26: 1423-1430.

[25] Midha R, Munro CA, Dalton PD, Tator CH, Shoichet MS. J Neurosurg. 2003; 99: 555-565.

OVERALL CONCLUSIONS

In this work we proposed the design of bicomponent electrospun conduit for peripheral nerve regeneration. Firstly, we have optimized the electrospinning process by the proper selection of polymer/solvent coupling, giving prominence to the effect of solvent permittivity, and process parameters in order to control the final morphology of fibrous membranes. Results have suggested that solvents with different permittivity play an active role in PCL polymer chain folding during the fiber deposition, thus drastically affecting the fiber crystallinity and the final morphological appearance of electrospun fibers in terms of fiber size scale and bead formation. By adopting a particular fiber morphology (i.e., size scale) and mode of assembly of polymer chains (i.e., crystallinity), it is possible to influence the adhesion and/or proliferation kinetics of cells, ultimately determining the course of their differentiation process. Although PCL electrospun fibrous scaffolds have already been proven feasible as favorable substrates for nerve cell culture, the results of cell attachment, viability, and neurite outgrowth studies reported here, demonstrated that the integration of gelatin with PCL fibers significantly improves the biointeraction of PC-12 pheochromocytoma nerve cells with the substrate. This improved bioactivity is related to the synergistic contribution of scaffold material topography, that is, submicrometric fiber diameter, and biochemical signals offered by gelatin biopolymer, as confirmed also by the comparative study with casted films.

Based on these preliminary results, PCL and PCL/Gelatin fibers were then collected on a rotating mandrel in order to produce electrospun conduits for peripheral nerve regeneration. We demonstrated that the use of rotating mandrel does not affect fibers morphology in both cases - PCL and PCL/Gelatin. Only mechanical properties of the electrospun conduits are strongly affected by the integration of gelatin in the fibers (PCL-Gelatin ratio is 50:50).

Further *in vitro* characterization with primary cells, i.e. DRGs, also confirmed that the fibrous scaffolds are able to support cell attachment and neurite extension, in particular PCL/Gelatin substrates improved neurite outgrowth from DRGs principal body. Conduits have been successfully implanted as artificial graft in an 18 weeks study in rat sciatic nerve model to repair a 5 mm gap after transection. Animal experiment, electrophysiology and histological results have shown that the PCL conduits induced better recovery comparing to PCL/Gelatin conduits, probably due to its higher stiffness and resistance to collapse. Despite the submicrometric size scale of fibers and the better *in vitro* response with primary cells, PCL/Gelatin electrospun scaffolds are not capable of sustaining nerve regeneration *in vivo*, where the device mechanical response assumes greater importance.

In perspective, we are trying to design novel electrospun conduits with higher degree of complexity: bilayered electrospun conduits made by the overlapping of a PCL/Gelatin nanotextured inner layer and PCL microfibers as outer layer. As consequence, the luminal bicomponent layer guarantees the required topographic and biochemical cues to improve cells activities, while the micro-structured outer layer ensures the mechanical stability required to guide the regenerating nerve, thus representing an innovative graft for peripheral nerve repair.